

**PREPARATION AND PROPERTIES OF  
CADMIUM-ZINC CHALCOGENIDE  
THIN FILMS FOR DEVICE  
APPLICATIONS**

Thesis

Submitted in partial fulfillment of the requirements for the degree of

**DOCTOR OF PHILOSOPHY**

by

**SANTHOSH T.C.M.**



**DEPARTMENT OF PHYSICS  
NATIONAL INSTITUTE OF TECHNOLOGY KARNATAKA,  
SURATHKAL, MANGALORE – 575025  
MAY, 2018**

## **DECLARATION**

*by the Ph.D. Research Scholar*

I hereby *declare* that the Research Thesis entitled “**Preparation and Properties of Cadmium-Zinc Chalcogenide Thin Films for Device Applications**” which is being submitted to the National Institute of Technology Karnataka, Surathkal in partial fulfillment of the requirements for the award of the Degree of **Doctor of Philosophy in Physics** in a *bonafide report of the research work carried out by me*. The material contained in this Research Thesis has not been submitted to any University or Institution for the award of any degree.

**Mr. Santhosh T.C.M.**

(Reg. No. 135016PH13F03)

Department of Physics

Place: NITK, Surathkal

Date:

## **CERTIFICATE**

This is to *certify* that the Research Thesis entitled “**Preparation and Properties of Cadmium- Zinc Chalcogenide Thin Films for Device Applications**” Submitted by **Santhosh T.C.M.** (Register Number: **135016PH13F03**) as the record of the research work carried out by him, is *accepted as the Research Thesis submission* in partial fulfillment of the requirements for the award of degree of **Doctor of Philosophy**.

**Prof. Kasturi V. Bangera**  
Research Guide

Chairman - DRPC

## **ACKNOWLEDGEMENT**

Ph.D. has been a truly life-changing experience for me and it would not have been possible without support and guidance that I received from many people.

First and foremost, I would like to express my sincere gratitude to respected supervisor Prof. (Mrs.) Kasturi V. Bangera for considering me as her research student. It has been an honor to be her Ph.D. student. I heartily thank her for her kindness, valuable suggestions, and constant encouragement, which I received during tough times in the Ph.D. pursuit. Her constant guidance, cooperation and moral support has always kept me going ahead. The research work presented here would have been impossible without support and guidance of my supervisor.

I would like to express my sincere gratitude to Prof. G. K. Shivakumar for his valuable suggestions and advice towards my research work.

I sincerely thank the members of RPAC Dr. M.N. Satyanarayan and Dr. Vidya Shetty K, for their valuable suggestions and excellent advice in accomplishing this research work.

I am grateful to the Head of the Department, Dr. M.N. Satyanarayan for supporting me to attend various conferences and workshops, which in turn helped me to understand the current research trends.

I offer my heartfelt gratitude to National Institute of Technology Karnataka, for providing financial assistance and wonderful work environment.

I heartily thank my research colleagues; Dr. Sadananda Kumar N. and Dr. Shashidhar, Mrs. Veena E, Mrs. Sowjanya V, Mr. Bharath S. P., and Mr. Biswajit Barman for their help, encouragement and best wishes. It was a great pleasure to work with them.

I thank all faculty members, staff and research students of the Department of Physics, for their kind and sincere support throughout my work.

I owe special thanks to my father Veeraiah T.C.M and mother Basamma K.M, who supported me and helped me throughout my life and during this study. Their constant encouragement and support enabled me to pursue my dreams. I rightly dedicate this

work to them. A very special thanks to my family members, Sachin T.C.M., Basavaraj B.A and Suchitra S. M, for their care and support along the way.

I am greatly thankful to friends outside the lab and institute, who have supported me in many circumstances during the course of my work. I would like to thank, Bindu, Sanjeev K. R., Komal Krishna, Dr. Raghavendra Hebbar and Dr. Praveen Naik.

There are many more whom I must remember with gratitude. Their names, though I might have failed to mention here, shall never be forgotten.

Mr. Santhosh T.C.M.

## ABSTRACT

The present work described in this thesis involves studies on cadmium selenide, both undoped and doped along with a study of ternary compounds  $\text{Cd}_{(1-x)}\text{Zn}_{(x)}\text{Se}$  and  $\text{CdSe}_{(1-x)}\text{Te}_{(x)}$  in thin film form obtained by depositing bulk compounds on glass substrates by thermal evaporation technique. The structural, morphological, optical and electrical properties were studied in order to understand the effect of doping and alloying with the intention of using these compounds in band gap engineering. The interest in these compounds is due to the fact that they are direct band gap materials and have their band gap energies in an attractive range of values. CdSe films were obtained in stoichiometric composition by varying deposition parameters such as substrate temperature and annealing duration. These films exhibit polycrystalline hexagonal crystal structure with a preferred growth along (002) direction. The optical band gap and electrical conductivity were found to be 1.68 eV and  $10^{-4} \text{ } \Omega\text{-cm}$  respectively. Further, CdSe thin films were doped with pure metals such as silver, bismuth and indium separately by varying the dopant concentration from 0-3%. The maximum electrical conductivity was obtained for 3% In doped CdSe thin films. Photocurrent measurements were carried out for undoped and doped CdSe thin films. 3% Bi doped CdSe thin films showed maximum photocurrent of 1.38  $\mu\text{A}$ . The effect of annealing duration on the formation of homogenous single phase ternary alloys of  $\text{Cd}_{(1-x)}\text{Zn}_{(x)}\text{Se}$  and  $\text{CdSe}_{(1-x)}\text{Te}_{(x)}$  thin films was studied. The band gap energy value was determined in both ternary systems by varying the composition  $x = 0, 0.2, 0.4, 0.6, 0.8$  and 1.

Heterojunction of undoped CdSe/p-Si, Ag doped CdSe/p-Si, Bi doped CdSe/p-Si and In doped CdSe/p-Si were fabricated and studied to consider their usefulness in optoelectronic devices. The electrical conduction in all the four diodes was found to takes place by thermionic emission at lower voltages and by space charge limited conduction mechanism at higher voltages. Among four diodes Bi doped CdSe/p-Si heterojunction has high rectification ratio of 894.1 at  $\pm 4 \text{ V}$ .

Keywords: CdSe, thin films, thermal evaporation, doping, ternary alloys, heterojunctions, diodes.

# CONTENTS

	<b>Page No.</b>
<b>CHAPTER 1 General Introduction</b>	
1.1 Introduction .....	1
1.2 Properties of Chalcogenide compounds .....	4
1.3 Literature Survey .....	6
1.4 Scope and objectives of the present work .....	15
<b>CHAPTER 2 Experimental and characterization techniques</b>	
2.1 Sample preparation technique .....	17
2.2 Thickness measurements methods .....	23
2.3 Characterization techniques	
2.3.1 Structural Characterization .....	25
2.3.2 Surface Morphological and Compositional analysis	27
2.3.3 Optical Characterization .....	29
2.3.4 Electrical Characterization .....	31
2.3.5 Photoconductivity .....	35
<b>CHAPTER 3 Preparation of CdSe thin films</b>	
3.1 Introduction .....	37
3.2 Experimental details .....	38
3.3 Optimization of deposition parameters .....	38
3.3.1 Effect of substrate temperature .....	38
3.3.2 Effect of annealing duration .....	42

## **CHAPTER 4 Effect of doping on the properties of CdSe thin films**

4.1 Introduction .....	47
4.2 Silver doped CdSe thin films .....	48
4.2.1 Experimental methods .....	48
4.2.2 Results and discussion .....	49
4.3 Bismuth doped CdSe thin films .....	55
4.3.1 Experimental methods .....	55
4.3.2 Results and discussion .....	56
4.4 Indium doped CdSe thin films .....	61
4.4.1 Results and discussion .....	61

## **CHAPTER 5 Preparation of ternary compounds and their properties**

5.1 Preparation of $\text{Cd}_{(1-x)}\text{Zn}_{(x)}\text{Se}$ thin films .....	66
5.1.1 Introduction .....	66
5.1.2 Experimental details .....	67
5.1.3 Results and discussion .....	68
5.2 Preparation of $\text{CdSe}_{(1-x)}\text{Te}_{(x)}$ thin films .....	75
5.2.1 Introduction.....	75
5.2.2 Experimental details .....	76
5.2.3 Results and discussion .....	77

## **CHAPTER 6 Heterojunctions of pure and doped CdSe films with silicon**

6.1 Introduction .....	84
6.2 Experimental details.....	85
6.3 Results and Discussion .....	86



**CHAPTER 7 Summary and conclusions**

7.1 Summary of the present work .....	94
7.2 Conclusions of the present work .....	94
7.3 Scope for the future work .....	96
<b>REFERENCES</b> .....	97
<b>PUBLICATIONS</b> .....	109
<b>CURRICULUM VITAE</b>	

## LIST OF FIGURES

	<b>Page No.</b>
Figure 1.1: Crystal structure of CdSe.....	6
Figure 2.1: Schematic diagram of thermal evaporation system.....	19
Figure 2.2: Photograph of thermal evaporation (PVD) system used to prepare CdSe thin films.....	20
Figure 2.3: X-Ray diffractometer Rigaku (Model Miniflex 600).....	25
Figure 2.4: Field Emission Scanning Electron Microscopy (Carl Zeiss).....	28
Figure 2.5: EDAX spectra of stoichiometric CdSe thin film.....	29
Figure 2.6: UV-Vis-NIR Spectrophotometer (model: 3700/3700DUV).....	30
Figure 3.1: XRD patterns of CdSe thin films deposited at different substrate temperature.....	39
Figure 3.2: FE-SEM micrographs of CdSe thin films deposited at different substrate temperature.....	40
Figure 3.3: EDAX spectra of CdSe thin films deposited at different substrate temperature.....	40
Figure 3.4: Tauc's Plot of CdSe thin film deposited at different substrate temperature.....	41
Figure 3.5: Variation of $\ln(R)$ with $10^3/T$ ( $K^{-1}$ ) of CdSe thin films deposited at a different substrate temperature ( $T_s$ ).....	42
Figure 3.6: XRD patterns of CdSe thin films annealed for two different durations.....	43

Figure 3.7: FE-SEM micrographs of CdSe thin films annealed for 1hr and 2hr.....	43
Figure 3.8: Tauc's plot of 1hr and 2hr annealed CdSe thin films.....	44
Figure 3.9: I-V characteristics of annealed CdSe thin films.....	45
Figure 3.10: Variation of $\ln(R)$ vs $1000/T(K^{-1})$ of CdSe thin films.....	45
Figure 3.11: Photo-response curves of as-deposited and annealed CdSe thin films.....	46
Figure 4.1: X-ray diffraction patterns of undoped CdSe thin films.....	49
Figure 4.2: XRD patterns of Ag doped CdSe thin films (a) Air annealed (b) Vacuum annealed.....	50
Figure 4.3: SEM micrographs of (a) Air annealed (b) Vacuum annealed undoped CdSe thin films.....	51
Figure 4.4: SEM micrographs of air annealed CdSe: Ag thin films.....	52
Figure 4.5: SEM micrographs of vacuum annealed CdSe: Ag thin films.....	52
Figure 4.6: Tauc's plot of undoped and CdSe: Ag thin films.....	53
Figure 4.7: Plot of $\ln(R)$ vs $1000/T, K^{-1}$ for undoped CdSe thin films.....	54
Figure 4.8: Plot of $\ln(R)$ vs $1000/T, K^{-1}$ for CdSe: Ag thin films with (a) 1%, (b) 3% and (c) 5% Ag.....	55
Figure 4.9: XRD spectra of CdSe and Bi doped CdSe thin films.....	57
Figure 4.10: FE-SEM micrographs of Bi doped CdSe thin films.....	58
Figure 4.11: (a) Tauc's plot and (b) transmittance spectra of CdSe and Bi (1%, 2%, 3%) doped CdSe thin films.....	58
Figure 4.12: Variation of $\ln R$ versus $1000/T, (K^{-1})$ for Bi doped CdSe thin films. ....	59

Figure 4.13: Photocurrent ( $\mu\text{A}$ ) v/s wavelength (nm) plot of 3% Bi doped CdSe thin films.....	60
Figure 4.14: X-Ray diffraction patterns of In doped CdSe thin films.....	61
Figure 4.15: FE-SEM micrographs of In doped CdSe thin films.....	62
Figure 4.16: a) Tauc's plot and b) Transmittance plot of In doped CdSe thin films.....	63
Figure 4.17: IV characteristics of In doped CdSe thin films.....	64
Figure 5.1: X-Ray diffraction patterns of $\text{Cd}_{(1-x)}\text{Zn}_x\text{Se}$ ( $x = 0 - 1$ ) thin films annealed for 1hr.....	68
Figure 5.2: X-Ray diffraction patterns of $\text{Cd}_{(1-x)}\text{Zn}_x\text{Se}$ ( $x = 0 - 1$ ) thin films annealed for 2 hr.....	69
Figure 5.3: Shift in the (002) peak for $\text{Cd}_{(1-x)}\text{Zn}_x\text{Se}$ ( $x = 0 - 1$ ) system.....	70
Figure 5.4: FE-SEM images of $\text{Cd}_{(1-x)}\text{Zn}_x\text{Se}$ thin films. a) CdSe, b) $\text{Cd}_{0.8}\text{Zn}_{0.2}\text{Se}$ , c) $\text{Cd}_{0.6}\text{Zn}_{0.4}\text{Se}$ d) $\text{Cd}_{0.4}\text{Zn}_{0.6}\text{Se}$ , e) $\text{Cd}_{0.2}\text{Zn}_{0.8}\text{Se}$ , f) ZnSe.....	71
Figure 5.5: Tauc's plot and transmittance spectra of $\text{Cd}_{(1-x)}\text{Zn}_x\text{Se}$ ( $x = 0.2 - 0.8$ ) films.....	72
Figure 5.6: Deposited $\text{Cd}_{(1-x)}\text{Zn}_x\text{Se}$ ( $x = 0-1$ ) thin films.....	72
Figure 5.7: Tauc's Plot of $\text{Cd}_{(1-x)}\text{Zn}_x\text{Se}$ thin films ( $x = 0 - 1$ ).....	73
Figure 5.8: Transmittance spectra of $\text{Cd}_{(1-x)}\text{Zn}_x\text{Se}$ ( $x = 0 - 1$ ) thin films.....	73
Figure 5.9: Variation of optical band gap v/s Zn concentration (at. %). ....	74
Figure 5.10: Variation of $\ln R$ vs $1000/T$ , ( $\text{K}^{-1}$ ) of $\text{Cd}_{(1-x)}\text{Zn}_x\text{Se}$ thin films....	75
Figure 5.11: X-ray diffraction of 120 min's annealed $\text{CdSe}_{(1-x)}\text{Te}_x$ ( $x = 0.2 - 0.8$ ) thin films.....	77

Figure 5.12: X-ray diffraction patterns of 150 min annealed CdSe <sub>(1-x)</sub> Te <sub>(x)</sub> (x = 0 - 1) thin films.....	78
Figure 5.13: Shift in the predominant peak of CdSe <sub>(1-x)</sub> Te <sub>(x)</sub> (x = 0-1) thin films.....	78
Figure 5.14: FE-SEM micrographs of 150 min annealed CdSe <sub>(1-x)</sub> Te <sub>(x)</sub> (x = 0-1) thin films.....	80
Figure 5.15: Tauc's plot of 150 min annealed CdSe <sub>(1-x)</sub> Te <sub>(x)</sub> (x = 0 - 1) thin films.....	81
Figure 5.16: Variation of band gap with Te concentration (at. %).....	82
Figure 6.1: Schematic representation of n-CdSe/p-Si heterojunction.....	86
Figure 6.2: (a) X-Ray diffraction pattern and (b) FE-SEM micrographs of CdSe thin film deposited on silicon wafer.....	86
Figure 6.3: Temperature-dependent I-V curves of.....	88
a) n-CdSe/p-Si,	
b) Ag doped n-CdSe/p-Si,	
c) Bi doped n-CdSe/p-Si,	
d) In doped n-CdSe/p-Si heterojunctions.	
Figure 6.4: Variation of ln (I) vs. V plot of .....	89
a) n-CdSe/p-Si,	
b) Ag doped n-CdSe/p-Si,	
c) Bi doped n-CdSe/p-Si,	
d) In doped n-CdSe/p-Si heterojunctions.	
Figure 6.5: Richardson's plot of .....	90
a) n-CdSe/p-Si,	

- b) Ag doped n-CdSe/p-Si,
- c) Bi doped n-CdSe/p-Si,
- d) In doped n-CdSe/p-Si heterojunctions.

Figure 6.6: $1/C^2$ vs. $V$ plot of n-CdSe/p-Si heterojunction.....	91
Figure 6.7: $1/C^2$ vs. $V$ plot of Bi doped CdSe/p-Si heterojunction.....	92
Figure 6.8: $1/C^2$ vs. $V$ plot of In doped CdSe/p-Si heterojunction.....	92
Figure 6.9: Band diagram of n-CdSe/p-Si heterojunction.....	93

## LIST OF TABLES

	<b>Page No.</b>
Table 1.1: Important properties of II-VI compounds.....	5
Table 3.1: XRD data of CdSe thin films deposited at different substrate temperature.....	39
Table 3.2: X-Ray diffraction and EDAX data for annealed CdSe thin films.....	43
Table 3.3: Optical band gap and activation energy data of annealed CdSe thin films.....	46
Table 4.1: XRD data of air annealed Undoped and Ag doped CdSe thin films.....	51
Table 4.2: XRD data of vacuum annealed undoped and Ag doped CdSe thin films.....	51
Table 4.3: Optical band gap of undoped and CdSe: Ag thin films.....	53
Table 4.4: Electrical conductivity data for undoped and CdSe: Ag thin films.....	54
Table 4.5: XRD data of undoped and Bi doped CdSe thin films.....	57
Table 4.6: Optical and electrical data of undoped and Bi doped CdSe thin films.....	59
Table 4.7: XRD and compositional data of In doped CdSe thin films.....	62
Table 4.8: Optical and electrical data of In doped CdSe thin films.....	63
Table 5.1: X-Ray diffraction data of Cd <sub>(1-x)</sub> Zn <sub>(x)</sub> Se (x = 0 - 1) evaporated thin films.....	70

Table 5.2: Compositional analysis of Cd <sub>(1-x)</sub> Zn <sub>(x)</sub> Se (x = 0 - 1) thin films.....	71
Table 5.3: Energy band gap and activation energy values of Cd <sub>(1-x)</sub> Zn <sub>(x)</sub> Se (x= 0 - 1).....	74
Table 5.4: Structural parameters of CdSe <sub>(1-x)</sub> Te <sub>(x)</sub> (x= 0 - 1) thin films.....	79
Table 5.5: Elemental analysis of CdSe <sub>(1-x)</sub> Te <sub>(x)</sub> (x = 0 - 1) thin films.....	81
Table 5.6: Optical band gap of CdSe <sub>(1-x)</sub> Te <sub>(x)</sub> (x= 0 - 1) thin films.....	82
Table 6.1: Structural and compositional data of CdSe thin films deposited on silicon wafer.....	87
Table 6.2: Rectification ratio of undoped and doped CdSe/p-Si heterojunctions.....	89
Table 6.3: Carrier concentration, barrier height, and ideality factor of n-CdSe/p-Si and doped n-CdSe/p-Si heterojunction.....	92



## NOMENCLATURE

### ABBREVIATIONS

Ag	Silver
Bi	Bismuth
Si	Silicon
Se	Selenium
Zn	Zinc
Te	Tellurium
CdSe	Cadmium selenide
ZnSe	Zinc selenide
CdTe	Cadmium telluride
CZS	$\text{Cd}_{(1-x)}\text{Zn}_{(x)}\text{Se}$
CST	$\text{CdSe}_{(1-x)}\text{Te}_{(x)}$
RF	Radio frequency
PVD	Physical vapour deposition
D C	Direct current
VPE	Vapour phase epitaxy
MBE	Molecular beam epitaxy
PLD	Pulsed laser deposition
TFT	Thin film transistor
XRD	X-ray diffractometer
FE-SEM	Field Emission Scanning Electron Microscope
EDAX	Energy dispersive analysis of X-rays
NIR	Near Infrared

Vis	Visible
UV	Ultra Violet
I-V	Current – Voltage
C-V	Capacitance- Voltage
C-F	Capacitance- Frequency
n-	n-type
p-	p-type
SCLC	Space Charge Limited Conduction
TED	Thermionic-emission diffusion model

### **SYMBOLS & UNITS**

eV	Electron volt
$\mu\text{m}$	micrometer
nm	nanometer
hr	hour
D	Crystallite size
a & c	lattice constants
d	Inter-planar distance
$2\theta$	Bragg angle
$\rho$	Resistivity
$\sigma$	Conductivity
n	Carrier concentration /cm <sup>3</sup>
R	Resistance
T	Temperature
E <sub>g</sub>	Energy band gap

$E_a$	Activation energy
at. %	Atomic percent
$h\nu$	Photon energy
$h$	Plank's constant
$k_b$	Boltzmann constant
$\text{\AA}$	Angstrom
$^{\circ}\text{C}$	Degree Celsius
$\alpha$	Alpha
A	Ampere
cm	Centimetre
$\mu$	micro
min	minute
$\lambda$	lambda
V	Volt
$\Omega$	Ohm
S	Siemen
s	second
T	Tesla
$\theta$	Theta
K	kelvin
$\epsilon_0$	Permittivity of Vacuum
$\epsilon_r$	Relative permittivity
$\nu$	Frequency
MHz	Mega Hertz

# CHAPTER 1

## GENERAL INTRODUCTION

### 1.1 INTRODUCTION

The thin film technology is a young and ever-growing field in the physical and chemical sciences which is a confluence of materials sciences, surface science, applied physics, applied chemistry and has become an identifiable unified discipline of scientific striving. It has their objectives in the provision for a scientific basis for the methods and materials used in thin film electronics. Thin film can be defined as thin material layer ranging from nm to  $\mu\text{m}$  of thickness (Chopra and Klerrer 1970). The main interest of thin films is due to some important properties that differ from those of the material in bulk. As the film becomes thinner, the surface properties become more important than the bulk.

In the thin films history, the scientific curiosity led to the development of two dimensional solid i.e. thin film physics. With the recent development of nano-science and nanotechnology attention has also been given to the attraction of nano-structured materials as well. Because of the huge surface-to-volume ratio of nano-particles and the high porosity of nano-particle layers and assemblies, a large number of analytic molecules can be absorbed by a nano-particle and within a nano-particle structure in a very short time. The material properties of thin films can be changed by changing the nano-particle size. At present the synthesis and characterization of nano-crystalline thin films have attracted great attention not only because of their exceptional properties but also due to their structural and temperature dependent properties along with great potential for many practical applications. The extensive use of nano-crystallite thin film devices contributed the development of nano-crystalline thin films technology. The scientific understanding about the dependence of films properties on various parameters resulted enormous number of successful application of nano-crystalline thin films in industrial, engineering, medical and other scientific purposes.

Optical and electrical properties of semiconducting films are essential requirements for proper applications in various optoelectronic devices. These properties

of the films are generally structure sensitive. The structural parameters such as lattice constant, grain size, etc. depend on the deposition conditions. CdSe is one of the prominent materials due to its near optimum direct energy gap and high absorption coefficient. It has become interesting because of its major contributions to new application in photo-electronic devices such as light emitting diodes, solar cells, photo-detectors, lasers and photo electrochemical cells, IR detector,  $\gamma$  detector and other optoelectronic devices. It is a well-known fact that the quality of the devices based on CdSe thin films strongly depends on the structural and electronic properties of the films obtained under various experimental conditions. A number of researchers have developed integrated circuits (IC) using polycrystalline CdSe thin films. Some other workers used CdSe thin films in gas and chemical sensors (Neudeck et al. 2002; Sen et al. 2008; Shalev et al. 2017; Singh et al. 2007; Yang et al. 2015). These technological advancements in thin films based on nano-science are expected to play increasingly important role in different area of technical fields.

Addition of impurities in the nanocrystals is another way of altering their band gap and other physical properties. The process called doping, is the intentional introduction of impurities into the semiconductor lattices. It is the primary means of controlling optical and electronic properties of bulk semiconductors. With the initiation of nanoscience and nanotechnology, doping of semiconductor or nanocrystals has also attracted a lot of recent attention from the scientific community, a significant effort has been made in experimental procedures to dope semiconductor nanocrystals by using different synthesis routes, feed, or processing conditions; however, in spite of this effort, the underlying doping mechanisms still remain indefinable. To realize technological applications based on nanocrystalline doped semiconductor materials, a fundamental phenomenon that determine their structure and properties is required. Understanding of fundamental properties will allow for the rational design and synthesis of new materials with precise control over their chemical, electrical, magnetic, mechanical, and optical properties.

An alloy is a mixture of metals or a mixture of a metal and semimetal element in a required composition. Alloys are used in a wide variety of applications. In some cases, a combination of elements may reduce the overall cost of the material due to important

properties. In other cases, the combination of elements imparts synergistic properties to the constituent metal elements such as corrosion resistance or mechanical strength. The possibility of tuning band gap and other properties by alloying would get material properties required for the device fabrication. The synthesis of ternary metal chalcogenides of group A<sub>II</sub>-B<sub>VI</sub> semiconductors in nanocrystalline form has been a rapidly growing area of research due to their important applications in wide spectrum of optoelectronic devices like lasers, photo-electrodes, light emitting diodes, sensors, transistors, radiation detectors (Benyettou et al. 2015; Fayek and El Sayed 2001; Krishnan 1992; Matsumura et al. 2002; Rennie et al. 1996). The abrupt growth of the world's energy demand from last several years has brought substantial consideration towards the energy scarcity problem. To accomplish this ever-increasing energy demand mankind has been focused towards emerging renewable energy sources such as solar, nuclear, wind, tidal energy etc. Among these solar energy is one of the best substitutes owing several rewards such as pollution free, abundantly available, inexhaustible and permanent source of energy. So, the nonstop conversion of solar energy into electrical energy is essential so as to accomplish the energy need of the present world (Chopra and Das 1983).

Most of the semiconductor devices contain at least one junction between p-type and n-type materials. These p-n junctions are fundamental to the performance of functions such as rectification, amplification, switching and other operations in the electronic circuits. For semiconductor device applications the difference in the energy band gap provides another degree of freedom that produces many interesting phenomena (Sze 1995). The successful applications of heterojunctions in various devices are due to the capability of epitaxy technology to grow lattice matched semiconductor materials on the top of the another with virtually no interface traps. Heterojunctions have been widely used in the various device applications (Streetman and Banerjee 2009). It is well known that photovoltaic devices are useful for solar energy conversion. These devices use p-n junction for direct conversion of solar energy into electrical energy. Due to simplicity in junction fabrication and inbuilt storage capacity, semiconductor/Si junction cells have attracted a great deal of interest over p-n junction solar cell (Raut et al. 2017). The physics of epitaxial heterojunction is matching of the lattice constant. This is physical requirement in atom placement. Large

lattice mismatch will cause dislocation at the interface and results in electrical defects such as interface traps. It turns out that if the lattice constants are not severely mismatched, good quality heteroepitaxy can still be grown, provided that the epitaxial layer thickness is small enough. The amount of lattice mismatch and the maximum allowed epitaxial layer are directly related. For a thick heteroepitaxy layer, dislocation at the interface are inevitable due to the physical mismatch of terminating bonds at the interface. If the heteroepitaxial layer is thin enough the layer can be physically strained (lattice constant becomes the same as the substrate). In addition to having different energy gaps, the electron affinities of these semiconductors are also different and need to be considered in device applications. This leads to different combination of  $E_C$  and  $E_V$  alignment at the interface. According to their band alignment heterojunctions can be classified into three groups

- a. Type I or straddling heterojunction
- b. Type II or staggered heterojunction
- c. Type III or broken- gap heterojunction.

In Type I heterojunction, one material has both lower  $E_C$  and higher  $E_V$ , naturally it must have smaller energy gap. In Type II heterojunction, the locations of lower  $E_C$  and higher  $E_V$  are displaced, so electrons being collected at lower  $E_C$  and holes being collected at higher  $E_V$  are confined in different spaces. A Type III heterojunction is a special case of Type II, but the  $E_C$  of one side is lower than the  $E_V$  of the other. The conduction band thus overlaps the valence band at the interface, hence the name broken gap. p-n junctions are of great importance both in modern electronics applications and in understanding semiconductor devices.

## **1.2 PROPERTIES OF CHALCOGENIDE COMPOUNDS**

Semiconducting thin films play a very important role in the research to the development of solar cells and many optoelectronic devices. Thin film devices are much useful in photovoltaic conversion in which the solar energy is converted into electrical energy. The study of semiconductor materials began in the early 19th century. Over the years, many semiconductors have been investigated. We see a group of compound semiconducting materials formed by combining elements of groups in the

periodic table such as III-V, II-VI, I-VII, II-V, V-VI, and IV-V compounds. Compound semiconductors which consist of various elements have a wide range of physical properties, which include band gap, crystal lattice structures, electron and hole mobility that can be used for many applications. The synthesis of binary metal chalcogenides of group II-VI (CdS, CdSe, ZnS, ZnSe, CdTe) in nanocrystalline form is a rapidly growing area of research due to their important nonlinear optical properties, luminescent properties, quantum size effect (Kois et al. 2013) and other important physical and chemical properties. In this group, cadmium selenide (CdSe), cadmium telluride (CdTe), zinc selenide (ZnSe) is widely used semiconductor whose band gap lies near the peak of the solar energy spectrum. Major attention has been given in recent years to investigate the structural, electrical and optical properties of these materials in thin film form, in order to improve the performance of the device and also for finding new applications (Tripathi et al. 2009). Cadmium selenide (CdSe) is of interest for its applications as high-efficiency thin film transistors, solar cells, photoconductors, photodetectors, gas sensors, photo-resistors.

**Table 1.1** Important properties of II-VI compounds.

<b>Molecular formula</b>	<b>CdSe</b>	<b>CdTe</b>	<b>ZnSe</b>
<b>Structure</b>	Wurtzite /Cubic	Cubic	Cubic
<b>Lattice parameter</b>	a = 4.31 Å, c = 7.02 Å / a = 6.062 Å	a = 4.30 Å	a = 5.66 Å
<b>Molar mass</b>	191.37 g/mol.	240.01 g/mol.	144.35 g/mol.
<b>Density</b>	5.82 g/cm <sup>3</sup>	5.85 g/cm <sup>3</sup>	5.27 g/cm <sup>3</sup>
<b>Melting point (K)</b>	1512	1365	1793
<b>Band gap (E<sub>g</sub>.)</b>	direct ~ 1.74 eV	direct ~ 1.54 eV	direct ~ 2.70 eV
<b>Conductivity(σ)</b>	n	n, p	n

To grow CdSe thin films various methods were employed by other researchers, such as thermal evaporation (Patel et al. 2009; Sarmah et al. 2008; Shreekanthan et al 2003), sputtering (Khalaf et al. 2016), electrodeposition (Chowdhury et al. 2012), spray pyrolysis (Yadav et al. 2010), chemical bath deposition (Kale and Lokhande 2000; Singh et al. 2011), SILAR (Pathan et al. 2003) etc. CdSe has found to form in both sphalerite (cubic, zinc blende) and also wurtzite (hexagonal) structure. Figure 1.1 shows



the crystal structure of CdSe. Although most of the researchers have reported hexagonal structure with the c axis oriented normal to the substrate surface (Yukselic et al. 2013). There are several studies indicating the cubic structure for the CdSe polycrystalline thin films. CdSe thin films with absorption edge at about 700 nm have a direct band gap of 1.74 eV.

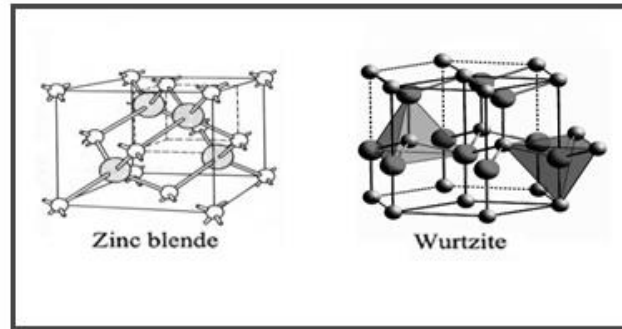


**Figure1.1** Crystal structure of CdSe

The conduction mechanism in compound thin film is mainly governed by the grain boundary defect. In pure compound films like CdSe the grain boundary contains a large number of defects due to dangling bonds (Al-Kabbi et al. 2013). The native defects of CdSe are excess cadmium and selenium vacancies. As a result of these defects CdSe often possesses n-type conductivity in bulk as well as in thin film, Selenium rich films might be expected to display p-type conduction. Those defects effectively act as either trapping or recombination centres and play an important role in the conduction processes. In these thin films concentration of native defects depends on film growth conditions.

### **1.3 LITERATURE SURVEY**

The II-VI semiconductors were grown in nanocrystalline thin film form by different growth processes are widely investigated due to their unique electronic, photo conducting properties, with a hope of exploring new potentialities for the fabrication of new scientific and technological devices. At present, a large number of scientists all over the world are very much concerned with the future prospect of utilizing solar energy in place of congenital fuel and electrical energy. As such thousands of researchers are studying different properties and aspects of photoconductivity material

in novel ways. As CdSe is regarded as a very prominent member of the II-IV group of semiconductor compounds, active research on this particular compound in both bulk and thin film form for intrinsic as well as an extrinsic category under different ambient conditions is going on. A significant amount of research has been conducted in the preparation and characterisation of semiconducting CdSe thin films. Among other high performance materials, cadmium selenide continues to attract attention as the material of choice for thin film applications. The brief literature survey is given below.

Arai et al. (1996) studied CdSe granular films prepared by a deposition method using a cluster beam, one can control easily the density of clusters on a substrate. One might expect such a granular film as a new type of materials with novel function. Such a material would also provide a suitable test to answer questions on how clusters interact with each other for the construction of their electronic states and for the redistribution of carriers. The surface states and connectivity of clusters can be controlled.

Rajendra et al. (2003) reported preparation of cadmium selenide thin films by thermal evaporation technique. They got homogeneous, stoichiometric thin films of cadmium selenide. The obtained films are found to be n-type with low resistance.

Cristian Baban et al. (2003) studied the influence of preparation conditions on the structure and optical properties of cadmium selenide (CdSe) thin films deposited by thermal evaporation under vacuum. The crystallite size increased when the substrate temperature and the temperature of the evaporation source are increased. Transmission spectra are observed to be strongly influenced by the deposition conditions.

Kale et al. (2004) reported the cadmium selenide nanocrystallites grown onto glass substrates from an aqueous alkaline medium, using chemical bath deposition method at room temperature. The grown films were nanocrystalline phase and air annealing increased the crystallinity of the CdSe films along with recrystallization process that changed nanocrystalline metastable cubic phase to stable hexagonal phase at the higher annealing temperature.

Saaminathan et al. (2005) studied cadmium selenide thin films prepared by pulse and pulse-reversal electroplating technique. They reported the effect of pulse and pulse

reversal plating on morphology of CdSe thin films. They showed improvement in the photoelectrochemical properties due to the effect of pulse reversal. Semiconductor parameters and the barrier height measurement have been tested for different conducting substrates. Titanium shows ohmic behavior and the other two substrates such as nickel and stainless steel act as rectifying contact for CdSe films. They reported preparations of the nanomaterials can be achievable by choosing the suitable duty cycle, ON time and OFF time with a period of micro/nanoseconds.

Nair et al. (1993) studied photosensitive properties of chemically deposited CdSe thin films. They discussed the improvement in photosensitivity of CdSe thin films on air annealing. Thickness of the films was maintained around  $0.5\mu\text{m}$ . Photosensitivity of thin films increased as the annealing temperature ( $200^{\circ}\text{C}$ ,  $300^{\circ}\text{C}$  and  $450^{\circ}\text{C}$ ) increases, but degradation in the photosensitivity was observed for the films which are air annealed beyond  $450^{\circ}\text{C}$ . The results are explained on the basis of improvement in crystallinity and increase in chemisorption of oxygen upon annealing the films in air.

Mahmoud et al. (2006) studied the effect of various growth parameters, like deposition rate and substrate temperature on the properties of CdSe thin films. The observed decrease in Hall coefficient and the resistivity with increased substrate temperature and deposition rate. The results show that the hall mobility decreases with increased substrate temperature, but increases with deposition rate. By this, it is concluded that grown CdSe films seem to be less sensitive to substrate temperature than the deposition rate.

Sarmah et al. (2008) studied effect of substrate temperature on the structural properties of CdSe thin films prepared by thermal evaporation. They observed improvement in crystallinity of the films with the increased thickness and also they reported, deposition temperature is the reason for the variation in lattice constants of the grown thin films over the bulk due to built-in strains present in the film grains. By this, they concluded that built-in microstrains and dislocation density of the deposited films are found to be dependent on the growth temperatures and the thickness of the films.

Murali et al. (2009) reported photoconductive properties of electron beam evaporated CdSe thin film. CdSe powder was synthesized in laboratory by chemical

method, used as source for the deposition of CdSe thin films. Grown films are polycrystalline hexagonal crystal structure. CdSe thin films with direct band gap of 1.65 eV was obtained.

Umme Farva et al. (2010) studied the CdSe nanocrystals of nearly equal to 3nm - 4 nm synthesized by hot injection method. They reported the effect of thermal annealing on the phase transformation and property of nanopowders. Annealing samples in a nitrogen atmosphere at 350<sup>0</sup>C resulted in the increased crystallinity of synthesized CdSe nanoparticles in hexagonal phase. They used annealed nanoparticles for the fabrication of bulk heterojunctions and hybrid solar cells showing improvement in the cell performances.

Shiyun Lou et al. (2011) reported the photoresponse properties of CdSe nanocrystalline films before and after annealing on ITO substrate. The photoresponse speed is improved after the annealing of the CdSe nanocrystal films due to lowering the height of the potential barriers existing between adjacent nanocrystals. There is an increase in the transport speed of photogenerated carriers. These investigations are helpful to improve the properties of photoelectrical devices.

Mahfoz Kotb et al. (2011) reported temperature dependence of D.C. conductivity of as-prepared and annealed CdSe thin films. The experimental results indicate that the electrical conduction taking place through the thermally activated process. They reported at higher temperatures, electrical conduction for the as-prepared film is taking place in the extended states while localized states conduction in the band tails is most likely to take place for annealed films.

Yukselici et al. (2013) reported growth of CdSe thin films on glass substrates by physical vapor deposition. They studied the optical and structural properties of grown CdSe thin films. The redshift in the asymptotic absorption edge with film thickness was related to an increase in the average size of grains grown during PVD process.

Kwang Heo et al. (2016) studied structural control of photoconductive CdSe nanowires through Bi assisted CVD process. Fabricated photodetectors and top-gated FET's based on CdSe NWs. CVD method opens wide range of possibility to exploit the precisely-controlled nanostructures for practical devices.

Kaur et al. (2016) reported thermally evaporated Sn doped CdSe thin films in argon environment. Doped films exhibit polycrystalline hexagonal crystal structure. A cubic phase of SnSe<sub>2</sub> forms as the annealing temperature increases beyond 363 K. The Urbach energy is calculated from the absorption coefficient and found to decrease with increasing annealing temperature, indicating a relaxation of distorted bonds and a decrease in the degree of disorder in the films.

Vanita et al. (2017) reported photoelectrochemical studies on electrodeposited indium doped CdSe thin films using aqueous bath. A band bending factor found to be enhanced from 0.31 to 0.49 after addition of indium. Red shifted and the enhanced spectral response observed with indium incorporation in CdSe thin films.

Subba Ramaiah et al. (2001) studied the Cu doped CdSe thin films and observed that p-doping is difficult to achieve with Cu acceptor levels in the thin films. Thin films deposited at a substrate temperature of 100<sup>0</sup>C developed crystallinity with pyramidal and conical shapes. The strong quantum confinement effect was observed in the small grain size of the films. XPS analysis strongly supported the structural analysis that the films exhibited only single phase. All the films exhibited p-type conductivity.

Perna et al. (2004) reported Zn doped CdSe thin films deposited using the pulsed laser ablation technique, starting from home-made doped CdSe pellet containing 1% Zn weight fraction. The structural quality of the CdSe: Zn films was lower than that of undoped CdSe, as shown by XRD and Raman spectra. Crystalline films were obtained in both cases with the (0 0 2) preferential orientation of the grains. The reflectivity and photoluminescence measurements of undoped CdSe are characterized by narrow excitonic features in the near band edge region, whereas the spectra of CdSe: Zn presented broader features due to optical transition involving the conduction and valence bands. The PL efficiency of CdSe: Zn persists up to room temperature, whereas that of undoped CdSe is scarcely visible for higher temperature.

Patil et al. (2016) synthesized and characterized Bi doped CdSe thin films by thermal evaporation method. They investigated the effect of different thickness and dopant concentration on the various properties of Bi doped CdSe thin films. XRD patterns confirm that the grown films are polycrystalline hexagonal crystal structure. Particle size varies from 10 nm to 13 nm. They got energy band gap in the range of 1.7

eV to 2.2 eV. They reported, Bi doped CdSe thin films can be used in development of efficient photovoltaic applications.

Abhijit et al. (2012) investigated Fe doped CdSe thin films prepared by simple and inexpensive computerized spray pyrolysis technique. Photo electrochemical characterization technique showed that the Fe doped CdSe thin films were highly photosensitive and more stable than undoped CdSe thin films.

Horak et al. (1982) reported carrier transport properties and plasma resonance of pure  $\text{Bi}_2\text{Se}_3$  and Cd doped  $\text{Bi}_2\text{Se}_3$  nanocrystals. Discussed point defects arising on introducing the impurities into the crystals. According to the results of spectral analysis the Zn atoms enter only the interstitial sites and behave as donors. Cadmium readily enters into the  $\text{Bi}_2\text{Se}_3$  lattice and forms substitutional defects, crystal formed are well cleavable and show a high degree of perfection.

Kriti Sharma et al. (2013) studied the indium-doped CdSe nanocrystalline thin films prepared by thermal evaporation using the Inert Gas Condensation method. The crystallinity of the films and the grain size decreases as the indium doping concentration increases. The results of photoluminescence measurements indicate that the photoluminescence intensity decreases as the indium doping concentration increases. The optical band gap values increase as the indium doping concentration increases. The dc electrical conductivity increases from undoped nanocrystalline CdSe to nanocrystalline CdSe:In 1% and decreases for nanocrystalline CdSe:In 5%.

Gupta et al. (1995) studies the optical properties of  $\text{Zn}_{(x)}\text{Cd}_{(1-x)}\text{Se}$  thin films. These films were deposited by the hot wall evaporation technique onto glass substrates. The optical band gap and effective mass of electron showed bowing effect, with bowing parameters which indicated good agreement with each other.

Arshad Mahmood et al. (2011) reported the ellipsometric analysis of  $\text{Cd}_{(1-x)}\text{Zn}_{(x)}\text{Se}$  thin films prepared by thermal evaporation technique. Thin films of CdZnSe with different composition ( $x=0, 0.2, 0.4, 0.6$  and  $0.8$ ) were deposited onto a glass substrate. The band gap increases with increasing Zn content in the films. The band gap of alloyed films engineered from 1.89 eV to 2.49eV.

Shinde et al. (2014) reported preparation and properties of flower like CdSe<sub>0.6</sub>Te<sub>0.4</sub> thin films. These films were deposited onto a well cleaned glass and FTO by Chemical bath deposition method was used. XRD patterns indicates these films are polycrystalline hexagonal crystal structure. The optical absorption study showed that the energy band gap of 1.61 eV.

Husain et al. (2003) reported optical, electrical and structural properties of Cd<sub>(1-x)</sub>Zn<sub>(x)</sub>Se sintered thin films for photovoltaic applications. All the thin films are polycrystalline cubic zinc blend structure. The band gap engineered from 1.69 eV to 2.58 eV by varying x from 0 – 1. The dark conductivity decreases from 3.55 x 10<sup>-6</sup> to 0.41 x 10<sup>-6</sup> /Ωcm.

Muthukumarasamy et al. (2007) investigated the structural phase transition in hot wall deposited CdSeTe thin films. The structural characterization of these films revealed that low proportion of CdSe in pseudobinary resulted in films with zinc-blende structure and a high proportion of CdSe gives rise to films with hexagonal crystal structure. For films with x= 0.4 and x= 0.6 both phases were found to be present.

Zeng et al. (2015) reported thin film solar cell based on CdSe<sub>x</sub>Te<sub>1-x</sub> nanocrystals and investigated the impact of composition on photovoltaic performances. The performance of the CdSe<sub>x</sub>Te<sub>1-x</sub> NC solar cells is influenced by charge generation, transport and injection comprehensively, however the photovoltaic performance is mainly determined by the electron injection. The better electron injection, the higher the photovoltaic performance. Finally, the performance is well improved by mixing CdSe<sub>x</sub>Te<sub>1-x</sub> NCs with conjugated polymer PPV and PCE of 3.35% is achieved.

Alam et al. (2013) fabricated CdTe/CdSe heterojunction solar cell structure using a simple, easy and low-cost electrodeposition method. CdSe layers have been grown by electrodeposition method and deposited layers showed n-type conductivity, high transmittance and low absorbance in the infrared region, crack-free surface with spherical grains. CdTe layers have been grown by electrodeposition method and deposited layers showed p-type conductivity, crack-free surface with granular shaped grains. After getting the good quality CdSe and CdTe layers, a fabrication of CdTe/CdSe heterojunction solar cell structure has been performed. I–V behavior of the metal contacts on CdTe films in dark condition showed anticipated rectifying behavior

indicating a diode character. Current vs. voltage measurements confirmed the ability to deposit a p–n junction by electrodepositing a CdTe thin film on a previously electrodeposited n-type CdSe film.

Athanassopoulou et al. (2012) reported the preparation and characterization of electrolytic deposition of CdSe on Ni substrates from CdSO<sub>4</sub> solutions containing excessive Cd<sup>2+</sup> and small amounts of SeO<sub>2</sub>. Rectification is not encountered for the as-deposited films formed under lower bath solution temperatures in which case ohmic characteristics are observed across the metal-semiconductor interface. After annealing in nitrogen gas, the overall electrical conductivity of the CdSe is increased by four orders of magnitude. They reported, change in conductivity may only by carrier doping and not for variation in carrier mobility. The showed rectification properties exhibited by I–V characteristics of Au/CdSe/Ni structures, it may possibly be utilized for photovoltaic conversion.

Krishna Kanta Haldar et al. (2014) studied the metal-semiconductor hetero-structures Au/CdSe tetrapod hetero-structures by using high-resolution transmission electron microscope, high angle annular dark field scanning transmission electron microscopic, and X-ray diffraction. The blue shifting of the plasmonic band and red shifting of the exciton band suggest a strong surface plasmon-exciton interaction between Au and CdSe in Au/CdSe tetrapod heterostructure. A significant photoluminescence quenching (83.4%) of CdSe nano-rod (NR) is observed in Au/CdSe tetrapod heterostructure. The radiative and non-radiative decay rates of CdSe nano rods are found to be modified in Au/CdSe tetrapod structures and the non-radiative rate changes from CdSe nanorods to Au/CdSe tetrapod structure. Current-voltage characteristics of Au/CdSe heterostructure exhibit the rectification property with a threshold voltage which can open up avenues for developing challenging devices.

Lingzhi Du et al. (2012) studied high-quality n-type CdSe nanobelts synthesized via chemical vapor deposition method in a Cd-enriched atmosphere. The electrical transfer properties and photovoltaic effect of CdSe nanobelts were studied by constructing nano FET and heterojunction device. The nano FETs have confirmed the n-type conductivity of CdSe nanobelts. The heterojunction exhibits an excellent rectifying behavior in the dark and also photovoltaic behavior.



Chen et al. (2003) studied MBE grown CdSeTe/Si composite substrate for low-wavelength IR HgCdTe application. The results indicate that the quality of films decreases as the alloy composition increases, which is possibly due to an alloy disordering effect. CdSeTe thin films with 4% Se incorporated exhibits excellent surface morphology low surface defects density.

Al-Kotb et al. (2013) investigated the CdSe films grown on a p-Si (100) by thermal evaporation technique. They reported the structural characteristics of CdSe films grown on silicon wafer, exhibits hexagonal phase with highly intensive peak of (002) plane. There is no effect of silicon orientation on both phase and crystalline qualities. The temperature dependent forward-bias I–V characteristics of the Au/CdSe/p-Si/Al heterostructure revealed the variation in barrier heights with a double Gaussian distribution. They explained the temperature dependence of ideality factor and barrier heights. They reported space-charge regions in diodes originate from traps in the band gap induced by structural defects presented in CdSe thin films.

Nawfal et al. (2012) studied growth of CdSe thin films using chemical bath deposition method at the different deposition temperature. They reported increase in the band gap of prepared films with increased deposition temperature, due to increase in the deposition rate and decrease in grain size. They observed decrease in optical band gap after annealing. CdSe/p-Si device was fabricated by depositing CdSe thin film on p-Si substrates shows diode characteristic.

## **1.4 SCOPE AND OBJECTIVES OF THE PRESENT WORK**

### **i. Scope of the present work**

CdSe is a binary semiconductor and is considered as a prominent member of the II-VI group due to its potential technological importance. Because of its high photosensitive nature and the suitable intrinsic band gap of 1.74eV, it is widely used in the fabrication of various optoelectronic devices. Structural, optical and electrical properties of semiconducting films are essential requirements for proper application in different thin film based optoelectronic devices and these properties are very sensitive to deposition conditions. Therefore, the study of such properties of the thin films with

respect to their different growing techniques as well as the growth conditions is a matter of great importance.

CdSe is basically n-type material in bulk as well as in thin film form having a high resistance. The present work is focused on increasing the n-type conductivity by doping it with suitable elements. Preparation of ternary compounds in stoichiometric form is another big challenge in thermal evaporation due to difference in the melting point and vapor pressure of the individual elements. The ternary compound thin layers with different composition are important for the solar cells and other optoelectronic device applications. Band edges of binary metal chalcogenides (CdSe, ZnSe and CdTe) can be tailored by alloying to give wide range of band gap values. Fabrication of heterojunctions with binary/ternary compound semiconductors with less interfacial traps and evaluation of these heterojunctions will be helpful for various device applications. The rectification ratio, barrier height and ideality factor are the most important characteristics of heterojunctions, which decide the device quality. The enormous gap between the potential of solar energy and its present utility is due to the modest energy density of the radiation, low conversion efficiencies of photovoltaic cell and cost of materials.

It is also to be mentioned that sufficient technical data on the properties of undoped and doped CdSe thin films are not available for a comprehensive database. So motivation behind the proposed work is to supplement more relevant data on some of the important optoelectronic properties of undoped CdSe, doped CdSe and alloyed CdSe thin films.

### **Objectives:**

- Preparation of Stoichiometric CdSe thin films and characterization.
- Optimization of the growth condition to obtain less resistive CdSe thin films.
- Doping of cadmium selenide thin films with other group elements.
- Study of structural, optical and electrical properties of the undoped and doped CdSe thin films.

- Study of the effect of annealing time and temperature on the structural, optical and electrical properties of the undoped CdSe and doped CdSe thin films.
- Preparation and characterization of  $\text{Cd}_{(1-x)}\text{Zn}_{(x)}\text{Se}$  and  $\text{CdSe}_{(1-x)}\text{Te}_{(x)}$  thin films and to examine the variation of energy band gap as a function of zinc and tellurium concentration in the ternary compounds so formed.
- Study of hetero-junctions of undoped and doped CdSe with silicon.

## CHAPTER 2

### EXPERIMENTAL AND CHARACTERIZATION TECHNIQUES

#### *Overview*

In this chapter details of thin film preparation methods and characterization of prepared thin film samples using different experimental techniques to study the structural, morphological, optical and electrical properties have been discussed.

#### 2.1 SAMPLE PREPARATION TECHNIQUES

Thin film semiconductor science is the developing field and studies on thin film semiconductor are pretty interesting. The several methods have been used to grow semiconducting thin films. The essential properties can be obtained by selecting proper method and deposition parameters. Thin film preparation methods can be broadly classified into two main categories such as physical and chemical methods. Physical vapor deposition is a technique where physical processes like evaporation, sublimation or ionic impingement on the substrate. Physical vapor deposition is the most common technique used for deposition of metal, alloys and many compound films. Under physical methods, thermal evaporation, pulsed laser ablation, sputtering and molecular beam epitaxy. Under chemical methods, spray pyrolysis technique, electrodeposition, chemical bath deposition (CBD), modified chemical bath deposition (M-CBD), electroless deposition, anodization, chemical vapor deposition (CVD), metal organo-chemical vapor deposition (MOCVD), Plasma enhanced chemical vapor deposition (PECVD).

The deposition process of thin film should meet some functional criteria like

- (a) Capability of depositing any material (metals, compounds, alloys),
- (b) Ability to form amorphous or crystalline films,
- (c) Stoichiometry should retain in the compounds (binary/ternary),
- (d) Reliable adhesion to different substrates (conducting/non-conducting), inconsistency of residual stress and defects,
- (e) Ability to deposit over a wide range of deposition parameters,

- (f) Ability to control the structural parameters like residual stress,
- (g) Dislocation density,
- (h) Capability to control deposition parameters such as deposition temperature, deposition rate, thickness etc.

The below sub-sections deal with the brief description of some of the typical physical and chemical methods which are commonly used to grow polycrystalline and epitaxial thin films of metal chalcogenides.

### **2.1.1 Physical methods**

#### **i. Thermal evaporation:**

Thermal evaporation is one of the most well-known physical vapor deposition (PVD) technique. It is a simple technique, one can evaporate a variety of materials like metals, semiconductors, dielectrics on the suitable substrates. Deposition of films by condensation from the vapor phase is commonly called physical vapor deposition (PVD). The preparation of thin films with controlled parameters requires an operating environment which does not disturb the process of thin film formation. A number of research works have been done for the attainment of high vacuum ( $10^{-6}$  torr) to reduce the interaction between residual gases and the surface of the growing film. There are several factors which are considered to build high vacuum systems, such as the cost of working, cost of installation and cost of maintenance. Figure 2.1 shows the schematic diagram of thermal evaporation system; it can be seen that a pumping system comprising a diffusion pump backed by an oil-sealed rotary pump.

The pressure at different stages was measured using cold cathode ionization gauges (Pirani gauge (GH1, GH2)- $10^{-3}$  Torr, Penning gauge-  $10^{-6}$  Torr). Such a system which is capable of maintaining a residual pressure in the order of  $10^{-6}$  Torr is used in the present study (Figure 2.2). In thermal evaporation system, the material is created in a vapor form by means of resistive heating. During heating some surface atoms acquire thermal energy sufficient to break bonds with other surface atoms then they leave the surface as vapor. The vapor atoms thus created are transported through the vacuum to get deposit on the substrate. The ambient is the vacuum otherwise, there will be a scattering of vapor atoms due to a collision between vapor atoms and gas atoms.

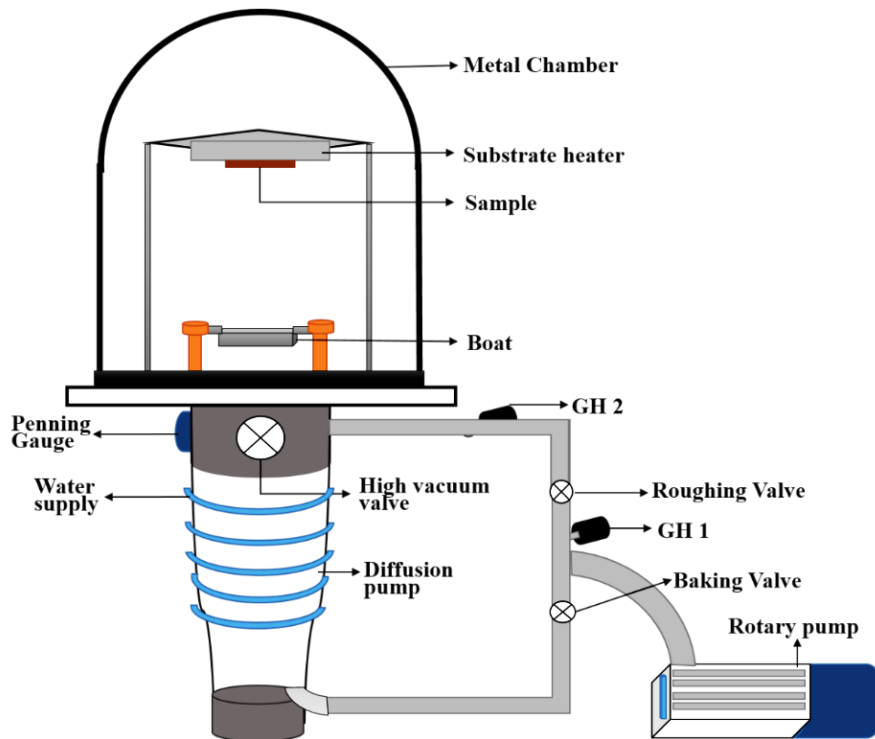


**Figure 2.1** Schematic diagram of thermal evaporation system.

Primarily residual gas molecules are present in the system because of desorption from the surface inside the vacuum system, liberation from the vacuum system and backstreaming from the pumps. Only at the pressure  $\leq 10^{-5}$  Torr, the vapor beams will arrive at substrate because of the larger mean free path between the collisions. The evaporant material taken in the boat which is heated to a sufficiently high temperature to produce desired vapor pressure ( $\geq 10^{-2}$  Torr). In case of most of the materials, this temperature is in the range of  $1000^{\circ}\text{C}$  to  $2000^{\circ}\text{C}$ . The temperature requirement for the source (boat) is that it should not react with the evaporant and it should have negligible vapor pressure ( $10^{-2}$  Torr) at the deposition temperature. The shape of the source should have a capability of holding the evaporant material in any form (powder or wire). A variety of source is used to evaporate materials, depending on whether the evaporant material is available in foil, wire, ingot or powder form. The materials used for sources are tantalum (Ta), molybdenum (Mo) and tungsten (W).



**Figure 2.2** Photograph of thermal evaporation system used to prepare CdSe thin films.

ii. Laser ablation or pulsed laser deposition:

Pulsed laser deposition (PLD) is an improved thermal process used for the deposition of compounds with a controlled elemental composition. In laser deposition, a high-power pulsed laser (1 J/shot) is irradiated onto the target of source materials through a quartz window. A quartz lens is used to increase the energy density of the laser power on the target source. Atoms that are evaporated from the surface are collected on substrate surfaces to form thin films. The target material is heated to its melting point. Pulsed laser deposition includes thermal process and the plasma process. Optimization of deposition parameters like as vacuum level, background oxygen pressure, the distance between target and substrate, ablation energy and substrate temperature one can obtain a desired deposition rate and structural quality. The advantage of PLD technique is direct monitoring of *cell-by-cell* growth by reflective high-energy electron diffraction (RHEED) pattern. The major disadvantage of this excellent technique is the limited area of uniform deposition and ejection of the particle from the source target.

### iii. Molecular Beam Epitaxy (MBE):

Molecular beam epitaxy (MBE) is an evaporative method. This growth technique is mainly for research purposes; this technique provides thin film materials of amazingly good quality. In this technique, the growth rate is very low compared to other methods, which makes it of restricted use for production of devices. In MBE, the deposition of a thin film can be accurately controlled at the atomic level in an ultra-high vacuum ( $10^{-10}$  Torr). A substrate which is placed in the ultra-high vacuum chamber was sputtered with a low energy ion beam to remove surface contamination. This step is followed by a high temperature anneal to avoid damage on the growth surface during preparation. The substrate is then cooled to the growth temperature nearly  $500^{\circ}$  C and growth commences by directing atomic beams of the material selected for deposition, toward the surface of the substrate. The beams are emitted from crucibles which have been heated to melting temperatures well above the substrate temperature to induce evaporation and condensation. The elemental composition of the films can be chosen by accurate control of the atomic ratio of each metallic electron beam sources.

### iv. Sputtering

Sputtering involves knocking an atom or molecule out of a target material by accelerated ions from an excited plasma and condensing it on the substrate either in its original or in a modified form. The ejection of an atom is due to bombardment by positive ions, the process is known as cathodic sputtering. The ejection of atoms from the cathode surface by impinging of energetic positive ions of noble gases of high purity (Ar, He etc.) at a reduced pressure under a high dc voltage gives rise to the sputtering phenomenon. If there is no involvement of any chemical reaction between the bombarding gas ions and the cathode is known as “physical sputtering”. The deposition of a thin film by sputtering includes several aspects such as glow discharge pressure, the shape of the electrode, current, and voltage. There are numerous sputtering options such as A.C. asymmetric bias sputtering, D.C. bias sputtering, diode sputtering, reactive sputtering, ion plating, getter sputtering. All these above sputtering options yield useful sputtering rates only in the pressure ranging from 20 to  $100^{-3}$  Torr. The density of bombarding ions decreases at lower pressure reduces the sputtering yield.



### 2.1.2 Chemical methods

In chemical deposition method, thin films are deposited on the substrate from aqueous solution either by passing a current or by a chemical reaction under appropriate conditions. Large or small and uniform or non-uniform surfaces of all types, conducting or insulating can be coated with relative ease by this cost-effective method. The electrodeposition, spray pyrolysis, closed space sublimation (CSS), anodization, solution growth, screen printing etc. are different chemical deposition techniques normally used for the deposition of thin films.

#### i. Chemical vapor deposition

Chemical Vapor Deposition is a chemical process used to prepare high-purity and high-performance semiconductor thin films. In Chemical Vapor Deposition (CVD), the vaporized precursors are introduced into a CVD reactor and absorbed onto a substrate held at higher temperature, these adsorbed molecules will either thermally decompose or react with other gases/vapors to form crystals. The CVD process consists of three steps: (a) mass transport of reactants to the growth surface through a boundary layer by diffusion, (b) chemical reactions on the growth surface, and (c) removal of the gas-phase reaction byproducts from the growth surface. Nucleation in the gas phase is homogeneous, whereas nucleation on the substrate is heterogeneous. Catalysts, usually transition metal particles such as Fe, Ni, and Co are also used in the CVD process. For example, strain-growth is used to produce nanoparticles in the CVD process.

#### ii. Spray pyrolysis

Spray pyrolysis is a useful and active technique to deposit metal oxide thin films. It is an attractive method to prepare a wide variety of thin film materials for large industrial applications. By using this technique metal oxides, chalcogenides and even metal thin films can be deposited. Morphology of the films can be controlled by Spray Pyrolysis. The quality and properties of the thin films depend largely on the growth parameters. The most important parameter is the substrate temperature. The higher the substrate temperature, the rougher and more porous are the deposited films. If the temperatures are too low the resulting films are cracked. Optimizing the substrate temperature can lead to getting dense smooth films. The crystallinity, texture and other

physical properties of the deposited films mainly depend on deposition temperature. The precursor solution is the other important spray parameter which affects the surface topography and the properties of the deposited films. In addition, the film morphology and properties can be drastically changed by using various additives in the precursor solution. It is also called as modified CVD process occurs in film formation close to the surface of the substrate.

By looking into different methods, each method has its advantages and disadvantages. Since thermal evaporation is one of the best methods, met all most all the above-mentioned criteria. The simplicity and wide usage of vacuum evaporation to obtain materials of desired qualities, particularly for the preparation of ternary compounds and fabrication of devices on silicon substrates, are some advantageous attributes of thermal evaporation method.

## **2.2 THICKNESS MEASUREMENT METHODS.**

The effect of film thickness on the properties of thin films is quite influential. If the thickness of the film and deposition parameters are kept constant, one can achieve reproducible properties. Film thickness can be measured in two ways either by monitoring the rate of deposition while depositing or after the film deposition. There are several methods to determine the thickness of the films, such as (a) Multiple beam Fizeau fringes method, (b) Reflectance spectroscopy, (c) Gravimetric method.

### **i. Multiple beam Fizeau fringes method**

This method was developed by Tolansky in 1950, requires a sharp step in the film down to the substrate plane which can be made either by using a mechanical mask during deposition or by etching the film after deposition. Both the film and substrate surface must be highly reflective. This is accomplished by evaporating a metal such as silver or aluminum over both film and substrate. Interference fringes are generated by placing a reflective, but semitransparent, optically flat reference plate very close to the step region. At small distance between the two plates, multiple beam interference fringes appear with a spacing  $x$ . In the region of sharp step, fringes are shifted by a distance  $\Delta x$ . The thickness  $t$  of the film is then given by,

$$t = \left(\frac{\Delta x}{x}\right) \frac{\lambda}{2} \quad (2.2.1)$$

where ‘ $\lambda$ ’ is the wavelength of the light.

ii. Reflectance spectroscopy

Reflectance spectroscopy can also be used to determine the thickness of the films. A reflectance spectrum of the film, obtained by plotting reflectance (R) as a function of wavelength ( $\lambda$ ), exhibits maxima at wavelength,

$$\lambda_{max} = \frac{2n_1 \cos(\theta')}{m} \quad (2.2.2)$$

Where  $n_1$ ,  $t$  is the refractive index and the thickness of the film respectively and  $\theta'$  is the angle between the reflected ray and the normal drawn to the plane of reflection at the film- substrate interface.  $m$  is an integer which can take value 1, 2, 3..... By subtracting the wavelength corresponding to two maxima an expression for thickness  $t$  of the film can be obtained as follows,

$$t = \frac{i\lambda_i\lambda_0}{2n_1(\lambda_i-\lambda_0)\cos(\theta')} \quad (2.2.3)$$

Where ‘ $i$ ’ is the number of complete cycles from ‘ $\lambda_0$ ’ to ‘ $\lambda_i$ ’. For two adjacent maxima or minima  $i = 1$  and for maxima and an adjacent minimum, or vice versa,  $i = 1/2$ . The angle  $\theta'$  is related to the incidence angle  $\theta$  by the relation,

$$2n_1 \cos(\theta') = 2\sqrt{[n_1^2 - n_0^2 \sin^2(\theta)]} \quad (2.2.4)$$

where  $n_0$  is the refractive index of the surrounding. In general, it is difficult to determine the wavelengths from reflectance vs wavelength ( $\lambda$ ) plots. However, reflectance vs.  $1/\lambda$  plots yield values which are easier to extract.

iii. Gravimetric method

In the present investigation, the gravimetric method was used to estimate the thickness of the deposited film. By gravimetric method thickness of the deposited film can be determined with the help of mass of the deposited layer ( $m$ ), the area of deposition ( $A$ ) and bulk density ( $\rho$ ) of the material is known. The mass of the deposited film can be determined by estimating the difference in mass between the bare substrate ( $m_1$ ) and the coated substrate ( $m_2$ ). Here the mass was measured using a high-resolution

microbalance (Sartorius). The thickness (t) of the film can be calculated from the following relation,

$$t = \frac{(m_2 - m_1)}{\rho A} \quad (2.2.4)$$

## 2.3 CHARACTERIZATION TECHNIQUES

CdSe, doped CdSe and ternary compound thin films were prepared using thermal evaporation, were characterized using various characterization techniques to evaluate structure, composition, optical and electrical properties. The brief details of the different characterization techniques and experimental procedures are given in the following sections.

### 2.3.1 Structural characterization

X-ray diffraction (XRD) studies were carried out to study the crystallographic aspects of the prepared thin films. Figure: 2.3 shows photograph of X-Ray diffractometer Rigaku (Model Miniflex600). Electrical and optical properties of the materials mainly depend on crystallographic nature of the films. In crystalline solids, atoms can be imagined to be orderly arranged in different set of equidistant parallel planes denoted by indices (h k l). When a beam of X-ray is allowed to pass through solid, diffraction takes place, when they satisfy Bragg's law. Diffraction analysis is useful whenever it is necessary to know the state of chemical combination of the elements involved or the particular phase in which they are present.



**Figure 2.3** X-Ray diffractometer Rigaku (Model Miniflex600).

Compared with ordinary chemical analysis, the diffraction method has the advantage that it is much faster, requires very small sample and is nondestructive. The basic law involved in the diffraction method of structural analysis is the Bragg's law. X-ray diffraction methods have strongly demonstrated the crystallinity of solids by exploiting the fact that the spacing between atoms is comparable to the wavelength of radiation. This results in easily detects by emitted beams of high intensity along certain directions when incident X-rays impinge at critical diffraction angles ( $\theta$ ). Then Bragg's law for X-ray diffraction is given by

$$2d \sin \theta = n\lambda \quad (2.3.1)$$

where 'n' is the order of diffraction, ' $\lambda$ ' is the wavelength of the X-rays, 'd' is the spacing between consecutive parallel planes and ' $\theta$ ' is the glancing angle. X-ray diffraction studies give a whole range of information about the crystal structure, orientation, average crystallite size and stress in the films. Experimentally obtained X-ray diffraction data of prepared sample are compared with the standard Powder Diffraction Files published by the Joint Council on Powder Diffraction Standards (JCPDS). This diffraction data is used to determine dimensions of the unit cell, crystal structure, standard deviation, and crystallinity. The average grain size of the film can be calculated using the Scherrer's formula

$$D = \frac{n\lambda}{\beta \cos\theta} \quad (2.3.2)$$

where 'D' is the average grain size, ' $\lambda$ ' is the wavelength of the X-ray and ' $\beta$ ' is the full width at half maximum intensity in radians. The lattice parameter 'a' and 'c' values for cubic and hexagonal crystallographic systems associated in the present investigation can be calculated from the following equations using the (h k l) values, where (h k l) is the Miller indices and the interplanar spacing (d) of individual peak in each diffraction patterns. For cubic system,

$$a = \frac{d}{\sqrt{(h^2+k^2+l^2)}} \quad (2.3.3)$$

for the hexagonal system,

$$\frac{1}{d^2} = \frac{4}{3} \frac{(h^2 + hk + k^2)}{(a^2)} + \frac{l^2}{c^2} \quad (2.3.4)$$

### 2.3.2 Surface morphology and compositional analysis

The surface morphology of the films was studied using scanning electron microscopy (FE-SEM). The uniformity of the thin film surface plays a significant role in determining the optical properties of thin films. When surface roughness increases, the films will be less transparent and the grain boundaries will affect the electrical properties of the thin film which depends on the growth technique and ambient growth conditions. A number of FE-SEM micrographs was taken at a different magnification at different spots to verify surface morphology and elemental composition, it remains the same throughout the deposited area of the grown samples.

#### (a) Field Emission- Scanning Electron Microscopy

Field Emission Scanning electron microscopy (FE-SEM) is one of the most widely used techniques for obtaining microstructural and surface features of thin films. FESEM is microscope that works with electrons instead of light. These electrons are liberated by a field emission source. The object is scanned by electrons according to a zig-zag pattern. Field emission scanning electron microscopy (FE-SEM) provides topographical and elemental information at magnifications of 10x to 300,000x, with the virtually unlimited depth of field. Applications of FE-SEM include semiconductor device cross-section analyses for gate widths, gate oxides, film thicknesses, and construction details, Advanced coating thickness and structure uniformity determination, small contamination geometry features and elemental composition information. In the present work, the surface morphology of the films was studied using Carl Zeiss model electron microscope operated at accelerating voltage of 5 kV (figure.2.4). Electrons are liberated from a field emission source and accelerated in a high electrical field gradient. Within the high vacuum column, these so-called primary electrons are focused and deflected by electronic lenses to produce a narrow scan beam that bombards the object. As a result, secondary electrons are emitted from each spot on the object. The angle and velocity of these secondary electrons related to the surface structure of the object. A detector catches the secondary electrons and produces an electronic signal. This signal is amplified and transformed to a video scan-image that

can be seen on a monitor it can be processed further. In order to avoid charging problems, a thin layer of 1.5 nm to 3 nm of gold or palladium is deposited on the specimen without altering the surface features.



**Figure 2.4** Field Emission Scanning Electron Microscopy (Carl Zeiss).

### **(b) Compositional analysis**

Energy dispersive X-ray analysis (EDAX) was used to estimate the elemental composition of the prepared thin films. EDAX analysis system works as an integrated feature of FE-SEM and cannot operate on its own without the latter. X rays are generated by the incident electrons within a volume similar to but rather larger than that for the backscattered electrons. Peak X-ray energies corresponding to the characteristics of the elements within that volume can be identified and the relative compositions of elements can be estimated. Thus the bulk composition of the sample and of the individual grains in a polycrystalline sample can be determined. The output of an EDAX analysis is an EDAX spectrum, which is a plot of how frequently an X-ray is received for each energy level. An EDAX spectrum normally displays peaks corresponding to the energy levels for which the most X-rays had been received. Figure 2.5 shows the EDAX spectra taken for CdSe thin film deposited at the optimized condition.

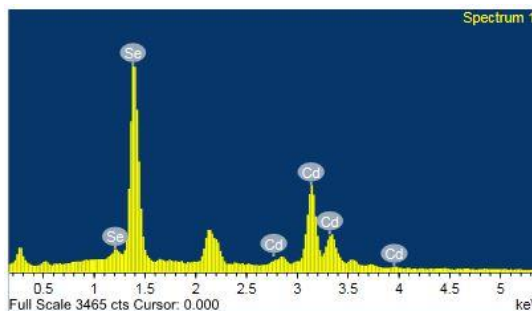


**Figure 2.5** EDAX spectra of stoichiometric CdSe thin film.

Each of these peaks is unique to an atom and therefore corresponds to a single element. The high intensive peak in a spectrum, the more concentrated the element is in the grown sample. An EDAX spectrum plot not only identifies the element corresponding to each of its peaks but the type of X-ray to which it corresponds as well.

### 2.3.3 Optical characterization

Optical characterization is one of the methods to explore the band structure of semiconductor under the illumination of light. A material under illumination, the incident light may get reflect, some part of the incident light may get absorb and some part may get transmitted through the sample. The amount of which reflection, absorption, and transmission depend on the band structure and energy of the incident light. The transmittance and absorption measurements reveal valuable information about the energy band gap ( $E_a$ ) and band structure of the semiconductor material. The result of band – band transition is fundamental absorption, remaining mechanisms are important if the energy of the incident light is less than the energy band gap of semiconductor material. Absorption due to the dopants occurs because of transition from donor levels to acceptor levels, these transitions generally results in the absorption in the far infrared region. Absorption may also occur due to the defects, impurities and grain boundaries etc. these introduce the localized energy levels in the band gap of the semiconductors. The intraband transition takes place in almost all the semiconductors due to the transition between the light hole and heavy hole bands in the valence band while free carrier absorption results from the transition to higher energy levels within the same energy band.

In the present investigation, optical absorption and transmission spectra of deposited thin films were obtained from UV-Vis-NIR spectrometer model 3600. UV-



Vis-NIR spectrophotometer consists of three detectors such as PMT (photomultiplier tube) for the ultraviolet and visible regions and an InGaAs detector and a cooled PbS detector for the near-infrared region. This spectrometer has high sensitivity across the entire measured wavelength range (300 nm to 3300 nm). The slit width of 1 nm and a scanning rate of 2 nm/min was fixed in the spectrophotometer. The glass substrates (which is used for deposition of thin films in the present case) are used as reference glass for the measurements. Tungsten halogen lamp (50 W) is used as an optical source with regulated power supply and control intensity of light. Photograph of the optical spectrophotometer is shown in figure 2.6.

The absorption coefficient can be deduced from the absorption or transmission spectra using the relation,

$$T = \frac{I}{I_0} = \exp(-\alpha t) \quad (2.3.5)$$

where 'I' is the transmitted intensity, 'I<sub>0</sub>' is the incident intensity of the light and 't' is the thickness of the film.



**Figure 2.6** UV-Vis-NIR Spectrophotometer (model: 3700/3700DUV)

In case of direct bandgap semiconductors is related to energy band gap by the equation

$$\alpha h\nu = B(h\nu - E_g)^n \quad (2.3.6)$$

where, n=1/2 for allowed direct transitions, n=2 for allowed indirect transitions, n=3 for forbidden indirect transitions and n=3/2 for forbidden direct transitions. 'B' is the parameter which depends on the transition probability. The plot of  $(\alpha h\nu)^2$  vs photon

energy ( $h\nu$ ) is called as Tauc's plot. In the case of direct transition,  $(\alpha h\nu)^2$  will show a linear dependence on the photon energy ( $h\nu$ ). A plot of  $(\alpha h\nu)^2$  against  $h\nu$  will be a straight line and the intercept on energy axis at  $(\alpha h\nu)^2$  equal to zero will give the bandgap energy ( $E_g$ ).

#### 2.3.4. Electrical characterization

The study of electrical properties of any semiconducting thin films is useful in the fabrication of various devices for different applications. The electrical properties of thin semiconducting films may depend on various factors like deposition method, thickness and homogeneity of the film, grain size, defect concentrations and elemental composition etc. The electrical resistance of thin films is mainly dependent on both geometry and structure of the solid thin film. Thin films deposited using vacuum deposition are usually polycrystalline in nature. In a thin film, a group of crystallites combined together by the grain boundaries generally treated as polycrystalline films. Electrical conductivity in this kind of films was controlled by grain boundaries. Grain boundaries regions are the highly disordered regions, characterized by the presence of defect states lead by non-stoichiometric thin films and incomplete atomic bonds. These defects in the thin films act as charge carrier traps and affect the electrical conductivity of the films. The overall conductivity of an intrinsic semiconductor is due to the combined effect of electrons and holes.

$$\sigma = en(\mu_n + \mu_p) \quad (2.3.7)$$

where 'n' indicates the density of electrons and holes in intrinsic semiconductors, ' $\mu_n$ ' is the mobility of electrons and ' $\mu_e$ ' is the mobility of holes. The mobility of holes and electrons is influenced by scattering in semiconductors, this is due to the phonons and ionized atoms. Defects in the semiconductor also contribute towards scattering but it is less compared to phonons. In this case, the relation will be

$$\sigma = \sigma_0 \exp\left(\frac{-E_g}{2k_b T}\right) \quad (2.3.8)$$

The resistivity ( $\rho$ ) of the films can be calculated applying Ohm's law, by the relation

$$\rho = \frac{RA}{L} \quad (2.3.9)$$

where 'R' is the resistance calculated from the slope of the current-voltage characteristic curves, 'A' is the area of the film deposited on the substrate and 'L' is the spacing between the electrodes. Semiconducting nature of films can be determined by using the following relation

$$R = R_0 \times \left( \frac{E_a}{k_b \times T} \right) \quad (2.3.10)$$

where 'R' is the resistance of the deposited film at ambient temperature 'T', 'R<sub>0</sub>' is constant, 'k<sub>b</sub>' is Boltzmann's constant and 'E<sub>a</sub>' is the activation energy. There are several methods to find the conductivity type of the films, most commonly used techniques are hall effect and hot probe methods, in the present investigation hot probe method was employed to determine the conductivity type of the deposited films. Highly conducting silver (Ag) was deposited on the thin film using thermal evaporation, as electrodes in a coplanar geometry with a 1mm gap (b/w the electrodes). The current-voltage (I-V) measurements were carried out using a Keithley source meter (Model SMU 2400). Temperature-dependent resistance measurement was carried out to estimate the activation energy (E<sub>a</sub>). The activation energy (E<sub>a</sub>) of charge carriers can be determined using the relation

$$E_a = \frac{2.303 \times k_b \times \text{slope}}{e} \quad (2.3.11)$$

where the slope was determined from the linear portion of the logarithmic resistance vs inverse temperature (1/T) plot.

The p-n junction theory serves as the foundation of the physics of semiconductor devices. The basic theory of current- voltage characteristics of p-n junction was established by Shockley. This theory was then extended by Sah, Noyce and Shockley and by Moll. The basic equations are used to develop the ideal static and dynamic characteristics of p-n junctions. Departures from the ideal characteristics due to generation and recombination in the depletion layer, to high injection and to series resistance effects are then discussed. Junction breakdown, especially that due to avalanche multiplication is considered in detail after which transient behavior and noise performance in p-n junctions are presented. Depending on the doping profile, device geometry and biasing condition a p-n junction can perform various terminal functions.

The thermionic conduction model was proposed by S.M. Sze and C.R. Crowell (1960, E.H. Rhoderick, Carlo Lamberti (2008). In the I–V analysis, according to the derivation of pure thermionic emission (TE) theory. According to this model the conduction occurs mainly due to thermionic emission and the forward current varies with the voltage according to following equation

$$I = I_s \exp\left(\frac{qV}{\eta kT}\right) \quad (2.3.12)$$

where ‘ $I_s$ ’ is the revers saturation current, ‘ $k$ ’ is the Boltzmann’s constant, ‘ $\eta$ ’ is the diode ideality factor, ‘ $T$ ’ is the temperature and ‘ $q$ ’ is the elementary charge. According to equation 2.3.12 the ideality factor should be unity. However, in applied cases, the diode current deviates from thermionic emission diffusion conduction mechanism at lower and high bias voltages. The deviation from the ideal nature can be attributed to the presence of defects and series resistance of diode. These factors contribute to different conduction mechanisms that are predominant at different bias levels. The series resistance arising from the bulk resistance of the semiconductors and metal-semiconductor interface affect the junction current and hence the device performance. Another factor affecting the device performance is the shunt resistance, which provides leaky paths for the charge carriers at reverse bias conditions and low forward bias. By considering the shunt resistance and series resistance equation (2.3.12) can be written as

$$I = I_0 \left\{ \exp\left[\frac{q(V-IR_s)}{nkT}\right] - 1 \right\} + \frac{V-IR_s}{R_{sh}} \quad (2.3.13)$$

where ‘ $R_s$ ’ is series resistance and ‘ $R_{sh}$ ’ is shunt resistance. The first term in above equation (2.3.13) corresponds to junction current and second term is shunt leakage current, which contributes to total current through the diode. Space charge limited conduction could be one of the possibilities. This linear variation in the current with square of the voltage implies that SCLC is the dominant conduction mechanism at higher voltages. The conduction through SCLC mechanism can be expressed by the equation

$$I = \left(\frac{AV^2 N_c \mu \epsilon_0 \epsilon_r}{8L^3 N_t}\right) \exp\left(\frac{-E_t}{kT}\right) \quad (2.3.14)$$

where ‘ $\epsilon_r$ ’ is the relative permittivity, ‘ $N_c$ ’ is the effective density of states, ‘ $N_t$ ’ is the concentration of the traps with activation energy ‘ $E_t$ ’, ‘ $L$ ’ is the thickness and ‘ $\mu$ ’ is

the hole mobility. The barrier height of the heterojunction can be determined by the equation for thermionic emission. In case of thermionic emission, saturation current ( $I_s$ ) is given as

$$I_s = AA^*T^2 \exp\left(\frac{-\phi_b}{kT}\right) \quad (2.3.15)$$

where ‘A’ is the area of the device, ‘A\*’ is the Richardson’s constant and ‘ $\phi_b$ ’ is the barrier height.

Capacitance – voltage (I-V) characteristics are useful for determining fundamental parameters in heterojunctions such as charge carrier concentration and barrier height. In revers bias condition, the variation of depletion region width of the heterojunctions and hence, variation of the junction capacitance with bias voltage can be approximated by

$$\frac{1}{C^2} = 2 \left[ \frac{(V - V_b + \frac{kT}{q})}{q\epsilon_0\epsilon_r NA^2} \right] \quad (2.3.16)$$

where ‘ $\epsilon_r$ ’ dielectric constant, ‘V’ is applied voltage, ‘ $V_b$ ’ is built in potential, ‘N’ is doping density and ‘A’ is the effective area of the diode. The junction capacitance at different bias voltages were measured by superimposing an ac supply of 50 mV modulation amplitude over dc bias voltage and frequency sweep from 20 Hz to 1 MHz.

In the present study characteristics of CdSe, (Ag, Bi and In) doped CdSe/p-Si heterojunctions were studied. Various diode parameters like ideality factor ( $\eta$ ), rectification ratio (RR), barrier height ( $\phi$ ) and interface state density was determined by temperature dependent current – voltage (I-V-T) and capacitance-voltage (C-V) characteristics. The heterojunction was evaluated by employing current-voltage measurements in dark using Keithley 2400 source meter. The conduction mechanism in heterojunctions can be explained by fitting it to suitable diode equations. In order to determine the barrier height at semiconductor interface, current - voltage was measured at different temperatures ranging from 303 K to 373 K in a step of 10 K. Barrier height at interfaces and the apparent carrier density in space charge region (SCR) were determined through capacitance-voltage (C-V) measurements. The junction capacitance measurements of heterojunctions were performed with an Agilent E4980A precision LCR meter at a frequency of 50 KHz with an oscillating voltage of 50 mV

superimposed on bias voltages. Bias voltage applied to the junction was varied from negative to positive depending on heterojunctions being studied.

### **2.3.5 Photoconductivity**

Photoconductivity is the process in which variation of electrical resistance or conductance of a material due to illumination. Photoconductivity is a powerful tool to understand the behavior of semiconductor thin solid films and it is also widely used to detect the presence of light and measure its intensity in light-sensitive devices. Some crystalline semiconductors like Si, Ge, CdSe, CdS and semimetal Se, are strongly photoconductive. Generally, semiconductors are fairly poor electrical conductors because they have only a less number of electrons that are free to move under a voltage. Semiconductors in bulk or in thin film form, with ohmic contacts deposited to ends, are used as a photoconductor. The photoconductivity process involves absorption of light, the excitation of charge carriers from their ground state to a higher state where they are free to contribute to the electrical conductivity and they return to their original state. The photoelectronic properties are mainly the electronic processes which are associated with photoconductivity mechanisms. The photoconduction in the semiconductor is generally explained to be due to increase in carrier concentration or mobility and lifetime of majority carriers. The basic principle involved in photoconductivity is that when photons of energy greater than that of the band gap of the semiconductors are incident on the semiconductor material, electrons and holes are generated resulting in the improvement of electrical conductivity. This phenomenon is called intrinsic photoconductivity. It is also possible to observe photoconductivity when the energy of the incident photon is less than that of the band gap. When the energy of the photon matches the ionization energy of the impurity atoms, they get ionized, creating extra carriers and hence an increase in conductivity can be observed. This phenomenon is called extrinsic photoconductivity. In a photo-conducting material, the photoexcited carriers to conductivity depend on the mobility and free lifetime.

The photoconductivity process includes the generation and recombination of charge carriers and their movement towards the electrodes. Photoconductivity is a complex process having several mechanisms like thermal and hot carrier relaxation process, charge carrier statistics, the effect of electrode and host recombination

mechanism. The study of photoconductivity process will be useful in understanding the physical properties of the semiconducting material and also offers many applications. A photon of energy greater than or equal to the band gap energy of a semiconductor material are incident on it, electrons and holes are generated in the conduction band and valence band respectively. This process will lead to increase in the conductivity of the semiconductor materials, denoted as intrinsic excitation. In case of doped materials, photoconductivity will take place even if the photon energy is less than the energy band gap. The energy of the incident photons equal to ionization energy of dopant impurities, they get ionized donating either hole to the valence band and electrons to the conduction band lead to increase the conductivity of the material. The sensitivity of any photoconductive material depends on the wavelength of the incident radiation. All photoconductivity measurements were carried out at room temperature. Current measurements are made with a Keithley 2400 source meter with an applied bias voltage of 5 V. Photocurrent of the samples were measured under the illumination of light of wavelength ranged from 300 nm to 1000 nm. The plot of relative response as a function of wavelength is called spectral response curve.

According to the model proposed by (R.L Petritz 1956) change in the conductivity ( $\Delta\sigma$ ) are the combined effect of a change in the carrier concentration and the effective carrier mobility ( $\mu^*$ ).

$$\Delta\sigma = q\mu^*\Delta\rho + q\rho\Delta\mu^* \quad (2.3.17)$$

Where  $\mu^*$  and  $\Delta\mu^*$  are

$$\mu^* = \mu \exp\left(\frac{-q\phi}{kT}\right) \quad (2.3.18)$$

$$\Delta\mu^* = -\frac{q\mu}{kT} \exp\left(\frac{-q\phi}{kT}\right) \Delta\phi \quad (2.3.19)$$

where ' $\phi$ ' is the barrier and ' $\phi\Delta$ ' is the change in the barrier height created due to the light.

## CHAPTER 3

### PREPARATION OF CdSe THIN FILMS.

#### *Overview*

This chapter represents preparation of CdSe thin films, effect of substrate temperature and annealing duration on the structural, electrical and optical properties of CdSe thin films grown by thermal evaporation technique.

#### 3.1 INTRODUCTION

Cadmium selenide (CdSe) is a prominent member of II–VI group. It has a direct band gap of 1.74 eV (Shyju et al. 2011) and often owns n-type conductivity in bulk as well as in thin film form. Due to its high photosensitive nature, it is widely used in the production of different optoelectronic devices such as photodetectors (Jin et al. 2012) (An et al. 2017), transistors (Van Calster et al. 1990), gamma ray detectors (Roth 1989) and PEC cells. To grow CdSe thin films various methods were employed by other researchers, such as thermal evaporation (Patel et al. 2009; Sarmah et al. 2008; Shreekanthan et al 2003), sputtering (Khalaf et al. 2016), electrodeposition (Chowdhury et al. 2012), spray pyrolysis (Yadav et al. 2010), chemical bath deposition (Kale and Lokhande 2000; Singh et al. 2011), SILAR (Pathan et al. 2003) etc. Thin films grown from bulk pure materials using various growth techniques usually contains defects. Defects such as traps, donors, acceptors, recombination centers, in the thin films can alter structural, optical, electrical properties and also the photoconductivity processes of the films. Ambient conditions and deposition techniques are the main things to achieve required electrical and optical properties of semiconducting thin films in appropriate devices for different applications. Properties of thin solid films such as physical, optical and electrical depend on deposition parameters. To attain desired properties of the material, deposition parameters like deposition rate, distance between source and substrate, substrate temperature and post-deposition heat treatment need to be optimized. In this study substrate temperature ( $T_s$ ) and annealing duration have been varied to get stoichiometric, less resistive CdSe thin films. The substrate temperature is one of the important factors which help to get stoichiometric crystalline films. Post



deposition heat treatment in a vacuum leads to stable good quality solid thin film. Therefore, the study of the influence of these parameters on the properties of thin films is a matter of great prominence.

### **3.2 EXPERIMENTAL DETAILS**

CdSe films have been grown by thermal evaporation technique under pressure less than  $10^{-5}$  Torr. The glass slides were used as substrates for deposition of CdSe thin films. The glass slides were cleaned with chromic acid, detergent, and acetone for removal of acidic, basic and organic impurities which adhere on the glass slides. Molybdenum boat was used to evaporate the CdSe powder of purity 99.995% (Alfa Aesar). The thickness of the films was measured by the gravimetric method and it was maintained at around 450 nm – 500 nm. The surface morphology and chemical composition of the grown thin films were analyzed using the scanning electron microscope (Carl Zeiss FE-SEM) with a linked Energy Dispersion X-ray (EDAX) detector, operating at an accelerating voltage of 5 KV. Structural studies of CdSe thin films were carried out with Rigaku Miniflex 600 X-ray diffractometer ( $\lambda = 1.54 \text{ \AA}$ ) in the  $2\theta$  range  $20^\circ - 60^\circ$ . The optical absorbance and transmittance spectra of prepared thin films were measured at room temperature in the spectral range 300 nm - 1200 nm using double beam spectrophotometer (Shimadzu 3600 UV–VIS-NIR). The thermal activation energy of CdSe thin films was determined from the logarithmic resistance vs inverse temperature plot. The resistance of CdSe films has been measured using the two-probe method in the temperature range of 300 K – 473 K, with silver (Ag) as a good ohmic contact.

### **3.3 OPTIMIZATION OF CdSe THIN FILMS**

#### **3.3.1 Effect of substrate temperature.**

CdSe thin films were grown at a substrate temperature ( $T_s$ ) of 303 K (room temperature) and another at 453 K by maintaining constant deposition rate and the distance between source to substrate. The X-Ray diffraction patterns of CdSe thin films deposited at 303 K and 453 K substrate temperature are shown in figure 3.1. XRD patterns of grown CdSe films exhibit polycrystalline hexagonal crystal structure. The XRD patterns of CdSe thin films deposited at 303 K and 453 K show a strong peak at

$2\theta = 25.31^\circ$  which is corresponding to (002) texture. Other small intensity peaks in XRD pattern of films deposited at 453 K located at  $45.6^\circ$  and  $49.5^\circ$  are corresponding to (103) and (112) respectively (Mahmoud et al. 2006).

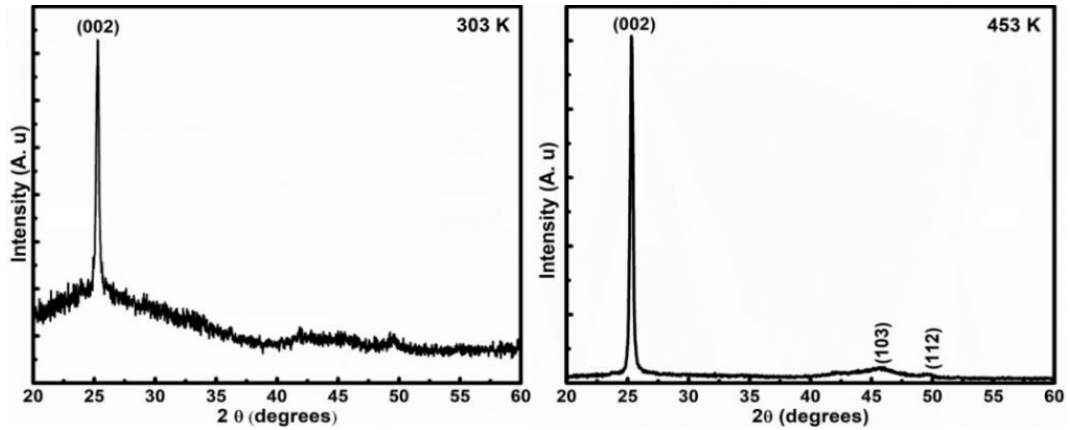


**Figure 3.1** XRD patterns of CdSe thin films deposited at different substrate temperature.

The average grain size was calculated using equation 2.3.2 shown in table 3.1. Lattice parameters were calculated using equation 2.3.3 and evaluated lattice parameters ‘a’ and ‘c’ are matching well with standard data [JCPDS card: 008-0459]. The grain size of deposited CdSe thin films increases from 21.60 nm to 26.85 nm as the substrate temperature increases from 303 K to 453 K.

**Table 3.1** XRD data of CdSe thin films deposited at different substrate temperature.

Substrate temp. (K)	Plane (hkl)	Inetr-planar spacing (d) Å	Grain size (D) nm	Atomic ratio Cd : Se
303	(002)	3.51	21.60	0.92
	(002)	3.51	26.85	0.97
453	(103)	1.98		
	(112)	1.83		

FE-SEM micrographs of CdSe thin films deposited at different substrate temperature are shown in figure 3.2. The surface morphology of deposited CdSe thin films shows a uniform distribution of grains throughout the deposited area. EDAX spectra of grown CdSe thin films shown in figure 3.3. reveals the presence of cadmium and selenium in both conditions. Films deposited at room temperature (303 K) are selenium-rich whereas films deposited at 453 K are near to stoichiometry (table. 3.1).

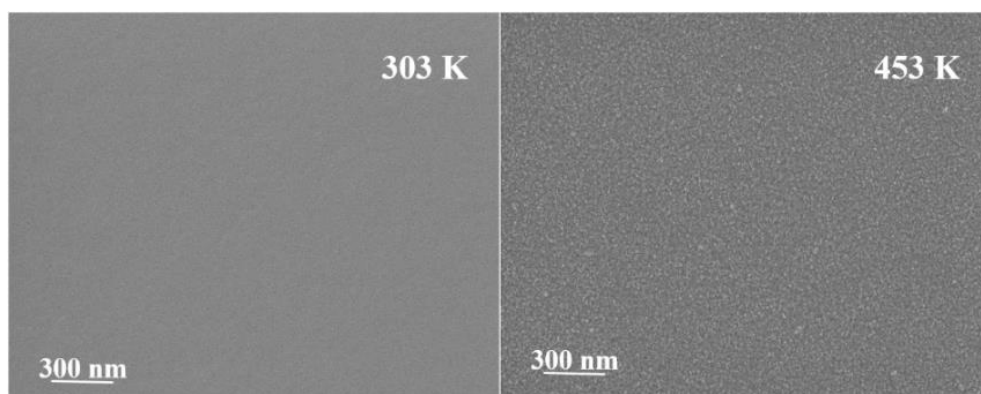


**Figure 3.2** FE-SEM micrographs of CdSe thin films deposited at different substrate temperature

The EDAX analysis of the undoped films revealed the dependence of the film composition on the annealing condition. This was expected in thermally evaporated compound materials. The vapor pressure and sticking coefficient of cadmium and selenium are different when CdSe powder is thermally evaporated, it dissociates into cadmium and selenium. Since cadmium and selenium have a different vapor pressure, varying amounts of cadmium and selenium reach the substrate where they recombine to form CdSe.

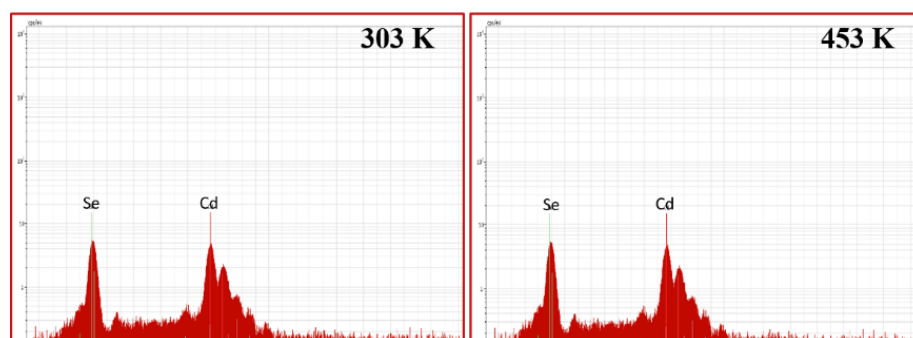


**Figure 3.3** EDAX spectra of CdSe thin films deposited at different substrate temperature.

The post deposition annealing of the films in vacuum also changed the film composition due to re-evaporation of excess selenium. The conductivity of the films depends on the composition of Cd: Se ratio. In the present work, the stoichiometric composition was achieved at a substrate temperature of about 453 K. Those deposited at suboptimum conditions were deficient or excess in any one of the elements.

The optical absorbance and transmittance measurements were carried out in the wavelength range from 300 nm – 1200 nm using UV-VIS-NIR-Spectrophotometer (Ali et al. 2013). Figure 3.4 shows the Tauc's plot of CdSe thin films deposited at a different substrate temperature ( $T_s$ ). The optical band gap energy ( $E_g$ ) of these films was determined with the help of absorption spectra using Tauc's relation. The Optical band gap ( $E_g$ ) was deduced by extrapolating the straight portion to energy axis and the energy value at  $\alpha = 0$ . provides the energy band gap ( $E_g$ ). The linear part in the plot describes the direct allowed transition and also the quality of deposited CdSe thin films. For direct allowed transition 'n' is taken as  $\frac{1}{2}$ . The energy bandgap of CdSe thin films deposited at 303 K and 453 K were found to be 2.02 eV and 1.89 eV respectively.

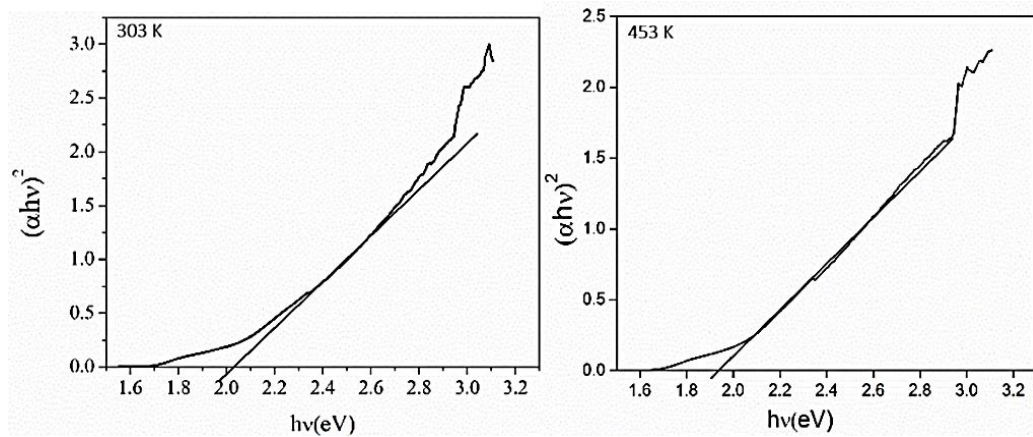


**Figure 3.4** Tauc's Plot of CdSe thin film deposited at different substrate temperature.

The electrical conductivity of CdSe films was measured by depositing silver on the top of the deposited CdSe film in a coplanar configuration. The conductivity of films deposited at both substrate temperatures ( $T_s$ ) is of the order of  $10^{-4}$  / $\Omega$ -cm. To measure the thermal activation energy of CdSe thin films, the resistance of the deposited films was measured in the ambient temperature ranging from 300 K - 473 K in hot air oven. It is observed that resistance of the films decreases as the temperature increases indicating semiconducting nature of deposited films. Figure 3.5 shows variation of  $\ln(R)$  v/s  $10^3/T$ , ( $K^{-1}$ ) plot. The thermal activation energy of the deposited CdSe films deposited at 303 K and 453 K determined using equation 2.3.11 was found to be 0.64 eV and 0.52 eV respectively. The conductivity of film deposited at 453 K shows a significant increase compared to the film deposited at 303 K. This increase in the conductivity may be due to increased grain size and reduced disorders in the film. It is

well known that the transportation of charge carriers in semiconducting thin films depends on the structural properties. The film deposited at 303 K is not stable mechanically as it peeled off from the substrate due to stress induced in the film.

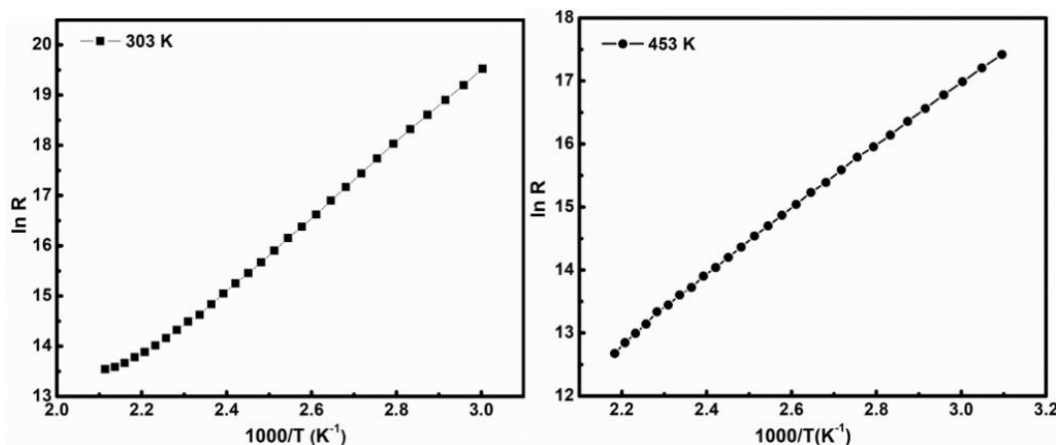


**Figure 3.5** Variation of  $\ln R$  with  $10^3/T$ , ( $K^{-1}$ ) of CdSe thin films deposited at a different substrate temperature ( $T_s$ ).

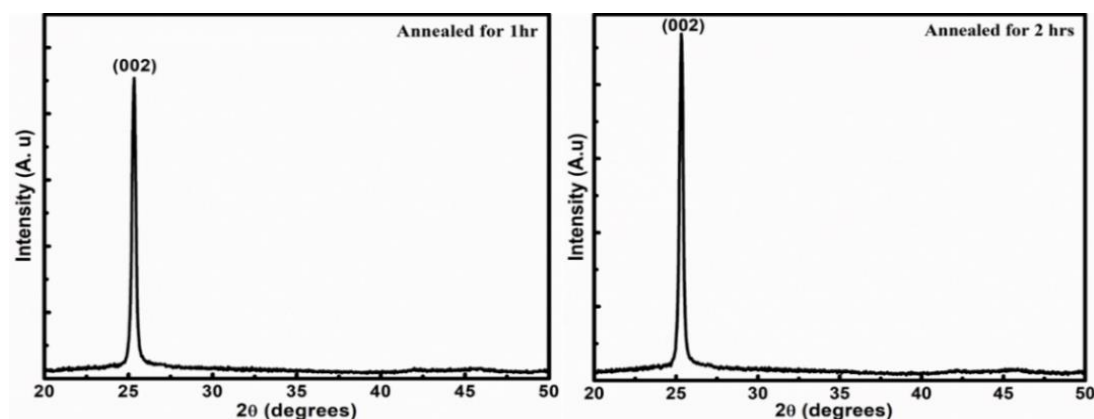
From the above results, it is observed that the CdSe film deposited at 453 K had improvement in mechanical stability, crystallinity, and low resistivity. Hence 453 K substrate temperature ( $T_s$ ) was maintained for further studies.

### 3.3.2 Effect of annealing duration

Since CdSe film grown at 453 K have a better structural and electrical properties, these films were annealed in vacuum immediately after the deposition at 453 K by varying the annealing duration. The effect of annealing time on the structural, morphological, optical, electrical and photoresponse properties has been studied.

Figure 3.6 shows the XRD patterns of annealed CdSe thin films, which are polycrystalline in nature and exhibit hexagonal crystal structure with a preferred orientation along (002) direction. The grain size in the films was evaluated using the well-known Scherrer's relation (2.3.2). As annealing time is increased, the (002) peak becomes narrower and the intensity increases. This indicates a marginal increase in the crystallite size with annealing time which is shown in table 3.2. An increase in the annealing time is expected to decrease the imperfections in the films leading to an improvement in the crystallinity. The structural parameters were calculated from the XRD patterns. Calculated d-spacing and lattice constants are matched well with

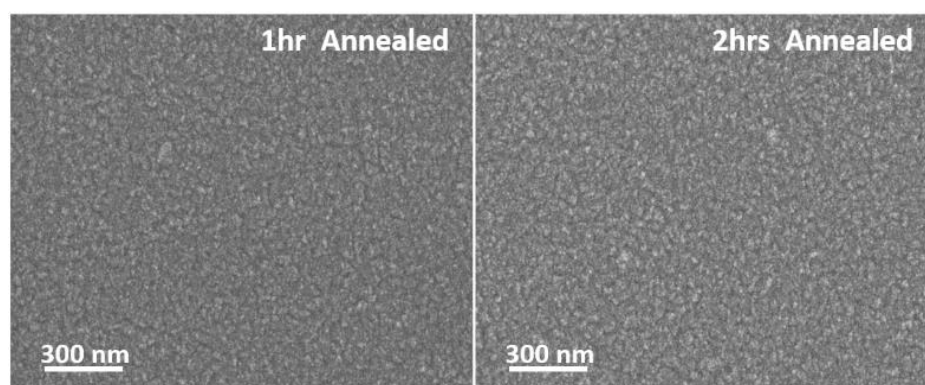
standard JCPDS data (008-0459). It is observed that there is no lattice distortion in the annealed films.



**Figure 3.6** XRD patterns of CdSe thin films annealed for two different durations.

**Table.3.2** X-Ray diffraction and EDAX data for annealed CdSe thin films.

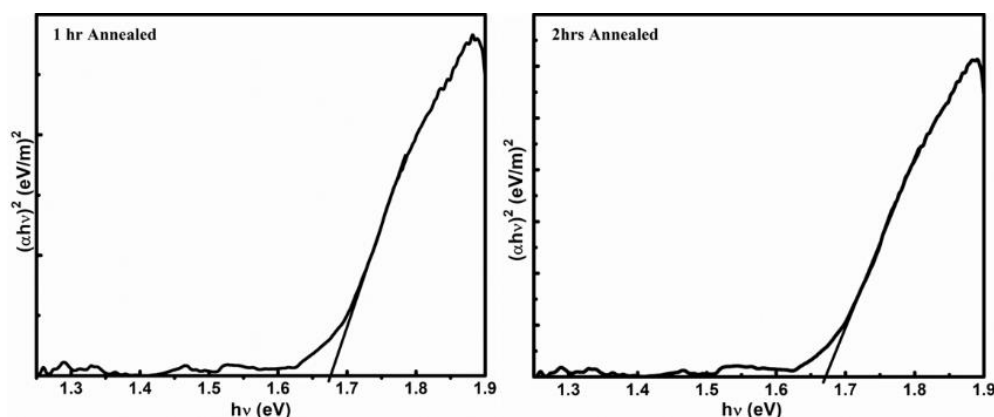
Annealing duration	Plane (h k l)	Crystallite size (D) nm	Inter-planer spacing (Å)	Atomic ratio Cd: Se
1 hr	(002)	32.9	3.51	1.01
2 hr	(002)	33.3	3.54	1.07



**Figure 3.7** FE-SEM micrographs of CdSe thin films annealed for 1hr and 2hr.

Figure 3.7 shows FE-SEM micrographs of annealed films. The deposited films were uniform, free from the pinhole and well covered to the glass substrate surface. It is interesting to note that the deposited films seem to be composed of densely packed nano size crystallites. Native defects in the prepared films reduced on annealing thereby increasing crystallite size.

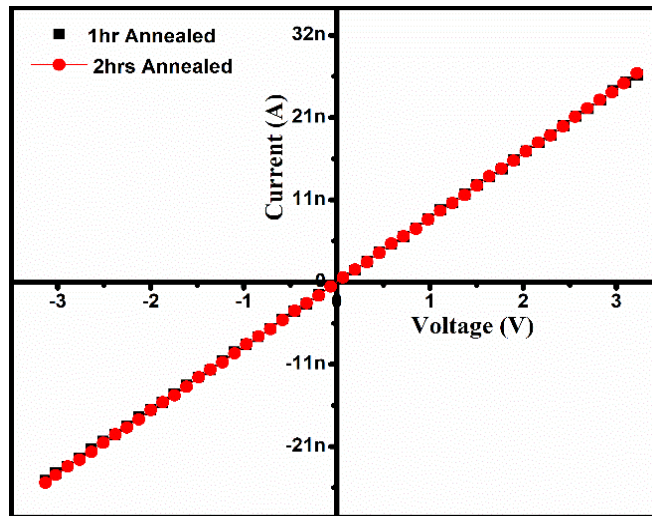
EDAX analysis reveals the presence of Cd and Se content in annealed films. It is observed that the selenium (Se) content in the films decreased as the annealing duration is increased from 1 hr to 2 hr, which may be due to the re-evaporation of selenium content from the substrate. This deviation in the stoichiometric ratio of CdSe thin films leads to an increase in the conductivity.



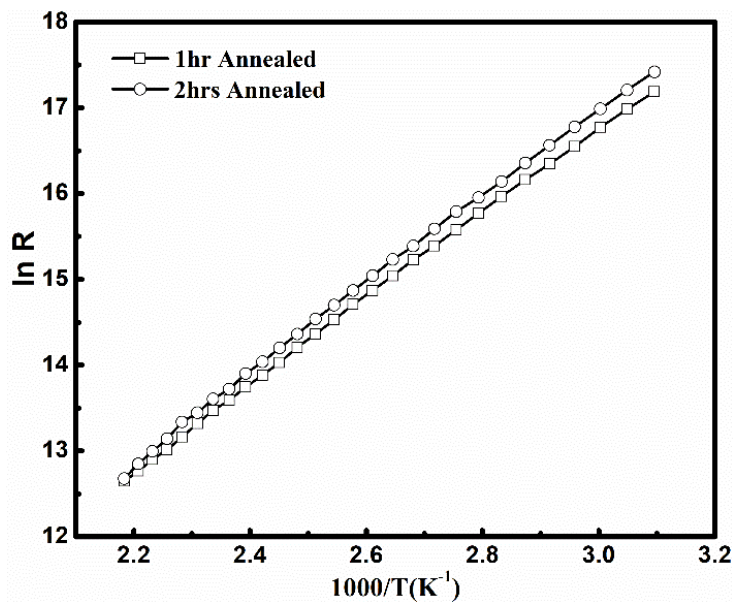
**Figure 3.8** Tauc's plot of 1hr and 2hr annealed CdSe thin films.

Figure 3.8 shows the Tauc's plot of annealed CdSe thin films. The optical band gap of 1.68 eV was determined from the Tauc's plot, but there is no significant change in the band gap values with varying annealing duration. The as deposited CdSe thin films have band gap of 1.89 eV, after annealing band gap decrease to 1.68 eV. The decrease in the band gap is may be due to the compositional variation as well as the improved crystallinity. The electrical conductivity of films was measured by depositing silver on the top of the CdSe film in a coplanar configuration. All the deposited films have an n-type conductivity which is determined from the hot probe method where the potential difference between hot and cold probe reveals the majority carriers type.

Figure 3.9 shows the I-V characteristics of annealed CdSe thin films reveals ohmic nature with silver contact. The conductivity of these films was found to be in the order of  $10^{-4}$  / $\Omega$ -cm. There is an increase in the conductivity by an order of magnitude after annealing the films at 453 K for 1 hr in a vacuum. However, while varying annealing duration there is no significant change in the conductivity of annealed CdSe films.



**Figure 3.9** I-V characteristics of annealed CdSe thin films.



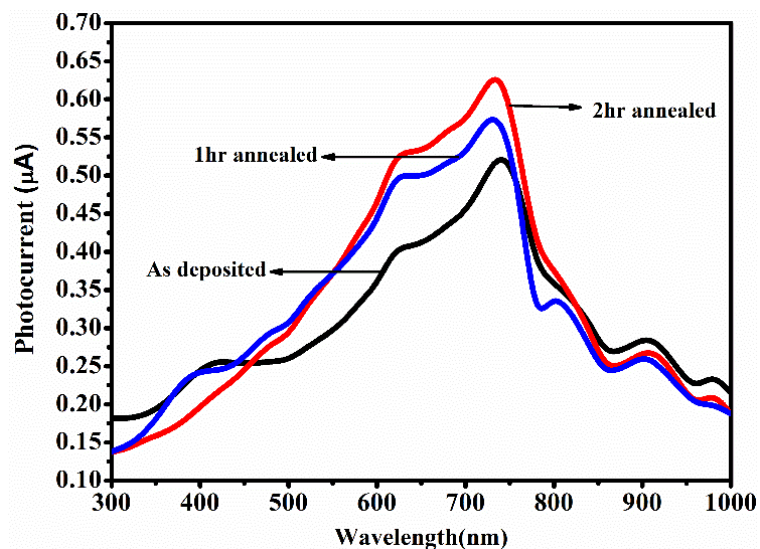
**Figure 3.10** Variation of  $\ln(R)$  vs  $1000/T, (K^{-1})$  of CdSe thin films.

Figure 3.10 shows the variation of  $\ln R$  vs  $1000/T, (K^{-1})$  of annealed films. The plot shows linear behavior throughout the temperature range, corresponding to intrinsic conduction in the annealed films. The activation energy of annealed CdSe thin films determined using equation no. 2.3.9 is shown in table 3.3. Figure 3.11 represents the photocurrent vs wavelength curves for as-deposited and vacuum annealed CdSe thin films. The photocurrent is low for the as-deposited film and a marginal increase in the photocurrent of  $0.53 \mu A$  to  $0.64 \mu A$  was observed for annealed films. All the curves show a peak at  $738 \text{ nm}$  which corresponds to the bandgap energy of  $1.68 \text{ eV}$ .



**Table 3.3** Optical band gap and activation energy data of annealed CdSe thin films.

Annealing duration	Activation energy ( $E_a$ )	Energy band gap ( $E_g$ )
1 hr	0.45 eV	1.68 eV
2 hr	0.43 eV	1.68 eV



**Figure 3.11** Photo-response curves of as-deposited and annealed CdSe thin films.

The peak response at 738 nm of CdSe films indicates, that it can be useful in solar cells as a good absorber. Annealed films show high photocurrent than the as-deposited CdSe thin films. Post-deposition annealing of films leads to a slight increase in the crystallite size and reduced grain boundary. Increase in the photocurrent may be due to the lowering of intergrain potential barrier on annealing. Increase in the photocurrent also depends on the compositions of the film. The effect of substrate temperature and post-deposition annealing leads to getting sharper peaks in the photocurrent curves.

## CHAPTER 4

### EFFECT OF DOPING ON THE PROPERTIES OF CdSe THIN FILM

#### *Overview*

In this chapter an attempt has been made to dope CdSe with silver (Ag), bismuth (Bi) and indium (In). The effect of doping concentration on the structural, morphological, optical and electrical properties of doped CdSe thin films have been studied.

#### 4.1 INTRODUCTION

It has been a general practice to dope compound semiconductors with suitable dopants to modify the properties of the films to make them more suitable for potential applications. When the dopant concentrations are low, they do not normally affect the structure and morphology of the films. However, it may lead to drastic changes in electronic properties of the films. This might result from the dopant getting incorporated into the lattice of the material of the films.

In II-VI group of compounds, CdSe is one of the extensively studied compound semiconductor. With a band gap of 1.74 eV, it is considered as a promising material for device applications such as solar cell window absorber layer, photodetectors, gas sensors, field effect transistors (Al-Kabbi et al. 2013). Properties of thin films depend on growth techniques and preparation conditions. Several preparation techniques are used to prepare CdSe thin films including thermal evaporation (Baban and Rusu 2003), chemical bath deposition (Mane and Lokhande 2000), spray pyrolysis (Yadav et al. 2010) and solution growth method (Kaur et al. 2015). The electrical and optical properties of semiconducting thin films depend mainly on impurity concentration and a doping process. A number of researchers worked on the doping of cadmium selenide (CdSe) and also on photoconductivity, electrical and optical properties of Ag doped CdSe thin films obtained using solution growth, thermal evaporation, and ion exchange method. CdSe is basically n-type material in bulk as well as in thin film form having a high resistance. CdSe thin films with low resistivity can be used in heterojunction solar cells to lower the series resistance and to minimize the conduction Band-Fermi level

energy gap. Substrate temperature, deposition rate, vacuum condition, post-deposition annealing condition, and wafers play important role in the preparation of thin films. Tailoring the electrical and optical properties of cadmium selenide by doping makes it suitable for next generation solar cells because of its optical band gap lying the solar energy spectrum (Kaur and Tripathi 2016). In the recent year's various researchers used Bi, Pr, Nd and Sm to dope CdSe, these are the potential candidates for various applications. V.T Patil et al. studied the Bi doped CdSe thin films prepared by thermal evaporation. K. Heo. et al. reported the structural control on Bi doped CdSe nanostructures for practical applications (Heo et al. 2016).

However, the study of doping effect on the properties of CdSe thin films is still insufficient to evaluate the mechanism and its relation to the properties. The evaluation of any material for application is complete and meaningful only when its structure, composition, and properties are well known.

## **4.2 EFFECT OF Ag (SILVER) DOPING CONCENTRATION ON THE PROPERTIES OF CdSe THIN FILMS.**

### **4.2.1 Experimental details**

CdSe: Ag thin films were prepared on glass substrates using thermal evaporation technique at a pressure less than  $5 \times 10^{-6}$  Torr. Tantalum boat was used to evaporate cadmium selenide (CdSe) fine powder of purity 99.995% and silver (Ag) powder of 99.99% (Alfa Aesar). Substrates were dipped in chromic acid for 24 hr to eradicate the contamination on the surface of the substrate. These were further cleaned with detergent and rinsed with acetone. Cleaned substrates were heated to and maintained at 453 K for 2 hr prior to film deposition. Two sets of samples were prepared and annealed at two different conditions. One set of samples were annealed at 473 K for 2 hr in air and other in a vacuum. The thickness of the prepared films was determined by the gravimetric method and it was found to be in the range of 750 nm to 800 nm. The thickness of the deposited films was verified using transmission interference. Structural characterization has been carried out using X-Ray diffraction (Rigaku Miniflex 600) with  $\text{CuK}\alpha$  radiation of wavelength  $1.5406 \text{ \AA}$  in the  $2\theta$  range from  $20^\circ$  to  $60^\circ$ . Scanning electron microscope (Carl Zeiss) has been used to record the surface micrographs of undoped & CdSe: Ag thin films. Elemental analysis has been carried out using Energy

Dispersive X-ray (EDAX) attached to the SEM. Absorption spectra of undoped and CdSe: Ag thin films were recorded using Shimadzu make UV-Vis-NIR 3600 spectrophotometer in the wavelength range of 300 nm – 1200 nm. For electrical studies, silver contacts were deposited on CdSe: Ag thin films in coplanar structure. Resistance has been measured as a function of temperature ranging from 300 K to 473 K to evaluate the activation energy for conduction.

#### 4.2.2 Results and discussion

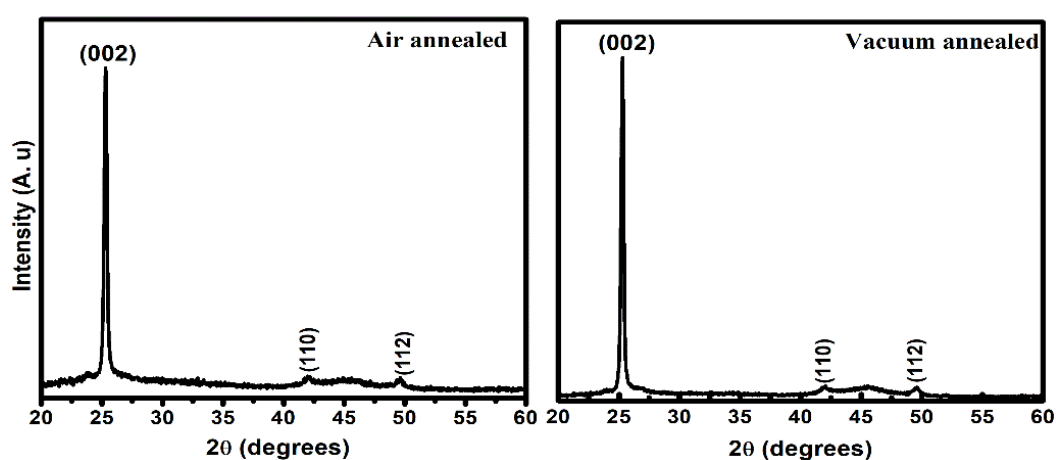


**Figure 4.1** X-ray diffraction patterns of undoped CdSe thin films.

Figure 4.1 shows the X-ray diffraction patterns of air annealed and vacuum annealed undoped CdSe thin films. The diffraction pattern peaks were indexed to the (002), (110) and (112) planes confirming the wurtzite phase of CdSe. The average crystallite size ( $D$ ) of the undoped CdSe thin films was estimated from full-width at half maximum (FWHM) of diffraction peaks according to Scherer's formula (2.3.2). The calculated lattice parameters were in good agreement with standard data for hexagonal lattice (JCPDs card 08-0459). Variation of crystallite size and lattice parameters of undoped CdSe thin films were tabulated in table 4.1 and table 4.2 for air annealed and vacuum annealed films respectively.

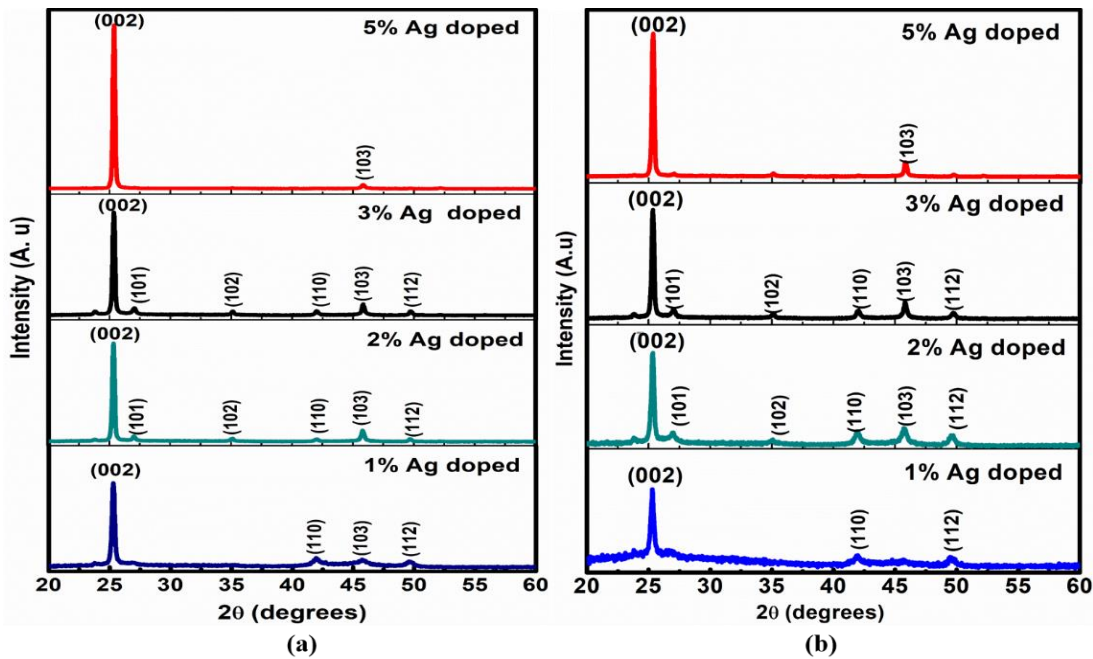


**Figure 4.2** XRD patterns of Ag doped CdSe thin films (a) Air annealed (b) Vacuum annealed.

Figure 4.2 (a) and Figure 4.2 (b) shows the XRD traces for air annealed and vacuum annealed CdSe: Ag thin films respectively. XRD analysis reveals that the films are polycrystalline in nature processing hexagonal crystal structure. XRD patterns show no peak corresponding to free silver or related compound. No significant change in grain size was observed for air annealed as well as for vacuum annealed CdSe: Ag films. An increase in the dopant concentration does not result in any changes in lattice parameter indicating that there is no lattice distortion.

The surface topography of the deposited films was examined through FE-SEM. Figure 4.3 shows FE-SEM micrographs of undoped CdSe thin films. It has been found that the CdSe thin films were uniform and featureless. It was also observed that crystallite size increases marginally on annealing the films in both air and vacuum. Figure.4.4 and figure.4.5 show FE-SEM micrographs of air annealed and vacuum annealed CdSe: Ag thin films respectively. Bright spots in the micrographs indicate the excess silver which is confirmed by the EDAX analysis.

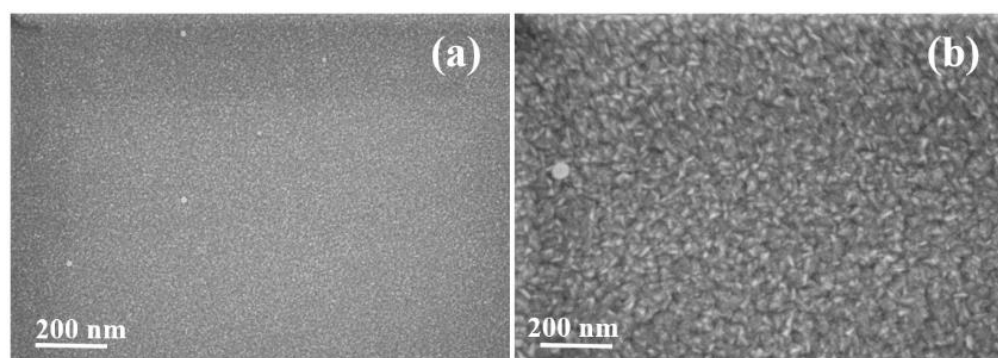
**Table 4.1** XRD data of air annealed Undoped and Ag doped CdSe thin films.

Sample	2 $\theta$ (degrees)	Plane (h k l)	Inter-planar spacing(d) (Å)	Grain size (D) (nm)
As deposited air annealed	25.28	(002)	3.52	35.23
Ag 1%	25.30	(002)	3.51	33.35
Ag 2%	25.33	(002)	3.51	39.69
Ag 3%	25.34	(002)	3.51	40.89
Ag 5%	25.35	(002)	3.50	43.29

**Table 4.2** XRD data of vacuum annealed undoped and Ag doped CdSe thin films.

Sample	2 $\theta$ (degrees)	Plane (h k l)	Inter-planar spacing (d) (Å)	Grain size (D) (nm)
As deposited vacuum annealed	25.29	(002)	3.52	31.58
Ag 1%	25.30	(002)	3.52	29.58
Ag 2%	25.31	(002)	3.51	32.29
Ag 3%	25.35	(002)	3.51	38.03
Ag 5%	25.44	(002)	3.50	39.52

It is observed that the surface roughness increases with increasing Ag concentration. Agglomeration of Ag in doped CdSe thin films has been studied by scanning electron microscopy. It has been reported that silver remains as separate clusters when used for doping CdSe thin films.

**Figure 4.3** SEM micrographs of (a) Air annealed (b) Vacuum annealed undoped CdSe thin films.

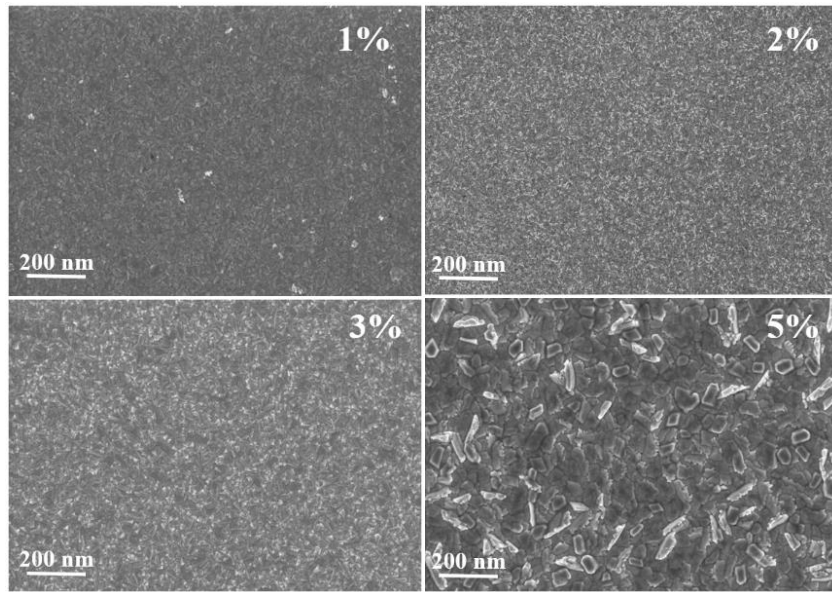


**Figure 4.4** SEM micrographs of air annealed CdSe: Ag thin films.

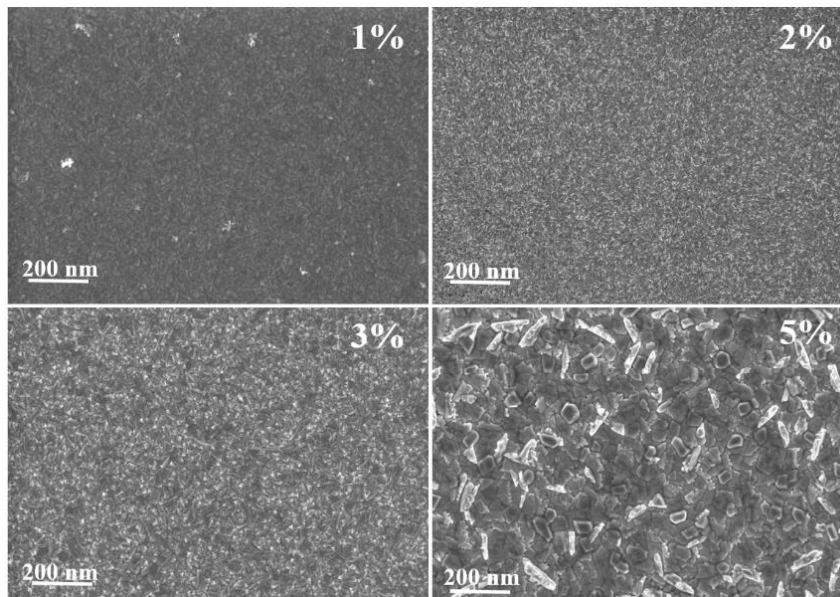


**Figure 4.5** SEM micrographs of vacuum annealed CdSe: Ag thin films.

Figure 4.6 (a) and figure 4.6 (b) show the plots of  $(\alpha h\nu)^2$  versus photon energy ( $h\nu$ ) for air annealed and vacuum annealed samples respectively. The optical absorption spectra of undoped and CdSe: Ag thin films, corrected for glass substrate absorption. The absorption spectra were analyzed to calculate the absorption coefficient ( $\alpha$ ), optical band gap and nature of transitions involved. Optical band gap ( $E_g$ ) values were determined by standard Tauc's method. The Optical band gap ( $E_g$ ) values were deduced by extrapolating the linear portion of the respective curves to  $(\alpha h\nu)^2 = 0$ .

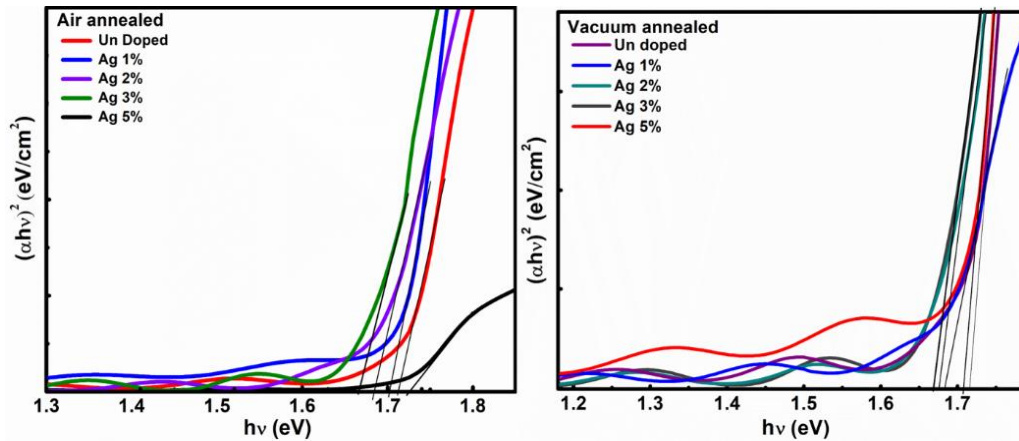


**Figure 4.6** Tauc's plot of undoped and CdSe: Ag thin films.

The optical band gap values for air annealed and vacuum annealed samples are listed in table 4.3. No significant change in the optical band gap was observed for air annealed and vacuum annealed CdSe: Ag films with increasing Ag concentration.

**Table 4.3** Optical band gap of undoped and CdSe: Ag thin films

Ag (Wt.%)	Air annealed $E_g$ ( eV)	Vacuum annealed $E_g$ ( eV)
0	1.71	1.72
1	1.70	1.68
2	1.69	1.67
3	1.66	1.66
5	1.72	1.71

Figure 4.7 shows the variation of logarithmic resistance versus inverse temperature of undoped CdSe thin films. Electrical resistivity and temperature dependence of resistance measurements have been carried out for undoped and CdSe: Ag (1% to 5%) thin films in the temperature ranging from 300 K to 473 K. The resistance of films decreased with increased temperature indicating the semiconducting nature. The hot probe method reveals that as-deposited, annealed and CdSe: Ag thin films have n-type conduction. The activation energy was calculated from the slope of the linear portion obtained from the plot of  $\ln R$  vs  $10^3/T$ , ( $K^{-1}$ ). The activation energy was found to be 0.44 eV and 0.39 eV for air annealed and vacuum annealed CdSe films respectively. The calculated values of electrical conductivity are listed in table 4.4 for air annealed and vacuum annealed films. Room temperature conductivity of undoped CdSe thin



films was found to be of the order of  $10^{-4} / \Omega\text{-cm}$ . In case of air annealed undoped CdSe films, the conductivity decreases as compared to that of as-deposited films, due to oxygen incorporation into CdSe thin films. The incorporated oxygen acts as an acceptor impurity in air annealed films (Sathyalatha et al. 1989).

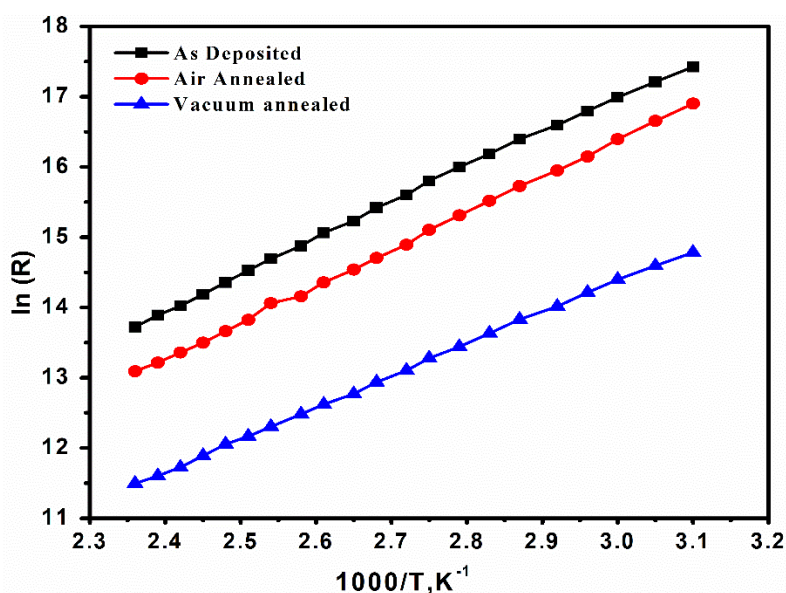


**Figure 4.7** Plot of  $\ln(R)$  vs  $1000/T, K^{-1}$  for undoped CdSe thin films.

In case of vacuum annealed CdSe films, conductivity increases as compared to undoped films, which may be due to re-evaporation of Se content from the deposited film while annealing as confirmed by EDAX analysis. The composition analysis using EDAX also reveals that addition of silver to the films result in a decrease in the concentration of both cadmium and selenium. This indicates that silver does not replace either cadmium or selenium preferentially.

**Table 4.4** Electrical conductivity data for undoped and CdSe: Ag thin films

Ag (Wt.%)	Air annealed $\sigma$ ( $/\Omega\text{-cm}$ )	Vacuum annealed $\sigma$ ( $/\Omega\text{-cm}$ )
0	$0.48 \times 10^{-4}$	$3.87 \times 10^{-4}$
1	$1.2 \times 10^{-3}$	$3.29 \times 10^{-6}$
2	$0.21 \times 10^{-2}$	$1.45 \times 10^{-2}$
3	$3.64 \times 10^{-1}$	$4.2 \times 10^{-1}$
5	3.66	1.04

A detailed study of variation of resistance with temperature for the case of CdSe: Ag films show that the electrical resistivity decreases with increase in the silver content in the films (Figure 4.8). Further, the activation energy for conduction is observed to decrease at higher temperature ranges which cannot be explained by the normal semiconducting nature of the films.

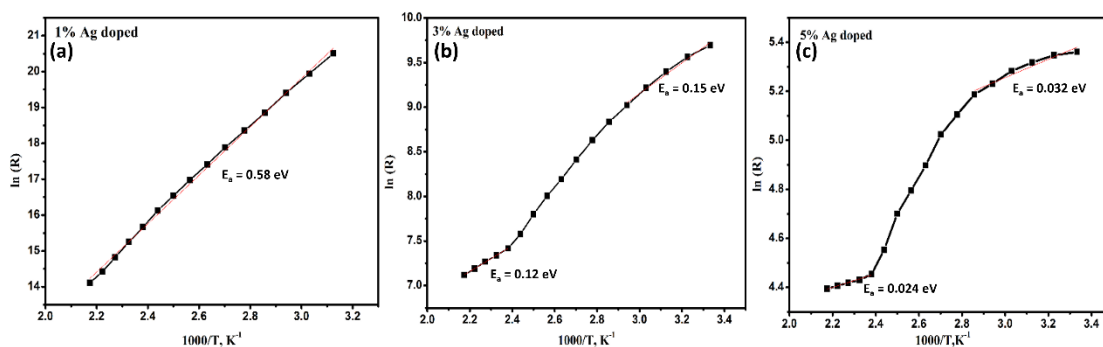


**Figure 4.8** Plot of  $\ln(R)$  vs  $1000/T$  ( $K^{-1}$ ) for CdSe: Ag thin films with (a) 1%, (b) 3% and (c) 5% Ag.

If the films show a transition from extrinsic conduction to intrinsic conduction, the activation energy should be higher at higher temperature range. These observations point towards the possibility of silver remaining as a metallic phase along with CdSe in the films. This is further confirmed by the fact that the x-ray studies did not show any variation in the crystal structure data and the minute amount of silver does not show up in the x-ray diffraction pattern. The X-ray peak analysis also points to the fact that the grain size and microstrain in the films are unaltered on the addition of silver. The Scanning electron micrographs show a rough surface with probable precipitates of silver in the film. It is concluded that silver does not dope CdSe thin films and does not replace any of the components in the film but remain as a passive additive in the films.

### 4.3 EFFECT OF Bi (BISMUTH) DOPANT CONCENTRATION ON THE PROPERTIES OF CdSe THIN FILMS

#### 4.3.1 Experimental details

Undoped, Bi doped CdSe thin films were deposited on glass slides using thermal evaporation technique at a residual pressure less than  $5 \times 10^{-6}$  Torr. Along with fine powder of CdSe (99.995 %), Bi lumps of 99.95% (SRL) was used as a dopant to prepare Bi doped CdSe thin films. The glass substrates dipped in highly concentrated chromic

acid for 24 hr to remove the additives on the surface and also it helps to increase the adhesion of deposited thin films. The glass slides were cleaned with a soap solution (labolin) further cleaned with lab grade acetone and gently rubbed with tissue paper. Molybdenum boat was used to evaporate source material. The deposition rate was maintained nearly  $37\pm 5$  nm/min. CdSe powder and dopant materials were co-evaporated from the single boat to prepare doped CdSe thin films. During deposition, the substrate temperature was maintained at 453 K and post-deposition annealing was carried out at 453 K for 1hr in vacuum. The thickness of the vacuum deposited films was evaluated by the gravimetric method and it was found to be in the range of 450 nm – 500 nm. Structural characterization has been carried out using Rigaku Miniflex X-Ray diffractometer with  $\text{CuK}\alpha$  radiation of wavelength ( $\lambda$ ) = 1.5406 Å. FESEM images of films were obtained by Carl Zeiss scanning electron microscope, elemental analysis has been carried out using energy dispersive X-ray spectroscopy (EDAX). Absorption spectra of CdSe and Bi doped CdSe thin films were recorded using Shimadzu make UV-Vis-NIR 3600 spectrophotometer in the wavelength range of 300 nm - 1200 nm. For electrical studies, silver contacts have been used. The variation of film resistance as a function of ambient temperature was determined. Photocurrent measurements were carried out using Xenon arc lamp (500 W) (Newport, model 66902) for both undoped and Bi doped CdSe thin films.

### 4.3.2 Results and discussion

Figure 4.9 shows the XRD pattern of CdSe and Bi (1%, 2%, and 3%) doped CdSe thin film prepared at 453K substrate temperature. The average grain size was calculated by well-known Scherrer's formula (Shah et al. 2012). The lattice parameters 'a' and 'c' were calculated using equation no. 2.3.3 and 2.3.4. (Hankare et al. 2011). Variation of crystallite size and lattice parameters of undoped and Bi doped CdSe thin films were tabulated in table 4.5. It is observed that lattice parameter increases as the Bi dopant concentration increases, it may be due to the larger radius of the Bi atom compared to Cd. The presence of a large number of peaks indicates that the films are polycrystalline in nature. The obtained diffraction patterns of undoped and Bi doped CdSe thin films exhibit hexagonal crystal structure and agree well with JCPDS data (008-0459).

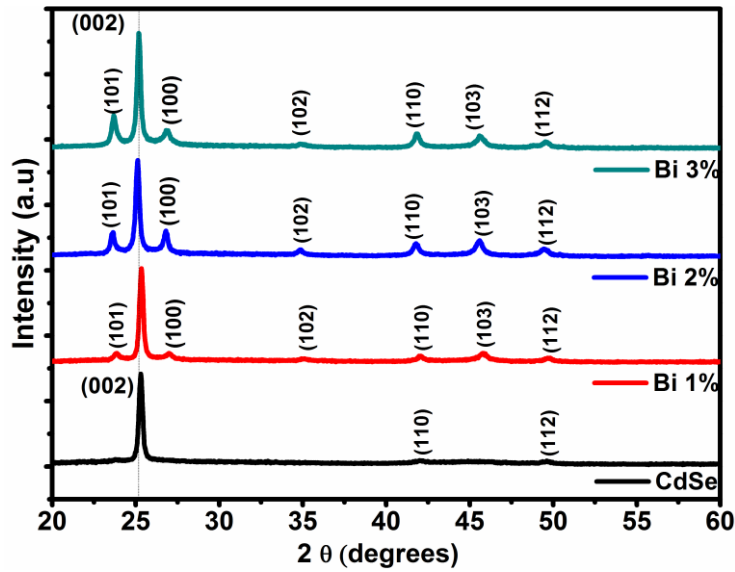


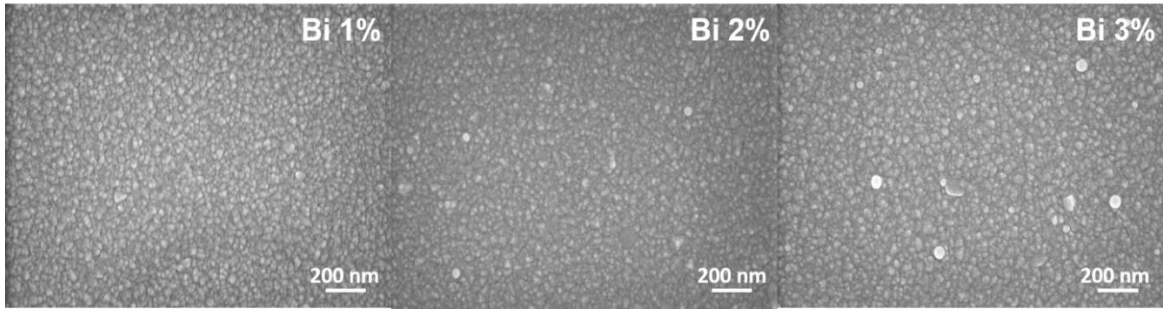
**Figure 4.9** XRD spectra of CdSe and Bi doped CdSe thin films.

As the Bi concentration increases, the (002) and (101) diffraction peak becomes more dominant and shifts towards the lower diffraction angle. The marginal increase in grain size was observed with increase in Bi dopant concentration. The increase in Bi content from 1 to 3 wt.% leads to increase in the crystallinity of the doped CdSe thin films as compared to undoped CdSe thin films. This kind of doping effect on the crystallinity of the CdSe thin films was observed by (Al-Ani et al. 2002; Mahalingam et al. 2010; Sharma et al. 2012) for Cu doped CdSe and In doped CdSe thin films.

**Table.4.5** XRD data of undoped and Bi doped CdSe thin films.

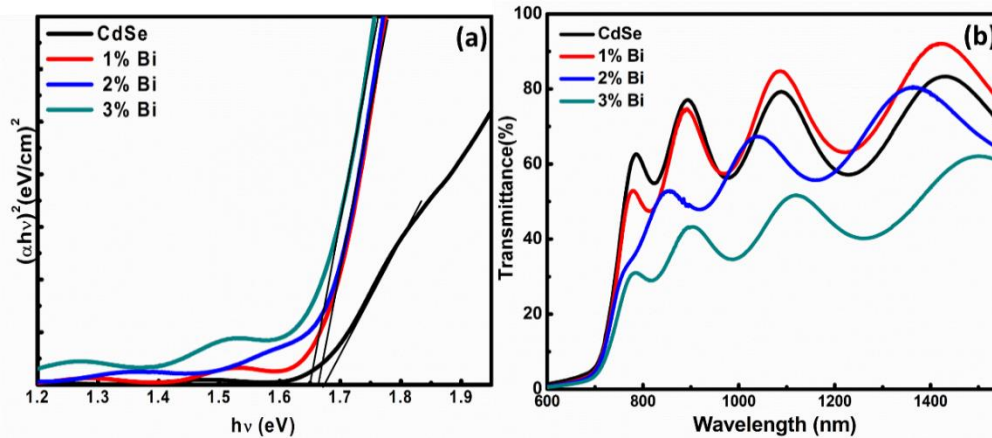
Sample	2θ (degrees)	Plane (h k l)	<i>d</i> (Å)	<i>D</i> (nm)	<i>a</i> (Å)	<i>C</i> (Å)	Cd (at.%)	Se (at.%)	Bi (at.%)
CdSe	25.30	(002)	3.516	32.68	4.295	7.03	50.36	49.63	
Bi 1%	25.30	(002)	3.514	32.35	4.299	7.03	49.47	49.42	1.11
Bi 2%	25.17	(002)	3.532	33.34	4.318	7.06	48.36	49.56	2.08
Bi 3%	25.10	(002)	3.540	33.87	4.323	7.08	46.76	49.83	3.41

Figure 4.10 indicates FE-SEM micrographs of Bi (1%, 2% and 3%) doped CdSe thin film. It is observed that the prepared thin films contain nano size grains which are uniformly distributed over the smooth homogeneous background and free from microscopy defect like cracks or peeling. EDAX analysis reveals the existence of Cd, Se, and Bi in the deposited films in a stoichiometric form.



**Figure 4.10** FE-SEM micrographs of Bi doped CdSe thin films.

The optical absorption and transmittance spectra were recorded in the 300 nm – 1200 nm wavelength range, using a Shimadzu 3600 UV-Visible model of the spectrophotometer. The optical band gap of these films has been calculated using the Tauc's relation (2.3.6) (Sharma et al. 2012). The plot of  $(\alpha h\nu)^2$  (vs)  $h\nu$  for CdSe and Bi doped CdSe thin films were shown in figure 4.11 (a). The band gap values were estimated from the  $(\alpha h\nu)^2$  versus photon energy ( $h\nu$ ) plot. The best fit to the experimental data was obtained for  $n = 1/2$ . The straight line portion is extrapolated to cut the x-axis, which gives the energy gap.



**Figure 4.11** (a) Tauc's plot and (b) transmittance spectra of CdSe and Bi (1%, 2%, 3%) doped CdSe thin films.

The Linear portion in undoped and Bi doped CdSe films supporting the interpretation of direct bandgap semiconductors. The obtained band gap values for CdSe and Bi doped CdSe thin films were tabulated in table 4.6. The obtained band gap of pure CdSe thin film is estimated to be 1.67 eV which is close to previously reported data of Murali et al. 2009. There is no significant change in the optical band gap for the Bi doped CdSe films compared to the undoped CdSe thin films. The optical

transmittance of doped CdSe films decreases as the Bi dopant concentration increases (Figure.4.11 (b)). This decrease in the transmittance may be due to scattering losses at the film surface (Nair et al. 1993) with an increase in the Bi dopant concentration.

The electrical measurements were carried out for Bi doped CdSe thin films. The resistance of the doped films was recorded as a function of ambient temperature. It is observed that the resistance decreases with increasing temperature indicating the semiconducting nature of the Bi doped CdSe thin films. The variation of resistance with temperature exhibits an Arrhenius behavior. Figure 4.12 shows the variation of  $\ln R$  versus inverse temperature of Bi doped CdSe thin films.

**Table.4.6** Optical and electrical data of undoped and Bi doped CdSe thin films.

Sample	Activation energy (eV)	Optical band gap ( $E_g$ )	$\sigma$ ( $/\Omega\text{-cm}$ )
Bi 1%	0.43	1.66	$0.64 \times 10^{-4}$
Bi 2%	0.40	1.66	$1.70 \times 10^{-4}$
Bi 3%	0.37	1.65	$8.47 \times 10^{-4}$

The thermal activation energies of the Bi doped CdSe thin films was calculated. The thermal activation energy was evaluated from the  $\ln R$  versus  $1000/T$ , ( $K^{-1}$ ), using the slope of the linear portion in the plot. Activation energy decreases with increasing Bi dopant concentration. This may due to the increase in the charge carrier concentration.

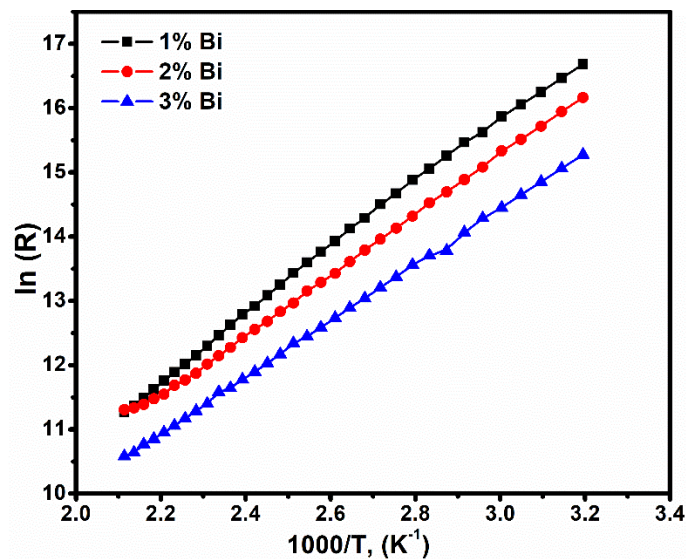


**Figure 4.12** Variation of  $\ln(R)$  versus  $1000/T$ , ( $K^{-1}$ ) for Bi doped CdSe thin films.

Bi doped CdSe films show single linear region having single slope represents the deep donor levels which contribute to conduction mechanism (Pejova et al. 2004). This has been interpreted by the literature as due to the energy brought by thermal agitation. Due to the thermal energy, ionization of the impurities takes place and this ionized charge carries move from deep donor levels in the band gap to the conduction band of the semiconductor sample. Electrical conductivity ( $\sigma$ ) increases with increasing Bi dopant concentration.

This increased electrical conductivity with Bi concentration can be interpreted by the increase in the number of free charge carriers from the Bi dopant atoms incorporated by substituting cadmium atoms. A similar observation has been made by (Chouikh et al. 2011) for Bi doped ZnO thin films deposited by spray pyrolysis.

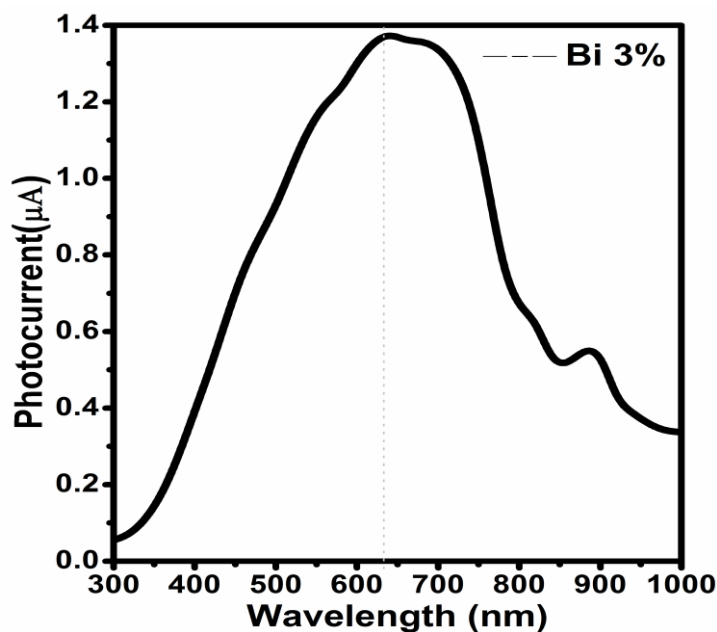


**Figure 4.13** Photocurrent ( $\mu\text{A}$ ) v/s wavelength (nm) plot of 3% Bi doped CdSe thin films.

Photocurrent ( $I_{Ph}$ ) was measured a function of wavelength for Bi doped CdSe thin films. The normalized spectral response curves of Bi doped CdSe thin films were shown in figure 4.13. Photocurrent curves showed a maximum at 620 nm, which corresponds to the band-edge emission of CdSe thin films (Figure 4.13). This reveals that the photoconductivity was mainly due to the photo-generated charge carriers that were excited by the incident photons with energy equal to or larger than the band gap.

Photoconductive thin films were widely used for photodetectors, and its efficiency depends on the fast rise of photocurrent upon illumination and sudden decay of the photocurrent upon termination of illumination (Nair et al. 1993). The maximum photocurrent ( $I_{Ph}$ ) value obtained in the present work was 1.38  $\mu\text{A}$  for 3% Bi doped CdSe films. Increase in the photocurrent indicates that the presence of Bi in the films acts as photoconductivity sensitizers.

#### 4.4 EFFECT OF In (INDIUM) DOPING CONCENTRATION ON THE PROPERTIES OF CdSe THIN FILMS

To prepare indium (In) doped CdSe thin films, fine powder of indium (In) (99.99% purity, Alfa aesar) was used as dopant material. Similar deposition parameters were maintained as given in section 4.3.1.

##### 4.4.1 Results and discussion

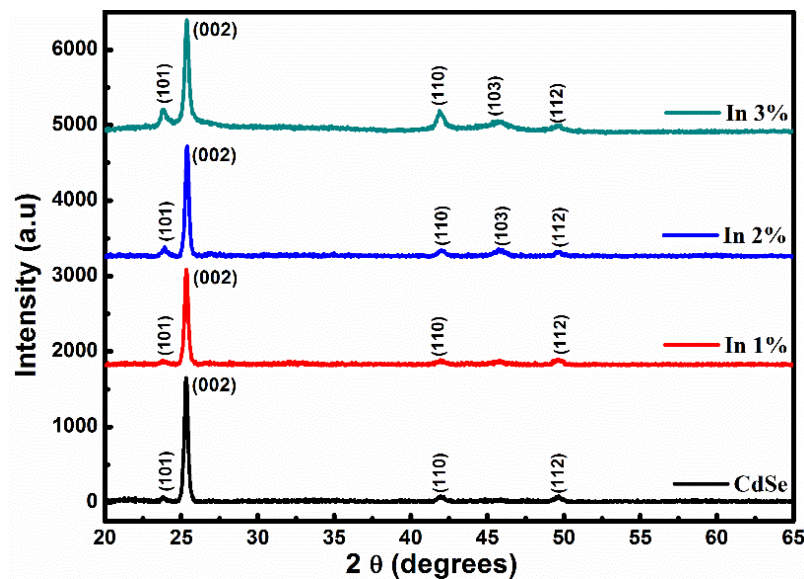


**Figure 4.14** X-Ray diffraction patterns of In doped CdSe thin films.

Figure 4.14 shows the XRD pattern of In (1%, 2% and 3%) doped CdSe thin film prepared at 453 K substrate temperature ( $T_s$ ) and vacuum annealed at the same temperature for 1hr. The presence of predominant (002) peak and other small peaks in the XRD patterns of In doped CdSe thin films indicates that the films exhibit polycrystalline hexagonal crystal structure. The average grain size was calculated by well-known Scherrer's formula (2.3.2) The lattice parameters 'a' and 'c' were



calculated using equations 2.3.3 and 2.3.4. Variation of grain size and lattice parameters with dopant concentration were tabulated in table 4.7. Obtained lattice parameters and inter planer spacing (d) values are agreeing well with JCPDS data (008-0459). As the In concentration increases, the (002) and (101) diffraction peak becomes more dominant and negligible shifts towards the higher diffraction angle ( $2\theta$ ). The increase in indium (In) content from 1% to 3 % leads to decrease in the crystallinity of the doped CdSe thin films as compared to undoped CdSe thin films. Similar kind of doping effect on the crystallinity of the CdSe thin films was observed by Sharma et al. 2013 for In doped CdSe thin films.

**Table 4.7** XRD and compositional data of In doped CdSe thin films.

Sample	$2\theta$ (degrees)	Plane (h k l)	d (Å)	D (nm)	a (Å)	c (Å)	Cd (at.%)	Se (at.%)	In (at.%)
In 1%	25.32	(002)	3.51	27.73	7.02	4.28	48.96	49.85	1.19
In 2%	25.35	(002)	3.51	26.94	7.02	4.29	47.70	50.21	2.09
In 3%	25.39	(002)	3.50	25.41	7.00	4.32	47.34	49.55	3.11

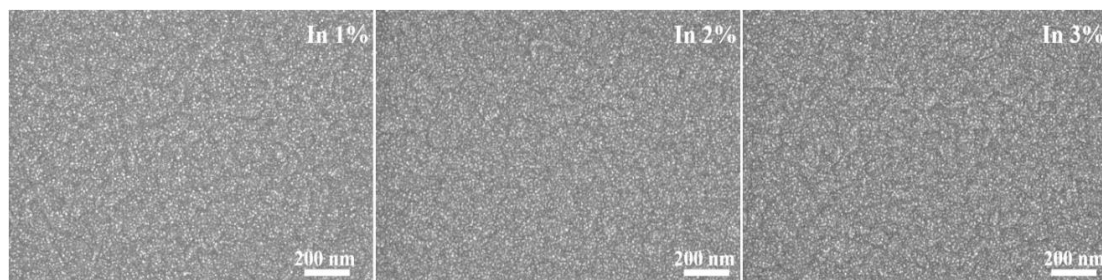


**Figure 4.15** FE-SEM micrographs of In doped CdSe thin films.

FE-SEM is a convenient technique to study the surface topography of grown thin film. Figure 4.15 shows the scanning electron micrographs of typical In doped CdSe thin films. FE-SEM micrographs of In doped CdSe thin films confirms the presence of densely packed grains. The surface morphology under FE-SEM study reveals that the deposited In doped CdSe thin films are uniformly coated over the substrates and free from microscopic defects like pin wholes and cracks. The grains are found to be closely packed with less inter grain spacing.

Energy dispersive analysis of X-rays analysis was carried out for the deposited In doped CdSe thin films. EDAX analysis reveals that the presence of cadmium, selenium, and indium in the deposited thin film and also silicon, calcium due to the composition

of the glass substrate used for deposition of In doped CdSe thin films. Table 4.7 provides the elemental composition in terms of atomic percentage of In doped CdSe thin films. The average atomic percentage of Cd, Se and In showing that the films are almost stoichiometric.

Room temperature optical absorption and transmission measurements were carried out using UV-Vis-NIR spectrometer in the wavelength ranging from 300 nm – 1500 nm. Figure 4.16 (a) and figure 4.16 (b) shows the Tauc's plot and transmittance spectra of In doped CdSe thin films. The optical energy band gap of In doped CdSe thin films was estimated from  $(\alpha h\nu)^2$  versus photon energy ( $h\nu$ ) curve, extrapolation of straight line portion in the plot for absorption coefficient ( $\alpha$ ) = 0 gives the energy band gap value.

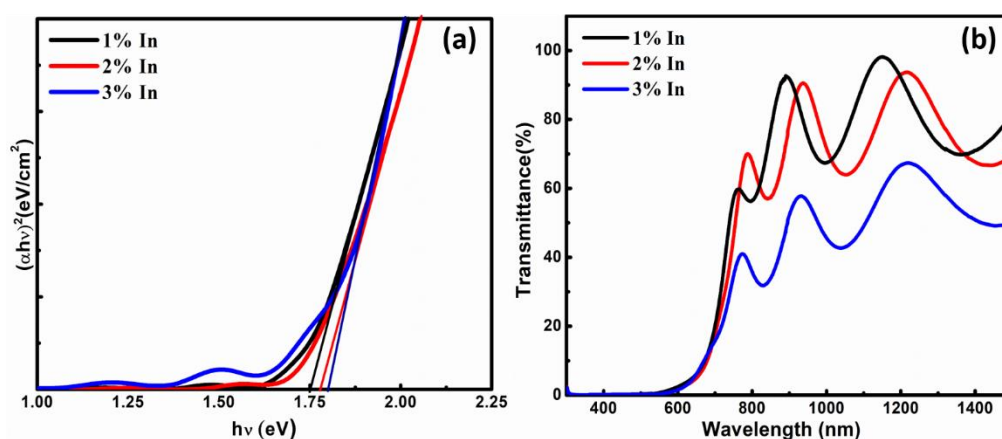


**Figure 4.16** (a) Tauc's plot and (b) Transmittance plot of In doped CdSe thin films.

This confirms that the deposited In doped CdSe thin films shows semiconducting nature with direct band gap. The estimated band gap values were tabulated in table 4.8. The band gap of the In doped films increase slightly with an increase in dopant concentration. It is well-known that increase in the band gap values arises from small grain size and resulting in the size effect of electronic states in the grown films.

**Table.4.8** Optical and electrical data of In doped CdSe thin films.

Sample	Activation energy (eV)	Optical band gap (eV)	$\sigma$ ( $\Omega$ -cm)
In 1%	0.37	1.74	67.7
In 2%	0.34	1.77	379.4
In 3%	0.32	1.80	1187.9

Transmittance spectra reveal that as the In dopant concentration increases transmittance decreases. It may be due to the scattering losses at the surface of In doped CdSe thin films. The electrical measurements were carried out in dark for In doped CdSe thin films. The resistance of the In doped films was recorded as a function of temperature. It is observed that the resistance decreases with increase in temperature indicating the semiconducting nature.

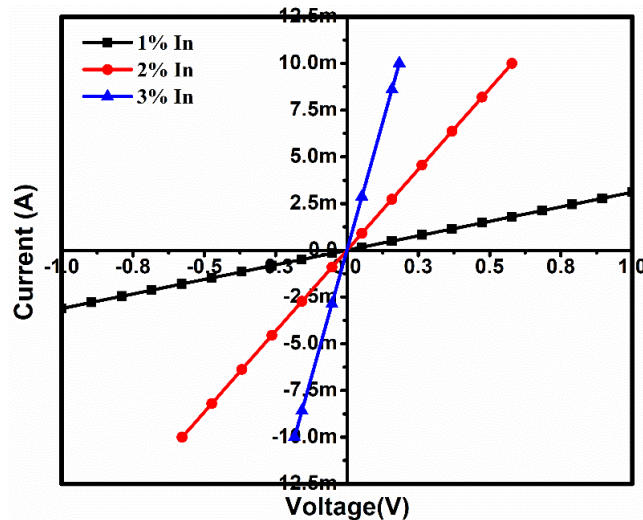


**Figure 4.17** I-V characteristics of In doped CdSe thin films.

The electrical conductivities of these polycrystalline In doped CdSe films was measured in dark at room temperature. The conductivity of the films was found to increase from  $10^{-4} / \Omega\text{-cm}$  to  $10^2 / \Omega\text{-cm}$ . The conductivity of doped films increases as the indium dopant concentration increases from 1% to 3%. The drastic increase in the conductivity of In doped films was observed as compared to undoped CdSe thin films. Increase in the conductivity may be due to the increased free charge carriers. The effect of In doping on electrical conductivity can be explained by identifying the possibilities of In incorporation into the host structure of CdSe. The first possibility may be a substitution of trivalent indium ( $\text{In}^{3+}$ ) to divalent cadmium ( $\text{Cd}^{2+}$ ). Another chance may be the formation of cadmium vacancies. Since CdSe with In is deposited at the same time, there is less chance for the formation of Cd vacancies. Thus, the substitution of a cadmium by an indium is more predominant which makes the In atom acting as a donor which causes the electrical conductivity to increase. The nature of majority charge carriers in the doped films was determined from the well-known hot probe method. All the In doped films show n-type conductivity. Figure 4.17 shows the I-V

characteristics of In doped CdSe thin films. I-V characteristics reveal that silver contact shows ohmic behavior. The thermal activation energies of the In doped CdSe thin films was studied. Activation energy decreases with increase in the dopant concentration. Obtained activation energy values were given in table 4.8.

## CHAPTER 5

### PREPARATION OF TERNARY COMPOUNDS AND THEIR PROPERTIES

#### *Overview*

In the present investigation, preparation and characterization of ternary compounds namely CdZnSe and CdSeTe have been carried out using thermal evaporation technique. Structural, optical and electrical properties of these thin films and effect of annealing duration on the formation of ternary compounds have been studied. These properties of ternary compounds will be helpful for optoelectronic device applications.

#### **5.1 PREPARATION AND CHARACTERIZATION OF CdZnSe THIN FILMS.**

##### **5.1.1 Introduction**

Cadmium selenide (CdSe) and zinc selenide (ZnSe) are the two important n-type materials in A<sub>II</sub>-B<sub>VI</sub> group semiconductors. CdSe has a band gap of 1.74 eV and ZnSe has a wider band gap of 2.7 eV at room temperature. The possibility of tuning properties by alloying would get material properties required for the device fabrication. The synthesis of ternary metal chalcogenides of group A<sub>II</sub>-B<sub>VI</sub> semiconductors in nanocrystalline form has been a rapidly growing area of research due to their important applications in wide spectrum of optoelectronic devices like lasers, photo-electrodes, light emitting diodes, sensors, transistors, radiation detectors (Al-Douri 2003; Husain et al. 2003).

Their physical and chemical properties are found to be strongly dependent on the relative concentrations of two elements and preparation methods to form an alloy. Thin films of Cd<sub>(1-x)</sub>Zn<sub>(x)</sub>Se have been synthesized using different techniques like thermal evaporation (Mahmood et al. 2011; Selva Priya et al. 2016), molecular beam epitaxy (Borkovska et al. 2008; Samarth et al. 1990), electron beam evaporation (Rao and Centre 1994) and chemical bath deposition (Chate et al. 2010), etc. The properties like crystal structure, optical properties and band structure of both ZnSe and CdSe are almost similar (Bagade et al. 2015, 2016). Murali et al. 2009 found that electron beam

evaporation technique prepared CdSe thin films shows good photoconductive response and having a high signal to noise ratio.

CdSe and ZnSe are well known to exist in either hexagonal or in cubic forms depending on the composition and deposition conditions (Husain et al. 2003). Band edges of these materials can be tailored by alloying, to give a wide range of band gap values. These are efficient absorbers in the visible region and hence can be used in solar cells. Since  $\text{Cd}_{(1-x)}\text{Zn}_{(x)}\text{Se}$  is more stable than CdSe, it may replace CdS as a window material in solar cells.

In the present investigation, bandgap engineering was successfully achieved by depositing  $\text{Cd}_{(1-x)}\text{Zn}_{(x)}\text{Se}$  (CZS) thin films in the stoichiometric form. Optimization of preparative parameters like deposition rate, substrate temperature and post-deposition annealing in a vacuum has been carried out to get good quality of highly adhesive, stable  $\text{Cd}_{(1-x)}\text{Zn}_{(x)}\text{Se}$  (CZS) thin films.

### **5.1.2 Experimental details**

The mixed  $\text{Cd}_{(1-x)}\text{Zn}_{(x)}\text{Se}$  thin films were deposited on glass substrates by the thermal evaporation technique at a pressure of  $10^{-5}$  Torr. The glass substrates dipped in highly concentrated chromic acid for 24 hr to remove the additives on the surface and also it helps to increase the adhesion of deposited thin films. The glass slides were cleaned with a soap solution (labolin) further cleaned with lab grade acetone and gently rubbed with tissue paper. Before deposition glass slides were kept in hot air oven and temperature was maintained at  $200^{\circ}\text{C}$  for 2 hr to remove the impurity content. Molybdenum boat has been used to evaporate CdSe (Alfa Aesar 99.995%), ZnSe (Alfa Aesar 99.995%) to prepare  $\text{Cd}_{(1-x)}\text{Zn}_{(x)}\text{Se}$  thin films, in which value 'x' was varied from 0, 0.2, 0.4, 0.6, 0.8 & 1. These films were deposited at 453 K and vacuum annealed at 453 K for 1hr and 2 hr separately.

The thickness of the deposited thin films was determined by the gravimetric method and it was found vary from 350 nm to 450 nm. The surface morphology and elemental composition of the grown thin films were analyzed using the scanning electron microscope (Carl Zeiss FE-SEM) with a linked electron dispersion X-ray (EDAX) detector, operating at an accelerating voltage of 5 KeV. The structural characterization

of the films was carried out by X-ray diffractometer (Rigaku Miniflex 600) using nickel-filtered copper  $K\alpha$  radiation with wavelength ( $\lambda$ ) = 1.5418 Å. The optical absorbance and transmittance spectra of prepared thin films were measured at room temperature in the spectral range 300 nm - 1500 nm using double beam spectrophotometer (Shimadzu 3600 UV-VIS-NIR). The resistance of thin films has been measured using the two-probe method in the temperature range of 300 K – 573 K, with silver (Ag) as an ohmic contact.

### 5.1.3 Results and discussion

X-ray diffraction (XRD) studies were carried out on prepared CdZnSe thin film samples and the diffraction patterns were analyzed to gain information about various structural aspects.

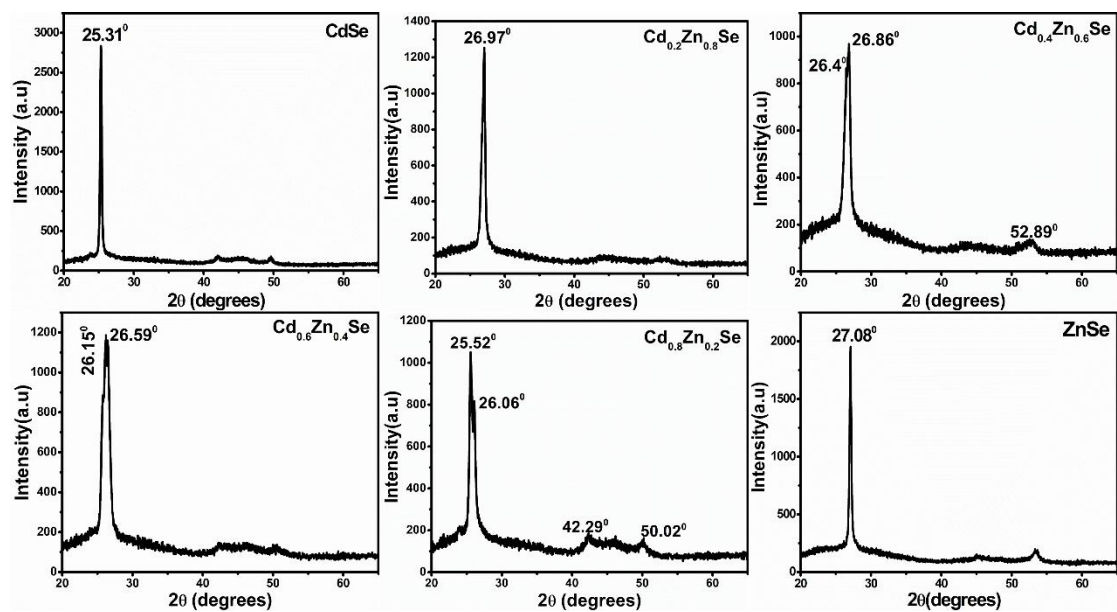


**Figure 5.1** X-Ray diffraction patterns of  $Cd_{(1-x)}Zn_{(x)}Se$  ( $x = 0 - 1$ ) thin films annealed for 1hr.

Figure.5.1 shows X-ray diffraction (XRD) patterns of 1hr vacuum annealed  $Cd_{(1-x)}Zn_{(x)}Se$  ( $x = 0 - 1$ ) thin films. It is observed that dominant peaks in XRD spectra of  $Cd_{(1-x)}Zn_{(x)}Se$  ( $x = 0.2 - 0.8$ ) system contains shoulder peaks, which indicates the presence of more than one phase. This is evidenced by the sideband peaks which appear on the right and left shoulder of each primary peak. Splitting of x-ray reflections which they ascribe to a distortion introduced by the Zn to CdSe.

Figure 5.2 shows X-ray diffraction (XRD) patterns of 2hr vacuum annealed  $\text{Cd}_{(1-x)}\text{Zn}_x\text{Se}$  ( $x = 0 - 1$ ) thin films. XRD measurements show that the preferred (002) reflection shifted continuously from  $25.24^\circ$  (of CdSe), to  $27.08^\circ$  (of ZnSe) with increasing ZnSe concentration from  $x = 0$  to 1 respectively (figure.5.3). The presence of high intensity (002) peak in all the compositions ( $x = 0 - 1$ ) reveals the formation of the alloys of  $\text{Cd}_{(1-x)}\text{Zn}_x\text{Se}$  ( $x = 0 - 1$ ) system as shown in figure 5.3. The relative intensity of peaks increased with increase in Zn concentration. XRD patterns exhibit the polycrystalline nature of the deposited films. The d-values for the various peaks were calculated using the Bragg's relation (Ahmad 2016). The surface of the deposited films was smooth and well adhered to the substrates.

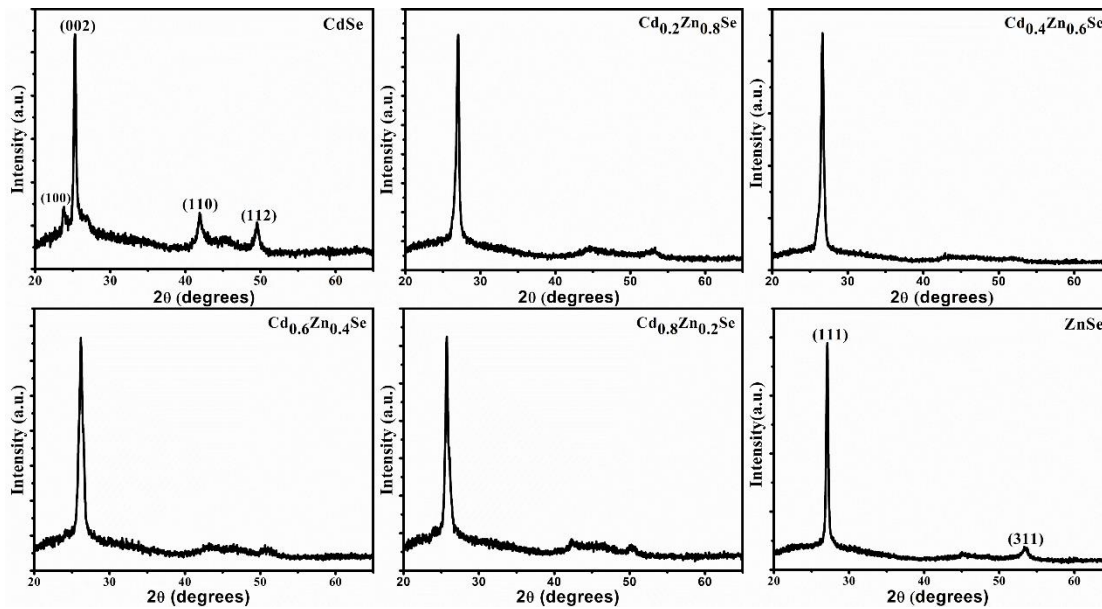


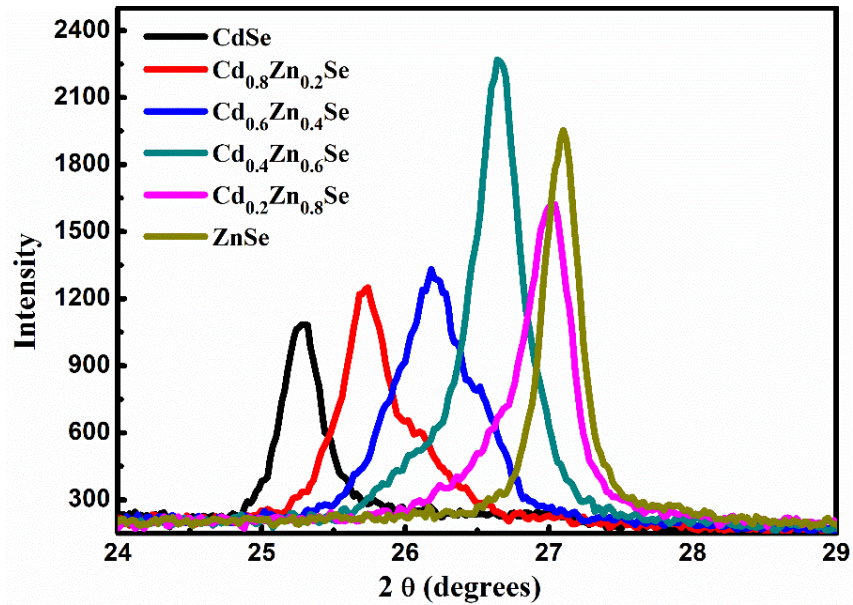
**Figure 5.2** X-Ray diffraction Patterns of  $\text{Cd}_{(1-x)}\text{Zn}_x\text{Se}$  ( $x = 0 - 1$ ) thin films annealed for 2 hr.

The obtained XRD patterns show that films of  $\text{Cd}_{(1-x)}\text{Zn}_x\text{Se}$  ( $x = 0, 0.2, 0.4, 0.6, 0.8$ ) have a hexagonal structure whereas  $\text{ZnSe}$  ( $x = 1$ ) has a cubic crystal structure as confirmed from the JCPDS data (for CdSe: 008-0459 & ZnSe: 005-0522) (Pawar et al. 2016). The lattice parameter's 'a' and 'c' for hexagonal structure can be calculated from the relation (Nasir et al. 2015). Earlier studies on films of  $\text{Cd}_{(1-x)}\text{Zn}_x\text{Se}$  system prepared using different techniques other than thermal evaporation revealed the presence of hexagonal (wurtzite) or mixed phase or cubic (zinc blende) depending on the composition of the films (Husain et al. 2003).



**Table 5.1** X-Ray diffraction data of  $\text{Cd}_{(1-x)}\text{Zn}_{(x)}\text{Se}$  ( $x = 0 - 1$ ) evaporated thin films.

Samples	2 $\theta$ (degree)	Plane (h k l)	Inter-planer spacing (d) Å	Grain size (D) (nm)	a (Å)	c (Å)
CdSe	25.24	(002)	3.52	26.85	4.30	7.04
	41.92	(110)				
	49.39	(112)				
Cd <sub>0.8</sub> Zn <sub>0.2</sub> Se	25.73	(002)	3.45	20.41	4.33	6.91
	42.42	(110)	2.12			
	50.12	(112)	1.81			
Cd <sub>0.6</sub> Zn <sub>0.4</sub> Se	26.17	(002)	3.40	20.63	4.28	6.80
	50.98	(112)	1.79			
Cd <sub>0.4</sub> Zn <sub>0.6</sub> Se	26.61	(002)	3.34	20.92	4.21	6.68
	51.60	(112)	1.76			
Cd <sub>0.2</sub> Zn <sub>0.8</sub> Se	26.98	(002)	3.30	22.13	3.96	6.60
	45.34	(103)	1.98			
ZnSe	27.08	(111)	3.29	29.81	5.69	

**Figure 5.3** Shift in the (002) peak for  $\text{Cd}_{(1-x)}\text{Zn}_{(x)}\text{Se}$  ( $x = 0 - 1$ ) system.

The crystallite size  $D$  (nm) of the investigated films was calculated by using the Scherer's formula (2.3.2) (table 5.1). Grain size decreases suddenly by introducing Zn into CdSe ( $x = 0.2$ ) and the marginal increase in the grain size was observed for the remaining compositions (0.2 - 1). The decrease in the grain size is an indication of deterioration of crystallinity of the films. The intensity of the peaks increases as the Zn concentration increases resulting in improved crystallinity of the deposited thin films.

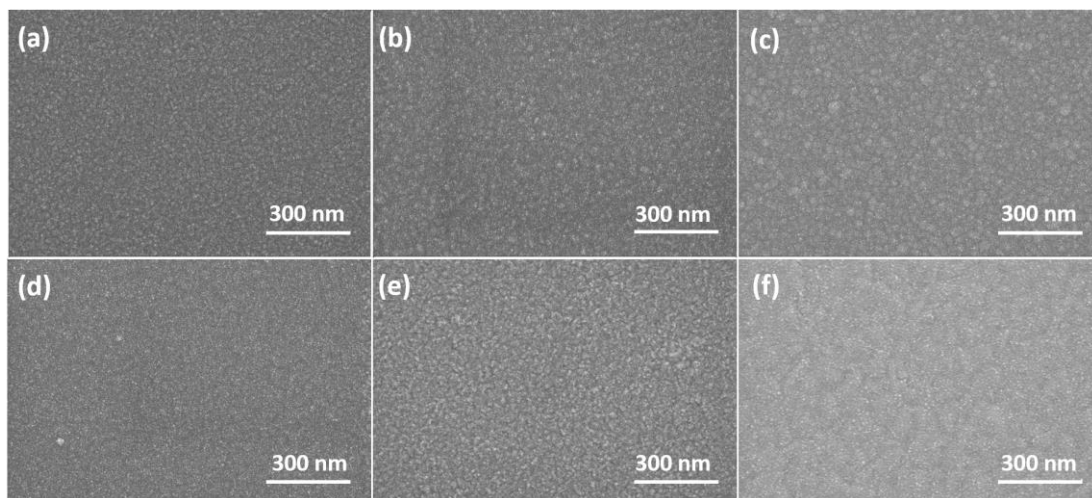


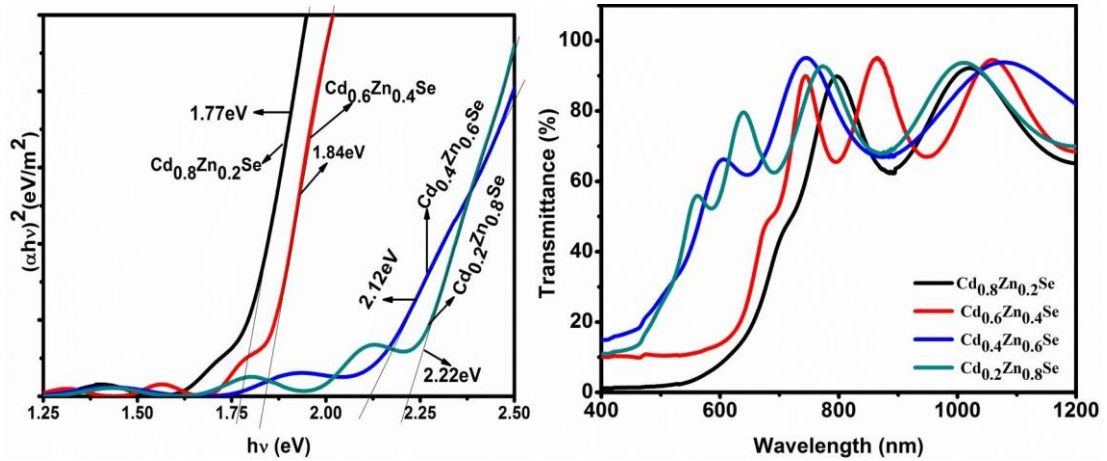
**Figure 5.4** FE-SEM images of  $\text{Cd}_{(1-x)}\text{Zn}_{(x)}\text{Se}$  thin films. a) CdSe, b)  $\text{Cd}_{0.8}\text{Zn}_{0.2}\text{Se}$ , c)  $\text{Cd}_{0.6}\text{Zn}_{0.4}\text{Se}$  d)  $\text{Cd}_{0.4}\text{Zn}_{0.6}\text{Se}$ , e)  $\text{Cd}_{0.2}\text{Zn}_{0.8}\text{Se}$ , f) ZnSe.

**Table 5.2** Compositional analysis of  $\text{Cd}_{(1-x)}\text{Zn}_{(x)}\text{Se}$  ( $x = 0 - 1$ ) thin films.

$\text{Cd}_{(1-x)}\text{Zn}_{(x)}\text{Se}$	Cd (at.%)	Zn (at.%)	Se (at.%)
<b>CdSe</b>	50.34		49.66
<b><math>\text{Cd}_{0.8}\text{Zn}_{0.2}\text{Se}</math></b>	40.19	9.21	50.6
<b><math>\text{Cd}_{0.6}\text{Zn}_{0.4}\text{Se}</math></b>	32.58	19.24	48.18
<b><math>\text{Cd}_{0.4}\text{Zn}_{0.6}\text{Se}</math></b>	19.81	30.70	49.50
<b><math>\text{Cd}_{0.2}\text{Zn}_{0.8}\text{Se}</math></b>	8.9	41.82	49.29
<b>ZnSe</b>		49.89	50.11

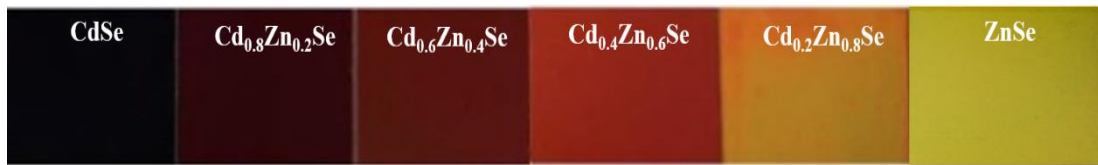
Morphological and compositional analysis has been carried out using FE-SEM and EDAX. Figure. 5.4 shows FE-SEM micrographs of  $\text{Cd}_{(1-x)}\text{Zn}_{(x)}\text{Se}$  ( $x = 0 - 1$ ) thin films. SEM micrographs of deposited films are homogenous throughout the deposited area with fine grains. EDAX analysis (table 5.2) confirms the presence of Cd, Zn, and Se in the deposited thin films. The stoichiometric composition was achieved for the deposited alloyed  $\text{Cd}_{(1-x)}\text{Zn}_{(x)}\text{Se}$  ( $x = 0 - 1$ ) films.

Optical absorbance and transmission measurements were carried out on deposited  $\text{Cd}_{(1-x)}\text{Zn}_{(x)}\text{Se}$  ( $x = 0 - 1$ ) thin films in the wavelength range of 300 nm – 1500 nm. Figure 5.5 represents the Tauc's plot and transmittance spectra of  $\text{Cd}_{(1-x)}\text{Zn}_{(x)}\text{Se}$  ( $x = 0.2 - 0.8$ ) thin films deposited at 453 K and vacuum annealed for 1hr. It is observed that there is an improper shift in the band edges. Optical band gap of  $\text{Cd}_{(1-x)}\text{Zn}_{(x)}\text{Se}$  ( $x = 0 - 1$ ) thin films varied from 1.67 eV to 2.61 eV.



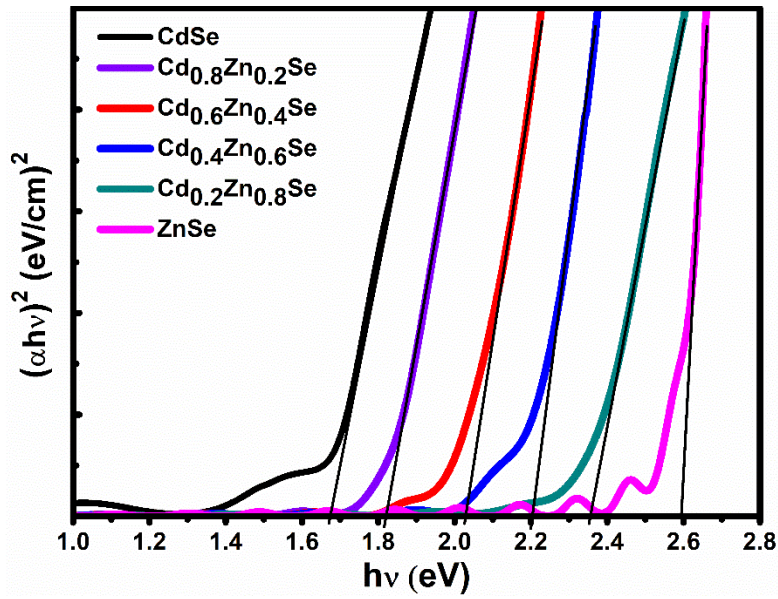
**Figure 5.5** Tauc's plot and transmittance spectra of  $\text{Cd}_{(1-x)}\text{Zn}_{(x)}\text{Se}$  ( $x = 0.2 - 0.8$ ) films

Figure 5.6 shows the variation in the visible color of  $\text{Cd}_{(1-x)}\text{Zn}_{(x)}\text{Se}$  ( $x = 0 - 1$ ) thin films deposited at 453 K and vacuum annealed for 2 hr. The color of deposited CdSe film is reddish black and changes to lemon yellow as Zn content increases.



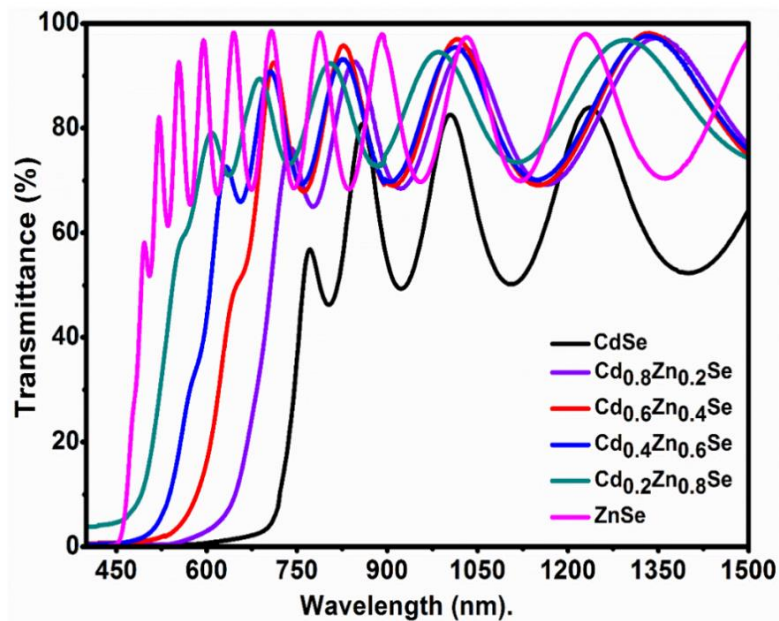
**Figure.5.6:** Deposited  $\text{Cd}_{(1-x)}\text{Zn}_{(x)}\text{Se}$  ( $x = 0 - 1$ ) thin films.

**Figure 5.7** shows the Tauc's plot and transmittance spectra of  $\text{Cd}_{(1-x)}\text{Zn}_{(x)}\text{Se}$  ( $x = 0 - 1$ ) thin films. The absorption edge for the deposited thin films was observed to shift to lower wavelength as the concentration of Zn is increased. The optical band gap energy ( $E_g$ ) of these films were determined with the help of absorption spectra using Tauc's relation (2.3.6). The Optical band gap ( $E_g$ ) was deduced by extrapolating the straight portion to energy axis at  $\alpha = 0$ . The calculated band gap of these films is tabulated in table 5.3. It is found that the optical energy band gap of the  $\text{Cd}_{(1-x)}\text{Zn}_{(x)}\text{Se}$  ( $x = 0 - 1$ ) thin films varied from 1.67 eV to 2.60 eV (figure.5.10). The band gap energy for pure CdSe and ZnSe thin films was found to be 1.67 eV and 2.60 eV respectively, close to previously reported data Samarth et al. 1990.



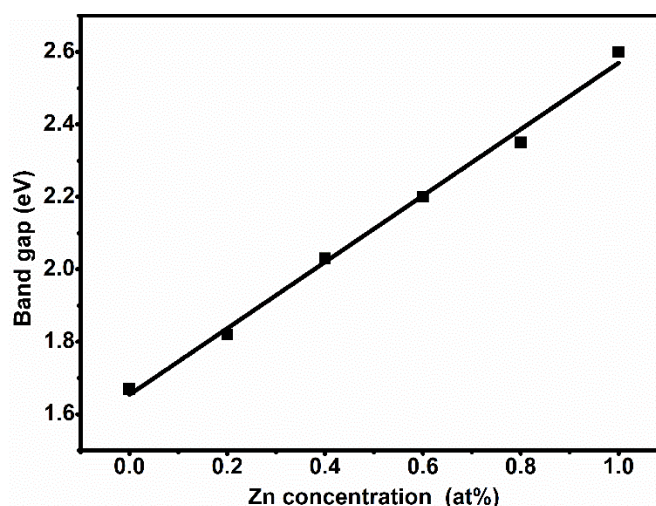
**Figure. 5.7** Tauc's Plot of  $\text{Cd}_{(1-x)}\text{Zn}_{(x)}\text{Se}$  thin films ( $x = 0 - 1$ ).

Figure 5.8 shows the transmittance spectra of  $\text{Cd}_{(1-x)}\text{Zn}_{(x)}\text{Se}$  thin films. Transmittance Spectra is one of the productive result helpful in understanding band structure and the energy gap of both amorphous and crystalline systems. Interference fringes in the transmittance spectra indicate the uniformity and quality of the deposited  $\text{Cd}_{(1-x)}\text{Zn}_{(x)}\text{Se}$  thin films. Increase in the transmittance was observed with an increase in Zn concentration. Absorption edges were blue shifted as the Zn concentration ( $x$ ) varied from 0 - 1.



**Figure 5.8** Transmittance spectra of  $\text{Cd}_{(1-x)}\text{Zn}_{(x)}\text{Se}$  thin films ( $x = 0 - 1$ ).

Figure 5.9 shows the variation of energy band gap ( $E_g$ ) with Zn concentration. The energy band gap ( $E_g$ ) is observed to be varying almost linearly with the incorporation of Zn into the CdSe (Figure.5.8). This is an evidence for the formation of homogeneous and alloyed  $Cd_{(1-x)}Zn_{(x)}Se$  thin films by thermal evaporation.



**Figure 5.9** Variation of optical band gap v/s Zn concentration.

Electrical measurements were carried out for the alloyed films. The electrical conductivity of the alloyed films was measured in dark, the conductivity decreases with increased incorporation of  $Zn^{2+}$  ions into the hexagonal CdSe. To evaluate the thermal activation energy, the resistance of the alloyed films was recorded as a function of temperature ranging from 300 K - 473 K. Resistance of alloyed films decreases with increase in temperature exhibiting the semiconducting behavior. Figure 5.10 shows the variation of  $\ln(R)$  versus inverse temperature for  $Cd_{(1-x)}Zn_{(x)}Se$  thin films.

**Table 5.3** Energy band gap ( $E_g$ ) and activation energy ( $E_a$ ) values of  $Cd_{(1-x)}Zn_{(x)}Se$  ( $x=0-1$ ).

Samples	Optical band gap (eV)	Activation energy (eV)
CdSe	1.67	0.37
$Cd_{0.8}Zn_{0.2}Se$	1.82	0.72
$Cd_{0.6}Zn_{0.4}Se$	2.03	0.76
$Cd_{0.4}Zn_{0.6}Se$	2.20	0.80
$Cd_{0.2}Zn_{0.8}Se$	2.35	0.85
ZnSe	2.60	-

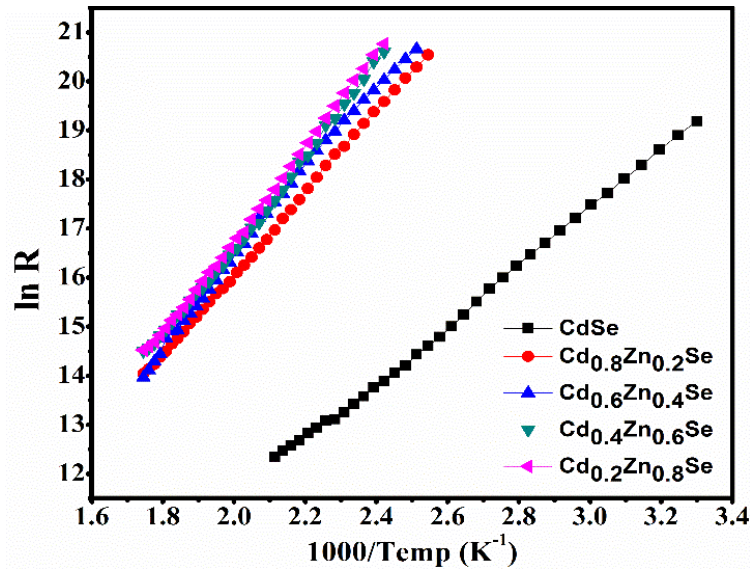


**Figure 5.10** Variation of  $\ln R$  vs  $1000/T$ , ( $K^{-1}$ ) of  $Cd_{(1-x)}Zn_{(x)}Se$  thin films.

Thermal activation energy ( $E_a$ ) was calculated from the slope of straight line parts of the plots. Table 5.3 it is found that activation energy increases from 0.37 eV to 0.85 eV with increase in Zn concentration ( $x = 0 - 0.8$ ) in the CdSe thin films.

## 5.2 PREPARATION AND CHARACTERIZATION OF CdSeTe THIN FILMS.

### 5.2.1 Introduction

In II-VI group, cadmium selenide (CdSe) and cadmium telluride (CdTe) are the two binary compound semiconductors. In recent years ternary alloys of these compound semiconductors are potential and interesting candidates in the field of optoelectronic devices (Chen et al. 2014; Kathalingam et al. 2010; Zeng et al. 2017; Zhao et al. 2016). The major advantages of these materials are their stability as nano-crystallites, excellent photoelectric properties with high optical absorption, and most favorable bang gap for solar energy conversion (Babu et al. 1991; Loizos et al. 1993; Loizos and Spyrellis 1989). The physical properties of  $CdSe_{(1-x)}Te_{(x)}$  system in sense of technological importance is of great interest in the production of advanced optoelectronic devices (Benyettou et al. 2015). These thin films have been prepared by various techniques like molecular beam epitaxy, thermal evaporation, electrodeposition, hot wall deposition. Both CdSe and CdTe exist in either hexagonal wurtzite or cubic zinc-blende structure. In case of  $CdSe_{(1-x)}Te_{(x)}$  system, lattice parameters, crystal structure and band gap

tuning can be done by controlling stoichiometry (Se/Te ratio) (Poplawsky et al. 2016; Shinde et al. 2013).

Earlier research work on cadmium chalcogenides indicates that the band gap of  $\text{CdSe}_{(1-x)}\text{Te}_{(x)}$  system can be tuned by varying Se & Te concentration. Some researchers observed linear variation in band gap (Kathalingam et al. 2010; Murali and Jayasutha 2009) and some of the studies reveal the band gap bowing behavior (Macdonald et al. 2012; Mourad et al. 2010; Zeng et al. 2015). To achieve high efficiency single and multijunction solar cells, controlling of the band gap of the absorber layer is required. The addition of CdSeTe layers results in the improved current collection at long wavelengths (Swanson et al. 2017). In the present work, an attempt has been made to grow  $\text{CdSe}_{(1-x)}\text{Te}_{(x)}$  thin films by varying  $x$  (0 to 1) using thermal evaporation method. Optical band gap of CdSeTe alloyed thin films was measured to evaluate material behavior as the tellurium incorporation increased in the films.

### 5.2.2 Experimental method

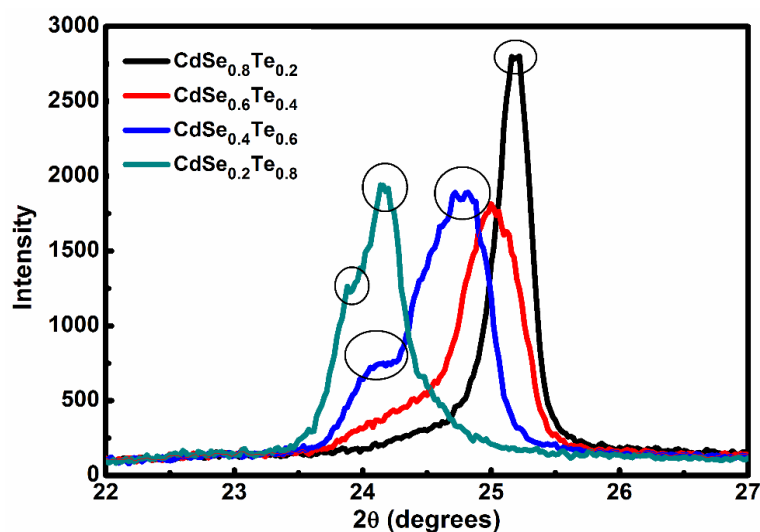
$\text{CdSe}_{(1-x)}\text{Te}_{(x)}$  thin films of different compositions ( $x = 0 - 1$ ) have been deposited on glass substrates by the thermal evaporation technique at a pressure of  $10^{-5}$  Torr. High purity CdSe (99.995%) and CdTe (99.99%) powders were used to prepare  $\text{CdSe}_{(1-x)}\text{Te}_{(x)}$  thin films in which value 'x' was varied from 0, 0.2, 0.4, 0.6, 0.8 & 1 and evaporated from a single boat source. Annealing duration was optimized to get good quality of thin films. The prepared thin films were subjected to characterization in order to understand the structural and optical aspects and to achieve properties for the technological requirements. Films were deposited at 453 K substrate temperature ( $T_s$ ) and post-deposition vacuum annealing was conducted at the same temperature. After deposition, vacuum annealing was done for two different durations, 120 min and 150 min. The thickness of the deposited thin films was estimated by gravimetric method and it is found to vary from 450 nm to 500 nm.

The surface morphology and chemical composition of the grown thin films were analyzed using the scanning electron microscope (Carl Zeiss FE-SEM) with a linked electron dispersion X-ray (EDAX) detector, operating at an accelerating voltage of 5 KV. Structural studies of  $\text{CdSe}_{(1-x)}\text{Te}_{(x)}$  thin films were carried out by Rigaku Miniflex 600 X-ray diffractometer ( $\lambda=1.54 \text{ \AA}$ ) in the  $2\theta$  range  $20^\circ - 65^\circ$ . The optical absorbance

and transmittance spectra of prepared thin films were measured at room temperature in the spectral range 300 nm - 1500 nm using double beam spectrophotometer (Shimadzu 3600 UV-VIS-NIR).

### 5.2.3 Results and discussion

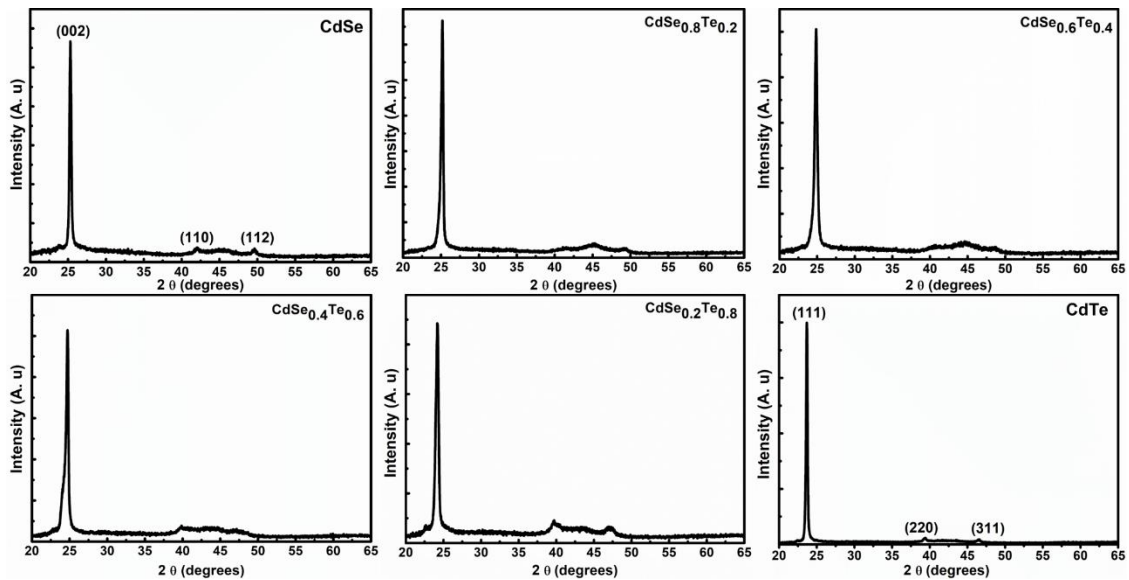
Figure 5.11 represents the X-ray diffraction (XRD) patterns of 120 min vacuum annealed  $\text{CdSe}_{(1-x)}\text{Te}_{(x)}$  ( $x = 0.2 - 0.8$ ) thin films. It is observed that predominant peaks in XRD spectra of  $\text{CdSe}_{(1-x)}\text{Te}_{(x)}$  system contain shoulder peaks, indicating the presence of more than one phase. The splitting of a strong peak in each composition is ascribed as distortion introduced by the Te to CdSe due to insufficient annealing duration. Substrate temperature, annealing temperature, annealing duration, vapor pressure, sticking coefficient, deposition rate and evaporation temperature are the key parameters having great importance in the formation of any binary or ternary compounds. Each element in this system having different vapor pressure leads to excess or deficiency of elements in the ternary compounds.



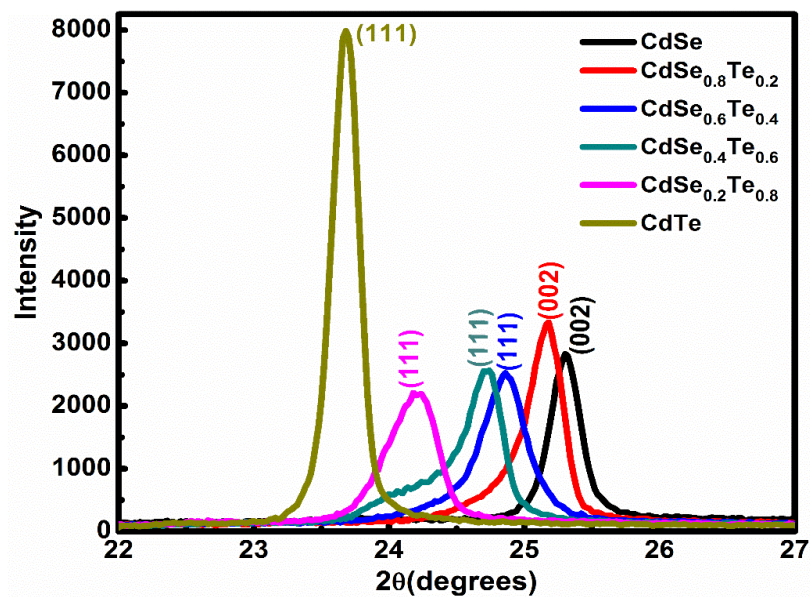
**Figure 5.11** X-ray diffraction of 120 min annealed  $\text{CdSe}_{(1-x)}\text{Te}_{(x)}$  ( $x = 0.2 - 0.8$ ) thin films.

Figure. 5.12 represents the XRD patterns of 150 min vacuum annealed  $\text{CdSe}_{(1-x)}\text{Te}_{(x)}$  ( $x = 0 - 1$ ) thin films. The XRD patterns of deposited films have more than one peaks indicates polycrystalline nature. The presence of sharp strong peak in each individual composition reveals the formation of  $\text{CdSe}_{(1-x)}\text{Te}_{(x)}$  ternary alloyed thin films.





**Figure 5.12** X-ray diffraction patterns of 150 min annealed  $\text{CdSe}_{(1-x)}\text{Te}_{(x)}$  ( $x=0-1$ ) thin films.



**Figure 5.13** Shift in the predominant peak of  $\text{CdSe}_{(1-x)}\text{Te}_{(x)}$  ( $x=0-1$ ) thin films.

The XRD pattern of the pure CdSe thin films shows a preferentially oriented peak along (002) at  $2\theta = 25.25^\circ$ , which is in good agreement with standard JCPDS data (008-0459) of CdSe powder for hexagonal crystal structure. Similarly, the X-ray diffraction spectra of pure CdTe thin films show a strong peak at  $2\theta = 23.68^\circ$ , which corresponds to (111) reflection having cubic zinc blende structure (JCPDS data: 010-0207).  $\text{CdSe}_{(1-x)}\text{Te}_{(x)}$  compound with  $x = 0.2$  is found to exhibit hexagonal crystal structure with

preferred orientation along (002) plane and other low intensive peaks at  $41.92^\circ$  and  $49.39^\circ$  corresponds to (103), (112) planes respectively.  $\text{CdSe}_{(1-x)}\text{Te}_{(x)}$  thin films with compositions  $x = 0.4, 0.6$  and  $0.8$  are cubic zinc blend with preferred oriented along (111) and other small intensive peaks of (220) & (311) plane.

The inter planer distance (d) of prepared thin films was evaluated using Bragg's relation, which is in good agreement with standard JCPDS data. Addition of Te to the lattice of CdSe increases the d- spacing from 3.52 ( $x = 0$ ) for pure CdSe to 3.75 ( $x = 1$ ) for pure CdTe which resulted in the peak shift towards lower diffraction angle ( $2\theta$ ). The lattice constant 'a' for the cubic system was determined using equation 2.3.3. The lattice parameters for hexagonal crystal system calculated using equation 2.3.4.

**Table 5.4** Structural parameters of  $\text{CdSe}_{(1-x)}\text{Te}_{(x)}$  ( $x = 0 - 1$ ) thin films.

Sample	$2\theta$ (degrees)	Plane (h k l)	Inter planer spacing (d) (Å)	Grain size (D) (nm)	a(H)	c(H)	a(C)
<b>CdSe</b>	25.24	(002)	3.52	26.85	4.30	7.04	CdSe
<b>CdSe<sub>0.8</sub>Te<sub>0.2</sub></b>	25.15	(002), (111)	3.53	29.47	4.31	7.07	6.12
	45.31	(103)	1.99				
	49.42	(112)	1.84				
<b>CdSe<sub>0.6</sub>Te<sub>0.4</sub></b>	24.84	(111)	3.58	21.12			6.20
<b>CdSe<sub>0.4</sub>Te<sub>0.6</sub></b>	24.71	(111)	3.59	25.40			6.22
	39.81	(220)	2.26				
	47.33	(311)	1.91				
<b>CdSe<sub>0.2</sub>Te<sub>0.8</sub></b>	24.22	(111)	3.66	28.77			6.35
	39.67	(220)	2.26				
	47.21	(311)	1.92				
<b>CdTe</b>	23.67	(111)	3.75	41.18			6.49
	39.33	(220)	2.28				
	46.49	(311)	1.95				

From the X-Ray diffraction patterns it is observed that as the 'Te' concentration increases crystal structure of  $\text{CdSe}_{(1-x)}\text{Te}_{(x)}$  system changes from hexagonal ( $x = 0 - 0.2$ ) to stable cubic zinc blende structure ( $x = 0.4 - 1$ ). Similar kind of observations was made by other researchers (Brill et al. 2005; Chen et al. 2003; Poplawsky et al. 2016) where films were prepared by different techniques. X-ray diffraction measurements shows that the strong peak in all the composition ( $x = 0 - 1$ ) shifted continuously towards lower diffraction angle ( $2\theta$ ) as the tellurium (Te) content increases from ( $x = 0$

– 1) (Figure 5.13). The X-ray diffraction studies reveal that the crystal structure of CdSe and CdTe are different but very closely related which allows the transition from one phase to another phase, depending on the selenium and tellurium contents (Muthukumarasamy et al. 2007). The crystallite size ‘D’ (nm) of the thin films was evaluated using Scherrer’s formula.

From the table 5.4 it is observed that the grain size increases at  $x = 0.2$  and decreases at composition  $x = 0.4$  but for higher tellurium content ( $x = 0.6 - 1$ ) grain size continuously increases. It may be mentioned that the decrease in the crystallite size occurs at  $x = 0.4$ , where there is a change in the crystal structure from hexagonal to cubic and associated lattice distortion due to the incorporation of tellurium into the CdSe lattice.

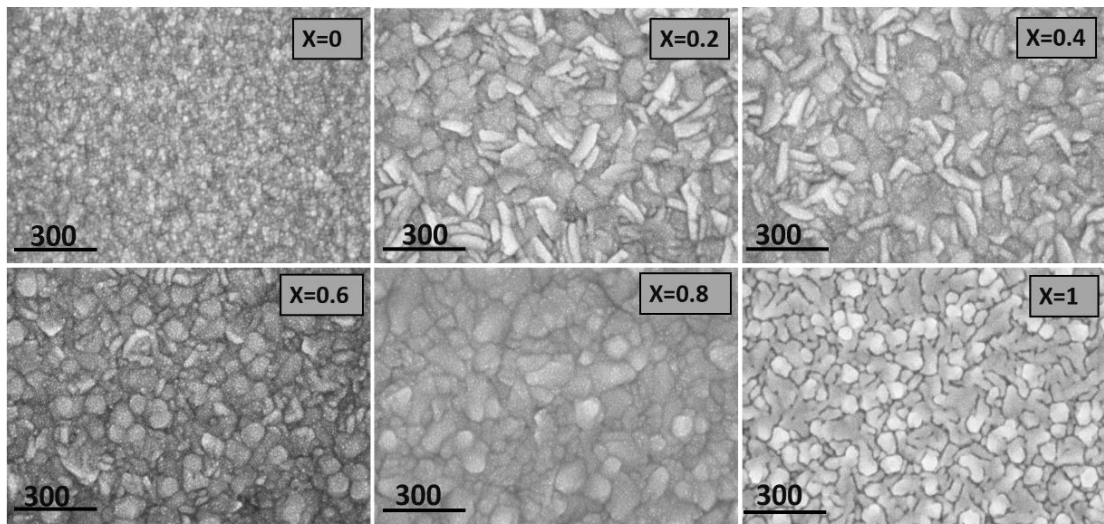


**Figure 5.14** FE-SEM micrographs of 150 min annealed  $\text{CdSe}_{(1-x)}\text{Te}_{(x)}$  ( $x = 0-1$ ) thin films.

Surface topography and elemental analysis have been carried out using Field Emission Scanning Electron Microscope (FE-SEM) and Energy Dispersive Analysis X-Ray (EDAX). Figure 5.14 shows the FE-SEM micrographs of 150 min vacuum annealed  $\text{CdSe}_{(1-x)}\text{Te}_{(x)}$  ( $x = 0 - 1$ ) thin films. The FE-SEM micrographs reveal that microstructure of  $\text{CdSe}_{(1-x)}\text{Te}_{(x)}$  thin films changes as the tellurium (Te) concentration increase. Energy dispersive X-ray analysis (EDAX) is a convenient method employed to extract the information regarding the existence of elements in the deposited films.

EDAX data of 150 min vacuum annealed  $\text{CdSe}_{(1-x)}\text{Te}_{(x)}$  ( $x = 0 - 1$ ) thin films was tabulated in the table 5.5.

**Table 5.5** Elemental analysis of  $\text{CdSe}_{(1-x)}\text{Te}_{(x)}$  ( $x = 0 - 1$ ) thin films.

$\text{CdSe}_{(1-x)}\text{Te}_{(x)}$	Cd (at.%)	Se (at%)	Te (at%)
<b>CdSe</b>	50.94	49.05	
<b>CdSe<sub>(0.8)</sub>Te<sub>(0.2)</sub></b>	50.81	40.11	9.08
<b>CdSe<sub>(0.6)</sub>Te<sub>(0.4)</sub></b>	51.04	30.96	18.00
<b>CdSe<sub>(0.4)</sub>Te<sub>(0.6)</sub></b>	50.68	17.55	31.77
<b>CdSe<sub>(0.2)</sub>Te<sub>(0.8)</sub></b>	50.33	8.91	40.76
<b>CdTe</b>	49.87		50.13

Compositional analysis confirms the existence of Cd, Se & Te contents in the prepared  $\text{CdSe}_{(1-x)}\text{Te}_{(x)}$  ( $x = 0 - 1$ ) thin films. Near stoichiometric composition was achieved for the  $\text{CdSe}_{(1-x)}\text{Te}_{(x)}$  alloyed films. In  $\text{CdSe}_{(1-x)}\text{Te}_{(x)}$  system, each element has different melting point and vapor pressure. In these elements, Selenium is having the lowest melting point compared to other two elements (Cd and Te) and also highest vapor pressure at the evaporation temperature. Due to this property of selenium, thin films will be selenium deficient. Sticking coefficient ( $S_{\text{Te}} > S_{\text{Cd}} > S_{\text{Se}}$ ) also plays an important role in the formation of stoichiometric alloyed compounds.

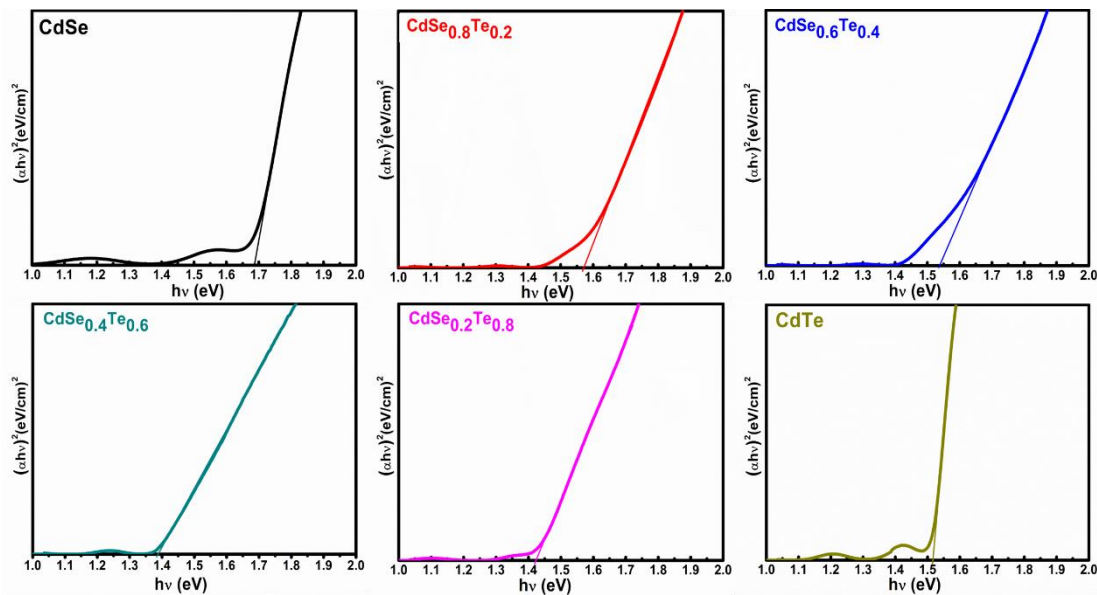


**Figure 5.15 A.** Tauc's plot of 150 min annealed  $\text{CdSe}_{(1-x)}\text{Te}_{(x)}$  ( $x=0-1$ ) thin films.

The optical band gap was determined from absorption spectra of thin films. Figure 5.15 shows  $(\alpha h\nu)^2$  vs photon energy ( $h\nu$ ) plots for 150 min vacuum annealed  $\text{CdSe}_{(1-x)}\text{Te}_{(x)}$  ( $x = 0 - 1$ ) thin films. The band gap values are tabulated in table 5.6. Extrapolation of straight line portion in the plot for absorption coefficient ( $\alpha$ ) = 0 gives the energy band gap value. Linear nature in the plots indicates direct bandgap nature of prepared thin films. The band gap of  $\text{CdSe}_{(1-x)}\text{Te}_{(x)}$  is shifted to lower values with an increase in the tellurium (Te) concentration in the CdSe films. The variation of band gap with CdTe concentration is shown in figure 5.16.

**Table 5.6** Optical band gap of  $\text{CdSe}_{(1-x)}\text{Te}_{(x)}$  ( $x=0 - 1$ ) thin films.

Sample	Band gap (eV)
CdSe	1.68
$\text{CdSe}_{0.8}\text{Te}_{0.2}$	1.57
$\text{CdSe}_{0.6}\text{Te}_{0.4}$	1.53
$\text{CdSe}_{0.4}\text{Te}_{0.6}$	1.39
$\text{CdSe}_{0.2}\text{Te}_{0.8}$	1.42
CdTe	1.51

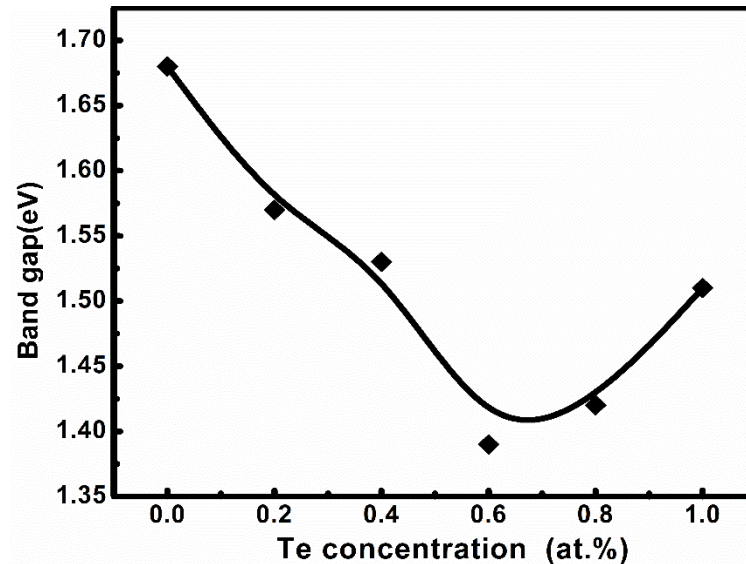


**Figure 5.16** Variation of band gap with Te concentration (at. %).

The band gap decreases from 1.67 eV (CdSe) to 1.39 eV ( $x = 0.6$ ) with an increase in Te concentration and then for higher Te concentration band gap increases to 1.51 eV corresponds to pure CdTe. It is observed that the variation in the band gap with

composition exhibits band gap bowing in a quadratic form. Similar band gap bowing behavior in  $\text{CdSe}_{(1-x)}\text{Te}_{(x)}$  system was reported by several workers (Benamar et al. 1999; Muthukumarasamy et al. 2009). Mismatch in the electro-negativity of anions like Te & Se playing an important role in band gap bowing in some of the II-VI ternary alloys, which was explained by Nacir Tit et al., using theoretical models (Tit et al. 2009).

## CHAPTER 6

### HETEROJUNCTIONS OF PURE AND DOPED CdSe FILMS WITH SILICON.

#### *Overview*

In this chapter, the electrical properties of pure n-CdSe/p-Si, (Ag, Bi and In) doped n-CdSe/p-Si heterojunctions prepared separately by thermal evaporation has been described. The temperature dependent dark current-voltage characteristics has been studied to understand the carrier transport mechanism in the fabricated diode. The capacitance-voltage characteristics of fabricated heterojunctions have been discussed.

#### 6.1 INTRODUCTION

The advances in nanoscience and nanotechnology in recent years have opened new opportunities for the applications of II–VI semiconductors. Heterojunctions belonging to II-VI group have received much consideration because of their potential optoelectronic applications over a wide range of wavelengths (Al-Kotb et al. 2014; Amir et al. 2008; Borah et al. 2008; Chaliha et al. 2010; Chen et al. 2003; Rao et al. 2013). These II-VI semiconductor thin films could be the building blocks for cheap and efficient solar cells. High ionicity of these compounds makes them good candidates for a variety of emerging areas, such as X-ray detectors for medical imaging and diagnostics, photovoltaic, photoconduction (Russak et al. 1980), biotechnology (Al-Kotb et al. 2014). Recently various materials (CdS, CdTe, ZnTe, ZnSe, ZnO, CdSeTe, CdZnTe, CdZnSe) have been developed to fabricate several devices such as a polymer, metallic oxide, ferroelectric, organics, inorganic nanomaterials etc. Among these materials, one-dimensional (1D), two- dimensional (2D) nanostructures are considered as ideal platforms for exploring innovative phenomena at the nanoscale, and investigating the sizes and dimensionality dependence of functional properties (Ashry and Fares 2012; Konda et al. 2007; Wu et al. 2017). Several techniques like molecular beam epitaxy, thermal evaporation (Borah et al. 2008; Chaliha et al. 2008), spray pyrolysis, CBD, sputtering etc. have been used for the fabrication of these junctions by a good number of researchers. The In doped CdSe films have high conductivity due to the incorporation of indium (In) and therefore, they are very suitable as a window layer

in solar cells (Ashry and Fares 2012). Cadmium selenide is a promising II-VI semiconductor for optoelectronic devices and its large absorption coefficient to the visible region of solar energy spectrum gives good efficiency and has led to the investigations of efficient CdSe based devices. According to previous studies by many authors have been reported that CdSe have n-type conductivity in bulk as well as in thin film form (Al-Kotb et al. 2014; Oduor and Gould 1995; Yacobi B.G. 2003). Because of the native defects in excess Cadmium in the film produces Selenium vacancies or Cd interstitials, both of which act as donors in CdSe. As a result, the non- stoichiometry is possible in II–VI selenide leads to deep levels, inducing in the sample high electrical resistivity (Zhang et al. 1998). Thus, the native defects play an important role in the determination of conduction processes in CdSe thin films (Kurokawa and Muto 2003; Raoult et al. 1989). Owing to its specific physical properties, polycrystalline CdSe thin films recommended as a capable candidate for solar cells (Kashiwaba et al. 1994), high-efficiency thin film transistors, light emitting diodes, and nanotransistors (Wang et al. 2006). These properties have led to many investigations of CdSe and Si-based heterojunctions and Schottky barrier junctions for photovoltaic applications. A number of studies have been made on CdSe/Si structures. Several carrier transport mechanisms involved in CdSe/p-Si junctions have been reported. In the present study, the characteristics of both pure n-CdSe/p-Si and doped n-CdSe/p-Si heterojunctions, fabricated using thermal evaporation have been investigated.

## **6.2 EXPERIMENTAL DETAILS**

The heterojunctions of pure n-CdSe/p-Si and doped n-CdSe/p-Si were fabricated using thermal evaporation technique to study their electrical properties. The base pressure in the vacuum chamber during deposition was maintained at  $10^{-5}$  Torr. Boron doped p-type silicon wafers of 0.5 mm thickness was used as substrate. High purity powders of CdSe (99.995%, Alfa aesar) was used to fabricate n-CdSe/p-Si heterojunction, CdSe (99.995%, Alfa aesar) and required an amount of Ag, In powder (99.99% Alfa aesar) and Bi lumps were used as a source materials to fabricate In doped n-CdSe/p-Si heterojunctions. For electrical measurements Ag (Alfa aesar, 99.999%) was used as a metal ohmic contact for n-CdSe and similarly, Al (Alfa aesar 99.99%) for a p-type Silicon wafer. The desired pattern of the sample for electrical studies was



defined through a mask placed on the Si wafer during the deposition. The CdSe thin films were deposited on Si wafers at 453 K and then annealed at the same temperature for 1 hour in vacuum to improve the quality of CdSe films and to reduce interfacial layer. The electrical transport mechanism and rectification ratio, barrier height, ideality factors were analyzed from the temperature dependence of current-voltage (I-V-T) and capacitance-voltage (C-V) characteristics of fabricated heterojunctions. current-voltage (I-V) and capacitance-voltage characteristics were done using computer-interfaced Keithley source meter 2400 and Agilent E4980A LCZ meter respectively. Schematic representation of heterojunction structure is shown in figure 6.1. Initially, CdSe thin film of thickness  $448 \pm 5$  nm was deposited on a silicon wafer. Aluminum (Al) is ohmic for p-Si, was deposited on a silicon wafer. Finally, silver (Ag) is ohmic for n-CdSe, was deposited on the top of the CdSe thin film.



**Figure 6.1** Schematic representation of n-CdSe/p-Si heterojunction.

### 6.3 RESULTS AND DISCUSSION

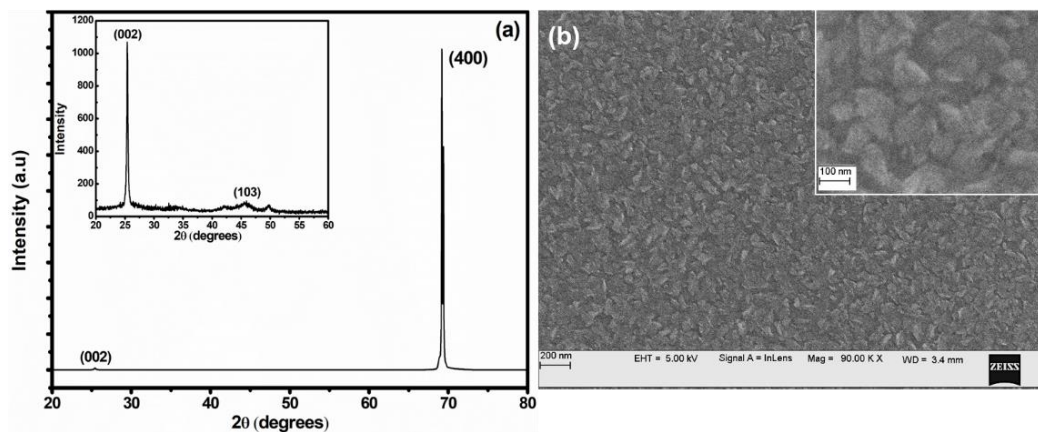


**Figure 6.2 (a)** X-Ray diffraction pattern and **(b)** FE-SEM micrographs of CdSe thin film deposited on silicon wafer.

Figure 6.2 (a) shows the XRD pattern of CdSe thin film deposited on silicon wafer, which illustrates the presence of high intensive diffraction peaks belongs to (002) and

(400) textures of hexagonal wurtzite structure of CdSe and cubic silicon wafer respectively. Other small intensive peaks of different texture such as (103) in the XRD patterns belongs to hexagonal CdSe thin films. The average grain size was calculated by well-known Scherrer's formula (eq. no. 2.3.2). The lattice parameters 'a' and 'c' were calculated using equations 2.3.3 and 2.3.4. Obtained lattice parameters and inter planer spacing (d) values are agreeing well with JCPDS data (008-0459 for CdSe, 001-0787 for Si). Figure 6.2 (b) shows the FE-SEM micrograph of CdSe thin film deposited on Si wafer. These films are uniform and homogenous. It is observed that the deposited CdSe thin films contains densely packed nano size grains without crack and pinholes. EDAX analysis has been carried out for undoped, (Ag, Bi and In) doped CdSe thin films deposited on silicon wafer. EDAX analysis reveals the presence of Si, Ag, Bi, In, Cd, and Se in respective deposited thin films. The structural and compositional data of CdSe thin films deposited on silicon wafer is given in table 6.1. There is no significant change in the structural properties of deposited Ag, Bi and In doped CdSe thin films was observed.

**Table 6.1** Structural and compositional data of CdSe thin film deposited on silicon wafer.

Sample	2 $\theta$ (degrees)	Plane (h k l)	d (Å)	D (nm)	a (Å)	C (Å)	Cd (at.%)	Se (at.%)
CdSe	25.37	(002)	3.51	40.4	4.30	7.01	49.03	50.97

There are several techniques, reported by many researchers on evaluation of series resistance ( $R_s$ ), ideality factor ( $\eta$ ), rectification ratio (RR) and barrier height ( $\phi_b$ ) from temperature dependent I-V studies (Borah et al. 2008; Castillo-Alvarado et al. 2010; Chand and Kumar 1996; Rao et al. 2013). In the present study, temperature dependence of current(I) - voltage(V) characteristics of undoped n-CdSe/p-Si, Ag doped n-CdSe/p-Si, Bi doped n-CdSe/p-Si and In doped n-CdSe/p-Si heterojunctions were studied by varying temperature from 303 K – 390 K. Figure 6.3 (a-d) shows the temperature-dependent I-V curves of undoped and (Ag, Bi and In) doped CdSe/p-Si heterojunctions. It is observed that the rectifying behavior of current with voltage can be evaluated as an indication of a typical p-n junction diode (Konda et al. 2007).

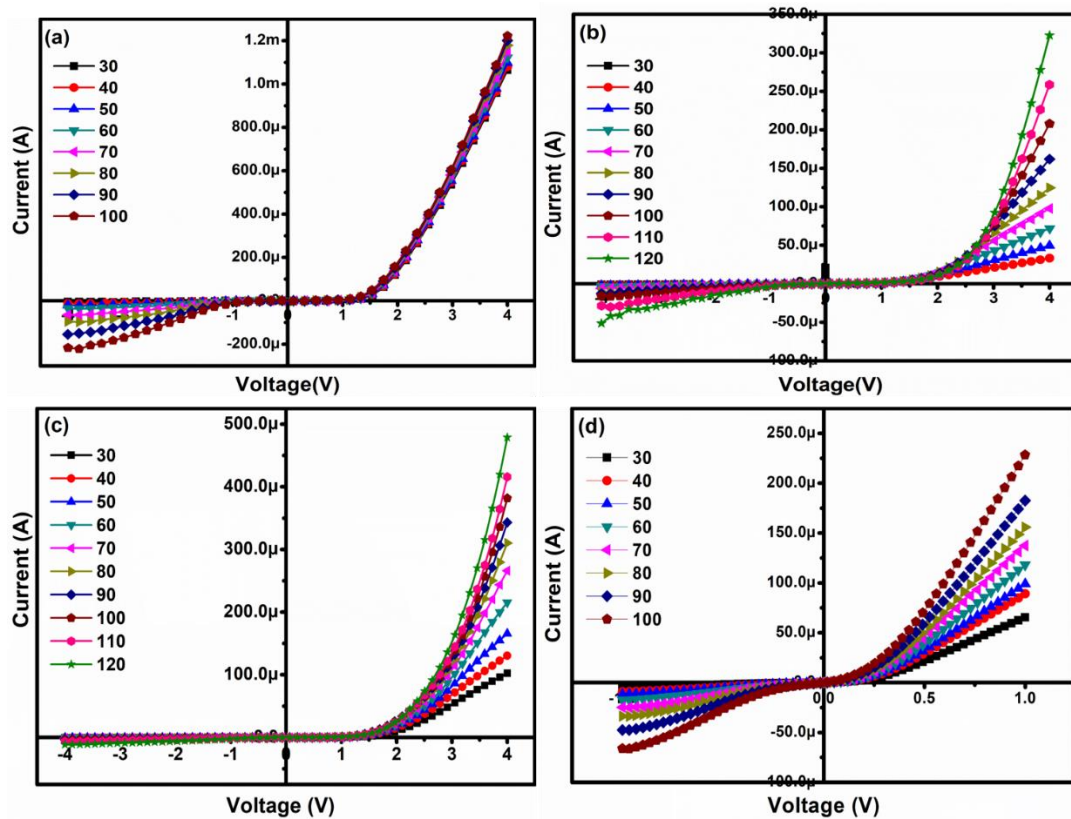


**Figure 6.3** Temperature-dependent I-V curves of **a)** n-CdSe/p-Si, **b)** Ag doped n-CdSe/p-Si, **c)** Bi doped n-CdSe/p-Si, **d)** In doped n-CdSe/p-Si heterojunctions.

The rectifying ratio (RR) of all the diodes were determined at different voltages ( $\pm 0.5$ ,  $\pm 1$ ,  $\pm 2$ ,  $\pm 3$  and  $\pm 4$ ) and data was tabulated in table 6.2. It is observed that undoped CdSe/p-Si and Bi doped CdSe/p-Si heterojunction have high rectification ratio (RR) among four diodes. Bi doped CdSe/p-Si heterojunction is having high rectification ratio of 894.1 at  $\pm 4$  V, compared to undoped CdSe/p-Si heterojunction. The linear dependence of the I-V characteristics at higher forward bias voltage was approximated using equation 2.3.13. Series resistance ( $R_s$ ) was estimated from the inverse of the slope in the higher forward bias region, which is found to be in the order of  $K\Omega$ . In order to verify the possibility of conduction through thermionic emission, a variation of  $\ln(I)$  was plotted against voltage (V) as shown in Figure 6.4. The non-linear nature at higher voltages in the Figure 6.4 hints the possibility of different conduction mechanism in higher voltages. Space charge limited conduction mechanism (SCLC) could be one of the possibilities. To verify this, the variation of current (I) with the square of the voltage ( $V^2$ ) was studied and it was found to be linear in higher voltages.

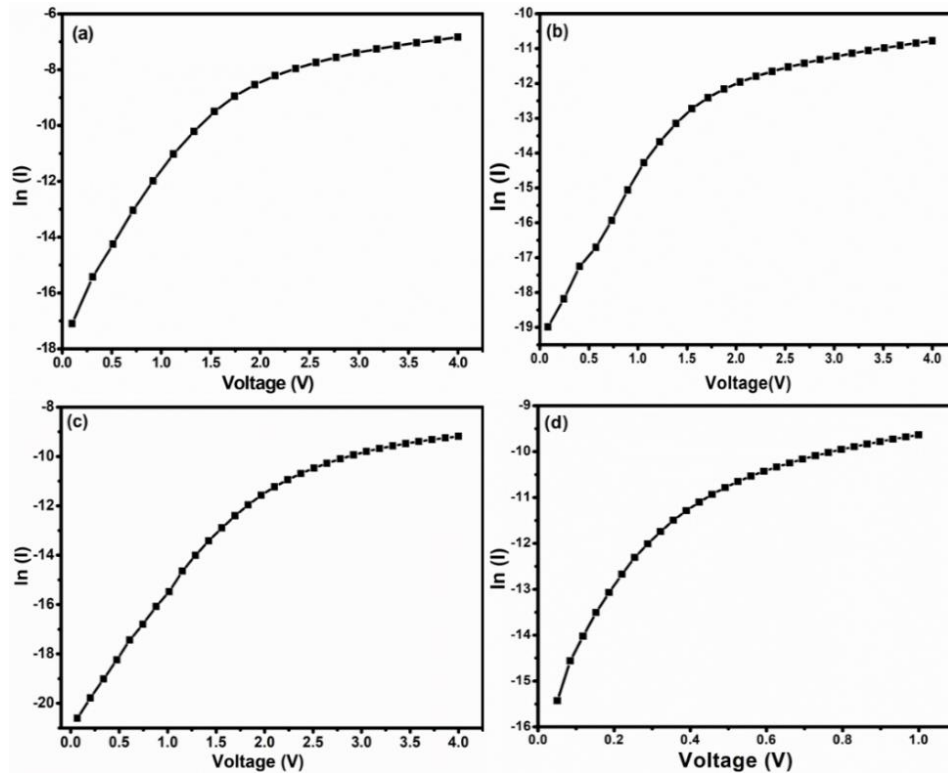


**Figure 6.4** Variation of  $\ln(I)$  vs.  $V$  plot of **a)** n-CdSe/p-Si, **b)** Ag doped n-CdSe/p-Si, **c)** Bi doped n-CdSe/p-Si, **d)** In doped n-CdSe/p-Si heterojunctions.

This linear variation of current ( $I$ ) with the square of the voltage ( $V^2$ ) implies that SCLC is the dominant conduction mechanism at higher voltages. The conduction through SCLC mechanism can be expressed by the equation 2.3.14 (An et al. 2017; Shinde et al. 2014).

**Table 6.2** Rectification ratio of undoped and doped CdSe/p-Si heterojunctions.

Heterojunctions↓ Voltage→	Rectification ratio				
	± 0.5	±1.0	±2.0	±3.0	±4.0
<b>CdSe/p-Si</b>	-	0.55	43.65	149.75	250.33
<b>Ag: CdSe/p-Si</b>	0.97	5.39	21.07	21.47	25.63
<b>Bi: CdSe/p-Si</b>	2.37	12.72	149.62	499.23	894.1
<b>In: CdSe/p-Si</b>	11.08	15.11	-	-	-

Figure 6.5 shows the Richardson's plot of undoped n-CdSe/p-Si and Ag, Bi and In doped CdSe/p-Si heterojunctions. The value of reverse saturation current ( $I_s$ ) can be evaluated from the temperature dependent I-V plot. The obtained value of reverse saturation ( $I_s$ ) at a different temperature is used to plot  $\ln(I_s/T^2)$  vs.  $1/T$ , ( $K^{-1}$ ) (Al-Kotb et al. 2014). The ideal barrier height of the heterojunction can be determined from the

slope of  $\ln(I_s/T^2)$  vs.  $1/T$ , ( $K^{-1}$ ) plot using equation 2.3.15 for thermionic emission conduction mechanism. The evaluated barrier height values of undoped, (Ag, Bi and In) doped CdSe/p-Si heterojunctions were tabulated in table 6.3.

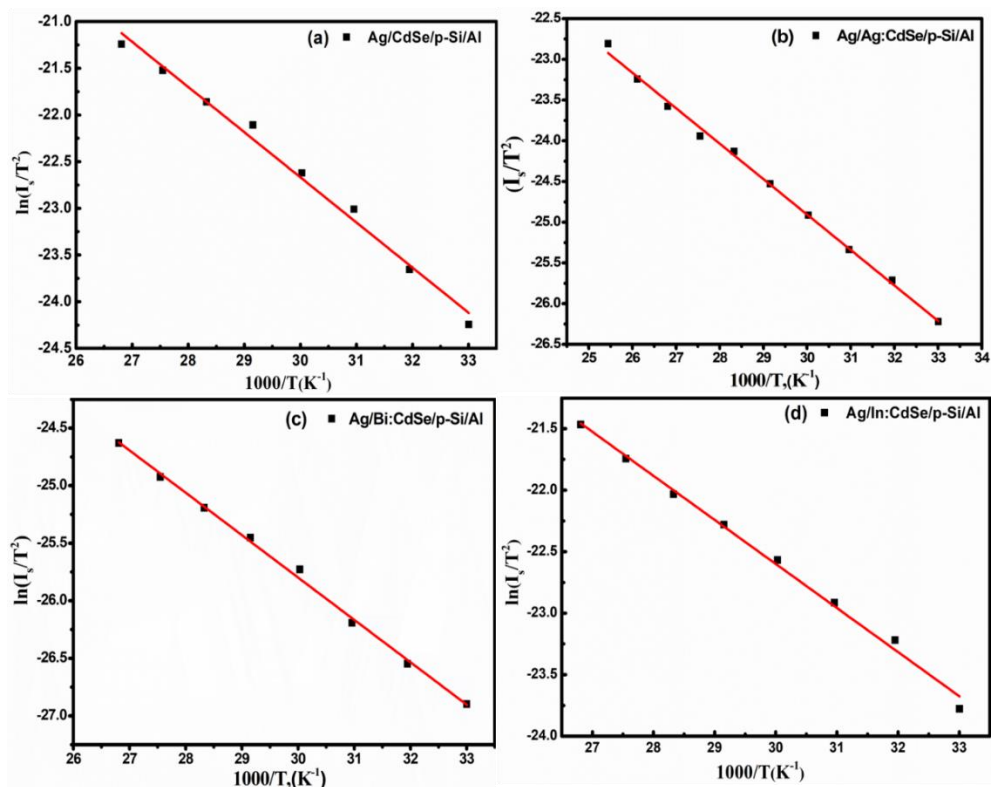


**Figure 6.5** Richardson's plot of **a)** n-CdSe/p-Si, **b)** Ag doped n-CdSe/p-Si, **c)** Bi doped n-CdSe/p-Si, **d)** In doped n-CdSe/p-Si heterojunctions.

The variation of the  $\ln(I_s/T^2)$  vs.  $1/T$ , ( $K^{-1}$ ) was found to be nearly linear for all four heterojunctions as shown in the Figure 6.5 (a-d). The obtained barrier height value determined from the Richardson's plot is slightly different from the reported value. Reverse saturation current ( $I_s$ ) in the temperature dependent I-V curves for all the diodes increases slightly with increasing temperature ( $T$ ). The small changes in the reverse saturation current ( $I_s$ ) with temperature ( $T$ ) is a symbol of slight change in the barrier height ( $\phi_b$ ) of the diode (Tripathi 2010). This deviation in the barrier height and ideality factor values are ascribed to the experimental conditions such as deposition methods and deposition parameters. The value of ideality factor decreases with temperature ( $T$ ), whereas the value of barrier height increases with temperature. The variation of ideality factor ( $\eta$ ) and barrier height ( $\phi_b$ ) as a function of temperature indicates the deviation

from pure thermionic emission- diffusion theory (Duman 2008). Such behavior of both  $\phi_b$  and  $\eta$  commonly observed in the ideal diode, that cannot be explained on the basis of tunneling, thermionic field emission or generation-recombination mechanisms. The possible reasons for this behavior could be the grain boundaries, defects and the interfacial states etc. (Chand and Kumar 1996).

Capacitance-voltage (C-V) measurement is the most commonly used method for the determination of carrier densities in semiconductor material when the capacitance of a reversely biased heterojunction is measured as a function of the applied reverse bias (Ashry and Fares 2012; Bozhkov et al. 2011). Capacitance-voltage (C-V) measurements has been carried for undoped, (Ag, Bi and In) doped CdSe/p-Si heterojunctions. Figure 6.6, Figure 6.7 and Figure 6.8 shows the variation of  $1/C^2$  with reverse voltage for n-CdSe/p-Si, (Bi and In) doped CdSe/p-Si heterojunctions, recorded at a frequency of 50 KHz. The linear nature of the graph indicates that the carrier concentration is uniform and the junction is an abrupt junction. It can be seen that  $1/C^2$  varies linearly with voltage (V). The slope of  $1/C^2$  vs. V is commonly used to determine the carrier density or doping density (Gowrish Rao et al. 2011). The value of carrier density (N) was determined from the slope of the plot using equation 2.3.16. The intercept at  $C^{-2}$  is equal to zero (0) gives the built-in potential ( $V_{bi}$ ) of the heterojunction. The determined carrier density (N) and built-in potential ( $V_{bi}$ ) values of undoped, (Bi and In) doped CdSe/p-Si heterojunctions were tabulated in table 6.3.

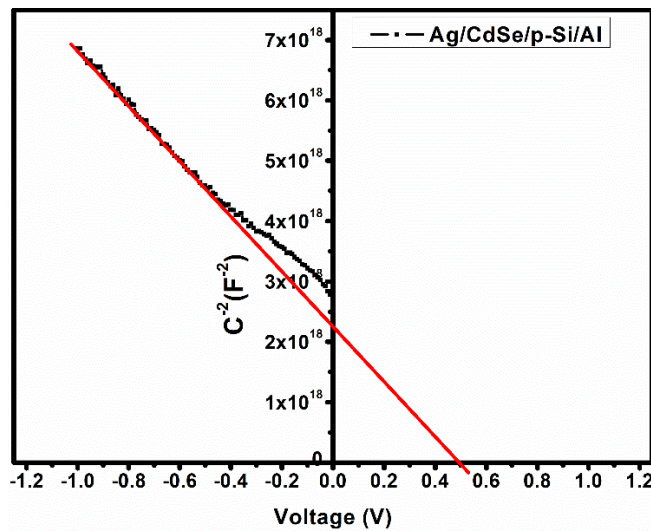


**Figure 6.6**  $1/C^2$  vs. V plot of n-CdSe/p-Si heterojunction.

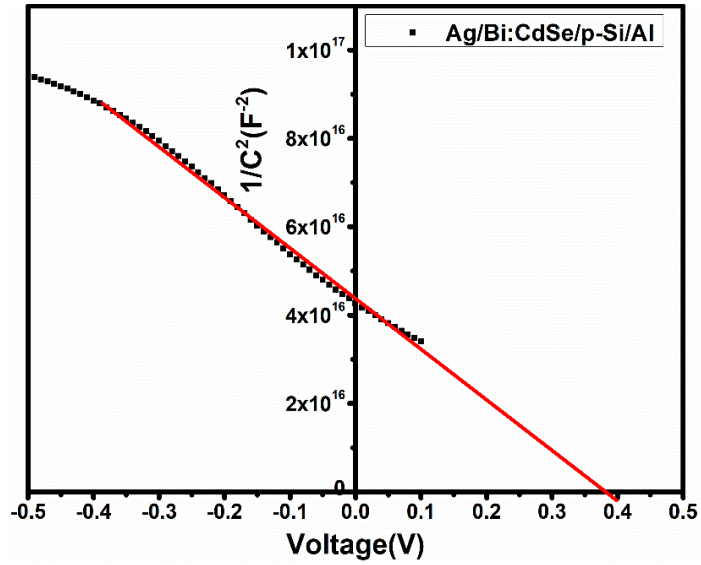


Figure 6.7  $1/C^2$  vs.  $V$  plot of Bi doped CdSe/p-Si heterojunction.

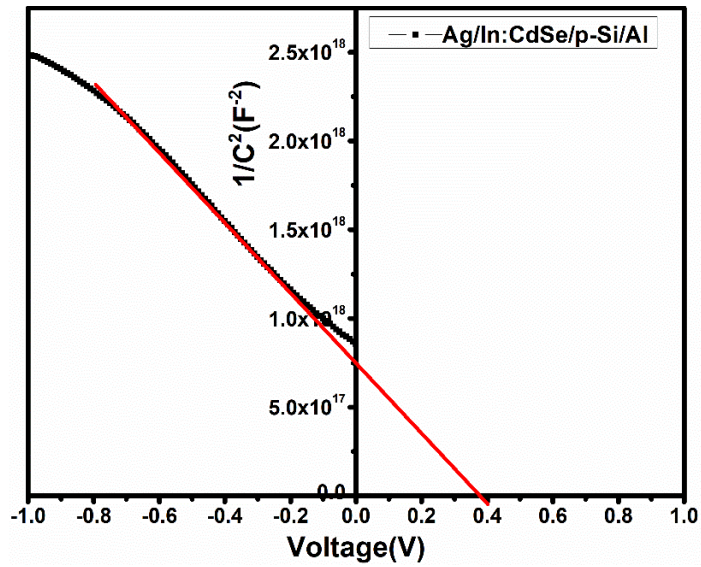
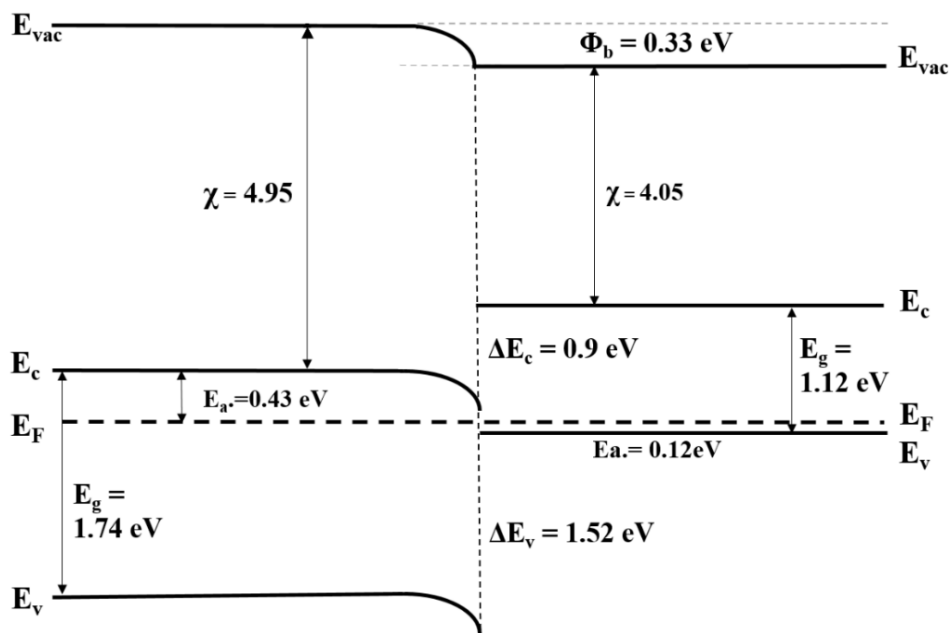


Figure 6.8  $1/C^2$  vs.  $V$  plot of In doped n-CdSe/p-Si heterojunction.

Table 6.3 Carrier concentration, barrier height, and ideality factor of n-CdSe/p-Si and doped n-CdSe/p-Si heterojunction.

Heterojunctions	From C-V studies		From I-V-T studies	
	$V_{bi}$ (eV)	$N$ ( $\text{cm}^{-3}$ )	$\eta$	$\phi_b$ (eV)
<b>CdSe/p-Si</b>	0.51 eV	$6.47 \times 10^{14}$	4.72	0.42 eV
<b>Bi: CdSe/p-Si</b>	0.38 eV	$1.39 \times 10^{15}$	5.61	0.32 eV
<b>In: CdSe/p-Si</b>	0.39 eV	$2.25 \times 10^{16}$	2.79	0.31 eV
<b>Ag: CdSe/p-Si</b>	-	-	8.45	0.38 eV

The band profile of n-CdSe/p-Si was constructed based on Anderson model. The values of electron affinities were taken from literature (Chaliha et al. 2008). Figure 6.9 shows the band diagram of n-CdSe/p-Si heterojunction. The conduction band offset  $\Delta E_c$  and valence band offset  $\Delta E_v$  were calculated from the difference between the electron affinities of CdSe ( $\chi = 4.95$  eV) and Si ( $\chi = 4.05$  eV). The band gap of CdSe was obtained from optical characterization which is approximated as 1.74 eV. The energy band gap of p-Si calculated from the study of variation of electrical resistivity with temperature was found to be 1.12 eV. Activation energy ( $E_a$ ) values were determined from the slope of the linear region of  $\ln(R)$  vs.  $1000/T$ , ( $K^{-1}$ ) plot. Activation energy for n-CdSe and p-Si values were found to be 0.43 eV and 0.12 eV respectively. The carrier concentration of CdSe thin films was determined from Hall measurements and it was found to be around  $10^{14} \text{ cm}^{-3}$ . The carrier density of p-Si was found to be around  $10^{18} \text{ cm}^{-3}$ . Based on these data, band diagram for n-CdSe/p-Si heterojunction has been proposed.



**Figure 6.9** Band diagram of n-CdSe/p-Si heterojunction.



## CHAPTER 7

### SUMMARY AND CONCLUSIONS

#### *Overview*

This chapter represents the summary of the work with the conclusions drawn from the present work. Scope for the future work is also included in this chapter.

#### 7.1 SUMMARY OF THE PRESENT WORK

The work presented in this thesis is broadly classified into seven chapters with several sections in each chapter. The first chapter covers introduction to thin films, properties of chalcogenides, literature survey, scope and objectives of the work. The second chapter contains experimental and characterization techniques employed in the present work. The third chapter describes detailed study on optimization of CdSe thin films by varying substrate temperature and annealing duration. The fourth chapter deals with preparation, results and discussion of Ag, Bi and In doped CdSe thin films. The fifth chapter describes the preparation, results and discussion of  $\text{Cd}_{(1-x)}\text{Zn}_{(x)}\text{Se}$  and  $\text{CdSe}_{(1-x)}\text{Te}_{(x)}$  ternary systems. The sixth chapter deals with fabrication and evaluation of undoped CdSe/p-Si and doped CdSe/p-Si heterojunctions. The seventh chapter contains summary and conclusions drawn from the present work.

#### 7.2 CONCLUSIONS

##### 7.2.1 Undoped and doped CdSe thin films

- Undoped CdSe, (Ag, Bi and In) doped CdSe thin films were deposited separately onto the amorphous glass substrates using thermal evaporation technique.
- Undoped CdSe as well as doped CdSe thin films are polycrystalline in nature exhibiting hexagonal crystal structure along (002) direction.
- The optical energy band gap of undoped CdSe thin films was found to be 1.68 eV. No significant change in the band gap of CdSe after doping.

- The electrical conductivity of undoped CdSe thin films was found to be in the order of  $10^{-4}$  / $\Omega$ -cm.
- In Ag doped CdSe films, silver does not get incorporated into the lattice of CdSe. Electrical conductivity is increased due to the presence of Ag as a separate metal phase.
- In Bi doped CdSe thin films electrical conductivity increased from  $10^{-4}$  / $\Omega$ -cm to  $8.47 \times 10^{-4}$  / $\Omega$ -cm with an increase in Bi dopant concentration (0% -3%). Bi doped CdSe thin films have better photo conducting properties.
- Indium (In) doped CdSe thin films have better electrical conductivity among all other dopant materials. Electrical conductivity of these films increased from  $10^{-4}$  / $\Omega$ -cm to 1187.9 / $\Omega$ -cm as the dopant concentration increases from 0 to 3%.

### 7.2.2 Cd<sub>(1-x)</sub>Zn<sub>(x)</sub>Se and CdSe<sub>(1-x)</sub>Te<sub>(x)</sub> (x = 0 -1) thin films.

- Cd<sub>(1-x)</sub>Zn<sub>(x)</sub>Se (x=0-1) films deposited at 453 K and 2hr vacuum annealed are polycrystalline hexagonal (wurtzite) crystal structure with strong preferential orientation along (002) direction. The optical band gap value varies from 1.67 eV (for pure CdSe) to 2.60 eV (for pure ZnSe) thin films. Transmittance increases from 85% to 95% as the Zn concentration increases from x= 0 to 1. Activation energy increases from 0.39 eV to 0.85 eV with an increase in Zn (x=0 to 0.8) concentration in the Cd<sub>(1-x)</sub>Zn<sub>(x)</sub>Se thin films. Cd<sub>(1-x)</sub>Zn<sub>(x)</sub>Se thin films with high transmittance and high resistivity can be used specifically as buffer layers for solar cells and also films with lesser Zn concentration in the ternary alloy can be useful for many optoelectronic device applications.
- CdSe<sub>(1-x)</sub>Te<sub>(x)</sub> films are found to be polycrystalline in nature. The structural studies of the prepared CdSe<sub>(1-x)</sub>Te<sub>(x)</sub> thin films reveal that a low percentage of CdTe in the pseudobinary system results in hexagonal wurtzite structure and a high proportion of Te gives rise to cubic zinc blende structure. Bandgap values showed a bowing behavior with increased Te concentration. The band gap of CdSe<sub>(1-x)</sub>Te<sub>(x)</sub> system can be tuned from 1.67 eV of pure CdSe to 1.51 eV of pure CdTe by varying Te concentration. Conductivity decreases as the Te

concentration increases.  $\text{CdSe}_{(1-x)}\text{Te}_{(x)}$  thin films with composition  $x = 0.2, 0.4$  may be used as window layer, and composition  $x = 0.6, 0.8$  may be used as absorber layers in CdTe based solar cell applications.

- It may be concluded that both  $\text{Cd}_{(1-x)}\text{Zn}_{(x)}\text{Se}$  and  $\text{CdSe}_{(1-x)}\text{Te}_{(x)}$  ( $x = 0 - 1$ ) ternary systems can be obtained in a stable form and with properties and characteristics determined by the composition. Thus, band gap engineering is an attractive possibility with these ternary systems.
- n-CdSe/p-Si and doped CdSe/p-Si heterojunction diodes have been fabricated. Barrier height has been determined from capacitance measurements and temperature dependent I-V characteristics of the junctions. Among four diodes Bi doped CdSe/p-Si heterojunction has high rectification ratio of 894.1 at  $\pm 4$  V.

### **7.3 SCOPE FOR THE FUTURE WORK**

The p-type doping of CdSe thin films is one of the major problems. It is predicted that p-type doping of CdSe will boost the commercialization of CdSe based semiconductor devices. Incorporating Cu into CdSe has shown some promise in this direction. Detailed studies on doping of CdSe with different group elements will be helpful in understanding the material behavior and also to improve the efficiency of the existing devices based on CdSe.

The ternary alloys based on CdSe, CdTe, ZnTe and ZnSe materials, such as CdZnSe, CdSeTe, CdZnTe and ZnSeTe are much useful in the fabrication of many optoelectronic devices. These materials can be used to engineer the lattice parameters and bandgap for heterostructure. The study of properties of such ternary alloys opens the door for many innovations. Employing low cost chemical methods to grow such ternary alloys with different composition for various large area devices may be an area worth pursuing.

## REFERENCES

Ahmad, S. M. (2016). "Study of structural and optical properties of quaternary  $Cu_xAg_{1-x}AlS_2$  thin films." *Optik (Stuttg.)*, 127(20), 10004–10013.

Al-Ani, S. K. J., Mohammed, H. H., and Al-Fwade, E. M. N. (2002). "The optoelectronic properties of CdSe: Cu photoconductive detector." *Renew. Energy*, 25(4), 585–590.

Al-Douri, Y. (2003). "Electronic and optical properties of  $Zn_xCd_{1-x}Se$ ." *Mater. Chem. Phys.*, 82(1), 49–54.

Al-Kabbi, A. S., Sharma, K., Saini, G. S. S., and Tripathi, S. K. (2013). "Effect of doping on trapping center parameters in nanocrystalline CdSe thin films." *J. Alloys Compd.*, 555, 1–5.

Al-Kotb, M. S., Al-Waheidi, J. Z., and Kotkata, M. F. (2014). "Opto-electronic characterizations of oriented nano-structure CdSe film/Si (0 0 1) heterostructure." *Superlattices Microstruct.*, 69, 149–163.

Ali, M., Syed, W. a. a., Zubair, M., Shah, N. a., and Mehmood, A. (2013). "Physical properties of Sb-doped CdSe thin films by thermal evaporation method." *Appl. Surf. Sci.*, 284, 482–488.

Amir, F. Z., Clark, K., Maldonado, E., Kirk, W. P., Jiang, J. C., Ager, J. W., Yu, K. M., and Walukiewicz, W. (2008). "Epitaxial growth of  $Cd_{1-x}Se_xTe$  thin films on Si(1 0 0) by molecular beam epitaxy using lattice mismatch graded structures." *J. Cryst. Growth*, 310(6), 1081–1087.

An, Q., Meng, X., Xiong, K., Qiu, Y., Jiang, M., Shan, C., Zhao, D., Chen, H., Shen, D., and Lee, S. H. (2017). "A high-performance fully nanostructured individual CdSe nanotube photodetector with enhanced responsivity and photoconductive gain." *J. Mater. Chem. C*, 5(28), 7057–7066.

Ashry, M., and Fares, S. (2012). "Electrical Characteristic Measurement of the

Fabricated CdSe / P-Si Heterojunction Solar Cell Under Radiation Effect.” *Am. J. Mater. Sci.*, 2(3), 72–76.

Baban, C., and Rusu, G. I. (2003). “On the structural and optical characteristics of CdSe thin films.” *Appl. Surf. Sci.*, 211(1–4), 6–12.

Babu, S. M., Rajalakshmi, T., Dhanasekaran, R., and Ramasamy, P. (1991). “Electrodeposition of CdSe<sub>x</sub>Te<sub>1-x</sub> by periodic pulse technique.” *J. Cryst. Growth*, 110(3), 423–428.

Bagade, C. S., Ghanwat, V. B., Khot, K. V., and Bhosale, P. N. (2016). “Efficient improvement of photoelectrochemical performance of CdSe thin film deposited via arrested precipitation technique.” *Mater. Lett.*, 164, 52–55.

Bagade, C. S., Mali, S. S., Ghanwat, V. B., Khot, K. V., Patil, P. B., Kharade, S. D., Mane, R. M., Desai, N. D., Hong, C. K., Patil, P. S., and Bhosale, P. N. (2015). “A facile and low cost strategy to synthesize Cd<sub>(1-x)</sub>Zn<sub>(x)</sub>Se thin films for photoelectrochemical performance: effect of zinc content.” *RSC Adv.*, 5(69), 55658–55668.

Benamar, E., Rami, M., Fahoume, M., Chraïbi, F., and Ennaoui, A. (1999). “Electrodeposition and characterization of CdSe<sub>(x)</sub>Te<sub>(1-x)</sub>, semiconducting thin films.” *Solid State Sci.*, 301–310.

Benyettou, S., Saïb, S., and Bouarissa, N. (2015). “Elastic, lattice dynamical and thermal properties of zinc-blende CdSe<sub>x</sub>Te<sub>1-x</sub> ternary alloys.” *Chem. Phys.*, 457, 147–151.

Borah, M. N., Chaliha, S., Sarmah, P. C., and Rahman, A. (2008). “Studies on current-voltage characteristics of ITO/(n)CdSe-Al heterojunctions.” *J. Optoelectron. Adv. Mater.*, 10(10), 2793–2799.

Borkovska, L., Korsunskaya, N., Kládko, V., Slobodyan, M., Yefanov, O., Venger, Y., Kryshchak, T., Sadofyev, Y., and Kazakov, I. (2008). “A new type of structural defects in CdZnSe/ZnSe heterostructures.” *Microelectronics J.*, 39(3–4), 589–593.

- Bozhkov, V. G., Torkhov, N. A., and Shmargunov, A. V. (2011). "About the determination of the Schottky barrier height with the C-V method." *J. Appl. Phys.*, 109(7), 73714.
- Brill, G., Chen, Y., Amirtharaj, P. M., Sarney, W., Chandler-Horowitz, D., and Dhar, N. K. (2005). "Molecular beam epitaxial growth and characterization of Cd-based II–VI wide-bandgap compounds on Si substrates." *J. Electron. Mater.*, 34(5), 655–661.
- Calster, A. Van, Vervaet, A., Rycke, I. De, Baets, J. De, and Vanfleteren, J. (1990). "Polycrystalline CdSe films for thin film transistors." *J. Cryst. Growth*, 86(1–4), 924–928.
- Castillo-Alvarado, F. L., Inoue-Chávez, J. A., Vigil-Galán, O., Sánchez-Meza, E., López-Chávez, E., and Contreras-Puente, G. (2010). "C-V calculations in CdS/CdTe thin films solar cells." *Thin Solid Films*, 518(7), 1796–1798.
- Chaliha, S., Borah, M. N., Sarmah, P. C., and Rahman, A. (2010). "Study of Au, Ni-(n)ZnSe thin film Schottky barrier junctions." *Int. J. Thermophys.*, 2030–2039.
- Chaliha, S., Sarmah, P. C., and Rahman, A. (2008). "Electrical and optical properties of thin film (n) CdSe / (p) CdTe heterojunction and its performance as a photovoltaic converter." *J. Optoelectron. Adv. Mater.*, 10(6), 1333–1339.
- Chand, S., and Kumar, J. (1996). "Evidence for the double distribution of barrier heights in Pd<sub>2</sub>Si/n-Si Schottky diodes from I-V-T measurements." *Semicond. Sci. Technol.*, 11(8), 1203–1208.
- Chate, P. A., Hankare, P. P., and Sathe, D. J. (2010a). "N-Type polycrystalline (CdZn)Se photoelectrode synthesis and its photoelectrochemical characterizations." *J. Alloys Compd.*, 506(2), 673–677.
- Chate, P. A., Hankare, P. P., and Sathe, D. J. (2010b). "Effect of indium doping on (CdZn)Se composite thin films." *J. Alloys Compd.*, 505(1), 259–263.
- Chen, Y. P., Brill, G., and Dhar, N. K. (2003). "MBE growth of CdSeTe/Si composite substrate for long-wavelength IR HgCdTe applications." *J. Cryst. Growth*, 252(1–3),

270–274.

Chen, Z., Zhang, H., Zeng, Q., Wang, Y., Xu, D., Wang, L., Wang, H., and Yang, B. (2014). “In situ construction of nanoscale CdTe-CdS bulk heterojunctions for inorganic nanocrystal solar cells.” *Adv. Energy Mater.*, 4(10), 1400235.

Chopra, K., and Klerrer, J. (1970). “Thin Film Phenomena.” *J. Electrochem. Soc.*, 117(5), 180C.

Chopra, K. L., and Das, S. R. (1983). “Why Thin Film Solar Cells?” *Thin Film Sol. Cells*, Boston, MA: Springer US, 1–18.

Chouikh, F., Beggah, Y., and Aida, M. S. (2011). “Optical and electrical properties of Bi doped ZnO thin films deposited by ultrasonic spray pyrolysis.” *J. Mater. Sci. Mater. Electron.*, 22(5), 499–505.

Chowdhury, R., Islam, M., Sabeth, F., Mustafa, G., Farhad, S., Saha, D., Chowdhury, F., Hussain, S., and Islam, A. (2012). “Characterization of Electrodeposited Cadmium Selenide Thin Films.” *Dhaka Univ. J. Sci.*, 60(1), 137–140.

Duman, S. (2008). “Temperature dependence of current-voltage characteristics of an In/p-GaSe:Gd/Au-Sb Schottky barrier diode.” *Semicond. Sci. Technol.*, 23(7), 75042.

Fayek, S. A., and Sayed, S. M. El. (2001). “Effect of composition and forming parameter on evaporated CdSeTe films deposited at room temperature.” *J. Phys. Chem. Solids*, 63(1), 1–8.

Gowrish Rao, K., Bangera, K. V., and Shivakumar, G. K. (2011). “Photoconductivity and photo-detecting properties of vacuum deposited ZnSe thin films.” *Solid State Sci.*, 13(11), 1921–1925.

Hankare, P. P., Jadhav, B. V., Chate, P. A., Sathe, D. J., and Mulla, I. S. (2011). “Synthesis and characterization of chemically deposited nickel substituted CdSe thin film.” *J. Alloys Compd.*, 509(6), 2948–2951.

Heo, K., Lee, H., Kim, T., and Lee, Y. (2016). “Author ’ s Accepted Manuscript

Structural Control of Photoconductive CdSe Nanostructures through a Bi-assisted VLS Process.” *Mater. Lett.*, 182, 129–133.

Husain, M., Singh, B. P., Kumar, S., Sharma, T. P., and Sebastian, P. J. (2003). “Optical, electrical and structural investigations on Cd<sub>(1-x)</sub>Zn<sub>(x)</sub>Se sintered films for photovoltaic applications.” *Sol. Energy Mater. Sol. Cells*, 76(3), 399–415.

Jin, W. F., Ye, Y., Gan, L., Yu, B., Wu, P. C., Dai, Y., Meng, H., Guo, X. F., and Dai, L. (2012). “Self-powered high performance photodetectors based on CdSe nanobelt/graphene Schottky junctions.” *J. Mater. Chem.*, 22(7), 2863–2867.

Kale, S. S., and Lokhande, C. D. (2000). “Thickness-dependent properties of chemically deposited CdSe thin films.” *Mater. Chem. Phys.*, 62(2), 103–108.

Kashiwaba, Y., Tada, A., and Ikeda, T. (1994). “Fabrication of thin-film p-CdS(Cu)/n-CdSe heterojunctions and their photovoltaic characteristics.” *Jpn. J. Appl. Phys.*, 33(11B), L1613–L1615.

Kathalingam, A., Kim, M. R., Chae, Y. S., Rhee, J. K., Thanikaikarasan, S., and Mahalingam, T. (2010). “Study on electrodeposited CdSexTe1-x semiconducting thin films.” *J. Alloys Compd.*, 505(2), 758–761.

Kaur, J., Singh, B., Sharma, K., and Tripathi, S. K. (2015). “Study of sub gap optical absorption parameters in Pb doped CdSe thin films.” *Aip Conf. Proc.*, 1591(June), 50009.

Kaur, J., and Tripathi, S. K. (2016). “Annealing-induced optical and sub-band-gap absorption parameters of Sn-doped CdSe thin films.” *Philos. Mag.*, 96(1), 45–57.

Khalaf, M. K., Alhilli, B. A. M., Khudiar, A. I., and Alzahra, A. A. (2016). “Influence of nanocrystalline size on optical band gap in CdSe thin films prepared by DC sputtering.” *Photonics Nanostructures - Fundam. Appl.*, 18, 59–66.

Konda, R. B., Mundle, R., Mustafa, H., Bamiduro, O., Pradhan, A. K., Roy, U. N., Cui, Y., and Burger, A. (2007). “Surface plasmon excitation via Au nanoparticles in n-CdSe/p-Si heterojunction diodes.” *Appl. Phys. Lett.*, 91(19).



Krishnan, V. (1992). "Electrosynthesis of Thin Films of CdZnSe: Composition Modulation and Bandgap Engineering in the Ternary System." *J. Electrochem. Soc.*, 139(1), 23.

Kurokawa, A., and Muto, J. (2003). "Properties of  $\mu\text{m}$ -thick CdSe prepared by vacuum deposition." *J. Mater. Sci. Mater. Electron.*, 14(1), 33–35.

Loizos, Z., Mitsis, A., Spyrellis, N., Froment, M., and Maurin, G. (1993). "Cadmium chalcogenide semiconducting thin films prepared by electrodeposition from boiling aqueous electrolytes." *Thin Solid Films*, 235(1–2), 51–56.

Loizos, Z., and Spyrellis, N. (1989). "Semiconducting  $\text{CdSe}_{(x)}\text{Te}_{(1-x)}$  thin films prepared by electrodeposition." 269 (December 1988), 399–410.

Macdonald, B. I., Martucci, A., Rubanov, S., Watkins, S. E., Mulvaney, P., and Jasieniak, J. J. (2012). "Layer-by-Layer Assembly of Sintered  $\text{CdSe}_x\text{Te}_{1-x}$  Nanocrystal Solar Cells." *ACS Nano*, 6(7), 5995–6004.

Mahalingam, T., Mariappan, R., and Ravi, G. (2010). "Characterization of electrodeposited indium doped CdSe." 7(12), 669–677.

Mahmood, A., R, S., Shah, a, Aziz, U., Ahmed, E., Ali, S., and Raza, Q. (2011). "Ellipsometric analysis of  $\text{Cd}_{1-x}\text{Zn}_x\text{Se}$  thin films prepared by a thermal evaporation technique." *Phys. Scr.*, 83(6), 65706.

Mahmoud, S. A., Ashour, A., and Badawi, E. A. (2006). "Processing parameters and transport properties of vacuum evaporated CdSe thin films." *Appl. Surf. Sci.*, 253(5), 2969–2972.

Mane, R. S., and Lokhande, C. D. (2000). "Chemical deposition method for metal chalcogenide thin films." *Mater. Chem. Phys.*, 65(1), 1–31.

Matsumura, N., Sakamoto, T., and Saraie, J. (2002). "Composition control of CdSeTe layers grown by molecular beam epitaxy." *J. Cryst. Growth*, 237–239(1–4 II), 1550–1553.

Mourad, D., Czycholl, G., Kruse, C., Klembt, S., Retzlaff, R., Hommel, D., Gartner, M., and Anastasescu, M. (2010). "Band gap bowing of binary alloys: Experimental results compared to theoretical tight-binding supercell calculations for  $\text{Cd}_x\text{Zn}_{1-x}\text{Se}$ ." *Phys. Rev. B - Condens. Matter Mater. Phys.*, 82(16).

Murali, K. R., and Jayasutha, B. (2009). "Photoelectrochemical characteristics of brush electrodeposited  $\text{CdSe}_x\text{Te}_{1-x}$  thin films." *Chalcogenide Lett.*, 6(1), 1–8.

Murali, K. R., Sivaramamoorthy, K., Kottaisamy, M., and Asath Bahadur, S. (2009). "Photoconductive studies on electron beam evaporated CdSe films." *Phys. B Condens. Matter*, 404(16), 2449–2454.

Muthukumarasamy, N., Balasundaraprabhu, R., Jayakumar, S., and Kannan, M. D. (2007). "Investigations on structural phase transition in hot wall deposited  $\text{CdSe}_x\text{Te}_{1-x}$  thin films." *Mater. Chem. Phys.*, 102(1), 86–91.

Muthukumarasamy, N., Jayakumar, S., Kannan, M. D., and Balasundaraprabhu, R. (2009). "Structural phase change and optical band gap bowing in hot wall deposited  $\text{CdSe}_x\text{Te}_{1-x}$  thin films." *Sol. Energy*, 83(4), 522–526.

Nair, M. T. S., Nair, P. K., Zingaro, R. A., and Meyers, E. A. (1993). "Enhancement of photosensitivity in chemically deposited CdSe thin films by air annealing." *J. Appl. Phys.*, 74(3), 1879–1884.

Neudeck, P. G., Okojie, R. S., and Chen, L. Y. (2002). "High-temperature electronics - A role for wide bandgap semiconductors?" *Proc. IEEE*, 90(6), 1065–1076.

Oduor, A. O., and Gould, R. D. (1995). "Space-charge-limited conductivity in evaporated cadmium selenide thin films." *Thin Solid Films*, 270(1–2), 387–390.

Patel, K. D., Jani, M. S., Pathak, V. M., and Srivastava, R. (2009). "Deposition of CdSe thin films by thermal evaporation and their structural and optical properties." *Chalcogenide Lett.*, 6(6), 279–286.

Pathan, H. M., Sankapal, B. R., Desai, J. D., and Lokhande, C. D. (2003). "Preparation and characterization of nanocrystalline CdSe thin films deposited by SILAR method."

*Mater. Chem. Phys.*, 78(1), 11–14.

Pawar, S. T., Kamble, S. S., Pawar, S. M., Sikora, A., Chavan, G. T., Prakshale, V. M., Deshmukh, P. R., and Deshmukh, L. P. (2016). *Chemo-synthesis and microstructural evolution of Zn<sub>1-x</sub>CoxSe thin films*. *Mater. Lett.*

Pejova, B., Grozdanov, I., and Tanuševski, A. (2004). “Optical and thermal band gap energy of chemically deposited bismuth(III) selenide thin films.” *Mater. Chem. Phys.*, 83(2–3), 245–249.

Poplawsky, J. D., Guo, W., Paudel, N. R., Ng, A., More, K. L., Leonard, D., Yan, Y., Green, M. A., Emery, K., Hishikawa, Y., Warta, W., Dunlop, E. D., Green, M. A., Emery, K., Hishikawa, Y., Warta, W., Dunlop, E. D., Paudel, N. R., Yan, Y., Yang, X., Yang, X., Wei, S.-H. H., Zhang, S. B., Zunger, A., McCandless, B. E., Hanket, G. M., Jensen, D. G., Birkmire, R. W., Ohata, K., Saraie, J., Tanaka, T., Nunoue, S. Y., Hemmi, T., Kato, E., Paudel, N. R., Poplawsky, J. D., More, K. L., Yan, Y., Tit, N., Obaidat, I. M., Alawadhi, H., Lane, D. W., Belyaev, A. P., Kalinkin, I. P., Baufay, L., Dispa, D., Pigeolet, A., Laude, L. D., Strauss, A. J., Steininger, J., Steininger, J., Strauss, A. J., Li, C., Wu, Y., Poplawsky, J. D., Pennycook, T. J., Paudel, N. R., Li, C., Poplawsky, J. D., Yan, Y., Al-Jassim, M. M., Jones, K. M., Wei, S.-H. H., Zhang, S. B., Stuckes, A. D., Farrel, G., Sebastian, P. J., Sivaramakrishnan, V., Davis, P. W., Shilliday, T. S., Woolley, J. C., Ray, B., Slack, G. A., Galginitis, S., Larson, D. J., Kranz, L., Choi, P.-P., Li, J., Diercks, D. R., Gorman, B. P., Wolden, C. A., Poplawsky, J. D., Hellman, O. C., Rivage, du, J. B., Seidman, D. N., Hellman, O. C., Vandenbroucke, J. A., Li, C., Michael, J. R., Kotula, P. G., Ziegler, J. F., Ziegler, M. D., Biersack, J. P., Nichterwitz, M., Unold, T., Yoon, H. P., and Thompson, K. (2016). “Structural and compositional dependence of the CdTe<sub>(x)</sub>Se<sub>(1-x)</sub> alloy layer photoactivity in CdTe-based solar cells.” *Nat. Commun.*, 7, 12537.

Rao, D. R., and Centre, M. S. (1994). “Electrical properties of polycrystalline Zn<sub>1-x</sub>CdxSe thin films grown by electron beam evaporation.” 13, 1637–1639.

Rao, G. K., Bangera, K. V., and Shivakumar, G. K. (2013). “Fabrication and characterization of thermal evaporated n-Si/ p-ZnTe thin film heterojunction diodes.”

*Curr. Appl. Phys.*, 13(1), 298–301.

Raoult, F., Fortin, B., and Colin, Y. (1989). “Standardization and stabilization of the resistivity-temperature characteristics of CdSe thin films by vacuum annealing.” *Thin Solid Films*, 182(1–2), 1–14.

Raut, V. S., Lokhande, C. D., and Killedar, V. V. (2017). “Photoelectrochemical studies on electrodeposited indium doped CdSe thin films using aqueous bath.” *J. Electroanal. Chem.*, 788, 137–143.

Rennie, J., Nishikawa, Y., Saito, S., Onomura, M., and Hatakoshi, G. (1996). “Operation voltage reduction in ZnSe-based light-emitting diodes due to the use of n-type AlGaAs and CdZnSe buffer regions.” *Appl. Phys. Lett.*, 68(21), 2971–2972.

Roth, M. (1989). “Advantages and limitations of cadmium selenide room temperature gamma ray detectors.” *Nucl. Inst. Methods Phys. Res. A*, 283(2), 291–298.

Russak, M. A., Reichman, J., Witzke, H., Deb, S. K., and Chen, S. N. (1980). “Thin Film CdSe Photoanodes for Electrochemical Photovoltaic Cells.” *J. Electrochem. Soc.*, 127(3), 725–733.

Sadananda Kumar, N., Bangera, K. V., and Shivakumar, G. K. (2015). “Properties of antimony doped ZnO thin films deposited by spray pyrolysis technique.” *Semiconductors*, 49(7), 899–904.

Samarth, N., Luo, H., Furdyna, J. K., Alonso, R. G., Lee, Y. R., Ramdas, A. K., Qadri, S. B., and Otsuka, N. (1990). “Molecular beam epitaxy of Zn<sub>1-x</sub>Cd<sub>x</sub>Se epilayers and ZnSe/Zn<sub>1-x</sub>Cd<sub>x</sub>Se superlattices.” *Appl. Phys. Lett.*, 56(12), 1163–1165.

Sarmah, K., Sarma, R., and Das, H. L. (2008). “Structural characterization of thermally evaporated CdSe thin films.” *Chalcogenide Lett.*, 5(8), 153–163.

Sathyalatha, K. C., Uthanna, S., and Reddy, P. J. (1989). “Electrical and photoconducting properties of vacuum evaporated pure and silver-doped CdSe films.” *Thin Solid Films*, 174(PART 1), 233–238.

Selva Priya, S., Lakshmi Shree, B., Therasa Ranjani, P., Karthick, P., Jeyadheepan, K., and Sridharan, M. (2016). “Electrical Properties of Thermally Evaporated CdSe and ZnCdSe Thin Films.” *Mater. Today Proc.*, 3(6), 1487–1493.

Sen, S., Bhandarkar, V., Muthe, K. P., Gupta, S. K., and Yakhmi, J. V. (2008). “Tellurium Thin Films Based Gas Sensor.” *12th Natl. Semin. Phys. Technol. Sensors*, (297), 240–245.

Shah, N. a., Nazir, a., Mahmood, W., Syed, W. a a, Butt, S., Ali, Z., and Maqsood, a. (2012). “Physical properties and characterization of Ag doped CdS thin films.” *J. Alloys Compd.*, 512(1), 27–32.

Shalev, E., Oksenberg, E., Rechav, K., Popovitz-Biro, R., and Joselevich, E. (2017). “Guided CdSe Nanowires Parallely Integrated into Fast Visible-Range Photodetectors.” *ACS Nano*, 11(1), 213–220.

Sharma, K., Al-Kabbi, A. S., Saini, G. S. S., and Tripathi, S. K. (2012). “Effect of Cu incorporation on structural and optical properties of nanocrystalline CdSe (nc-CdSe:Cu) thin films.” *J. Alloys Compd.*, 540, 198–203.

Sharma, K., Al-Kabbi, A. S., Saini, G. S. S., and Tripathi, S. K. (2013). “Indium doping induced modification of the structural, optical and electrical properties of nanocrystalline CdSe thin films.” *J. Alloys Compd.*, 564, 42–48.

Shinde, S. K., Dubal, D. P., Ghodake, G. S., Lee, D. S., Lohar, G. M., Rath, M. C., and Fulari, V. J. (2014). “Baking impact of Fe composition on CdSe films for solar cell application.” *Mater. Lett.*, 132, 243–246.

Shinde, S. K., Thombare, J. V., Dubal, D. P., and Fulari, V. J. (2013). “Electrochemical synthesis of photosensitive nano-nest like CdSe<sub>0.6</sub>Te<sub>0.4</sub> thin films.” *Appl. Surf. Sci.*, 282, 561–565.

Shyju, T. S., Anandhi, S., Indirajith, R., and Gopalakrishnan, R. (2011). “Solvothermal synthesis, deposition and characterization of cadmium selenide (CdSe) thin films by thermal evaporation technique.” *J. Cryst. Growth*, 337(1), 38–45.

Singh, A., Li, X., Protasenko, V., Galantai, G., Kuno, M., Xing, H., and Jena, D. (2007). “Polarization-sensitive nanowire photodetectors based on solution-synthesized CdSe quantum-wire solids.” *Nano Lett.*, 7(10), 2999–3006.

Singh, R. S., Bhushan, S., Singh, A. K., and Deo, S. R. (2011). “Characterization and optical properties of CdSe nano-crystalline thin films.” *Dig. J. Nanomater. Biostructures*, 6(2), 403–412.

Streetman, B. G., and Banerjee, S. K. (2009). *Solid State Electronic Devices*. Pearson/Prentice Hall.

Swanson, D. E., Sites, J. R., and Sampath, W. S. (2017). “Co-sublimation of CdSexTe1-xxx layers for CdTe solar cells.” *Sol. Energy Mater. Sol. Cells*, 159, 389–394.

Sze. (1995). *Physics of Semiconductor Devices Physics of Semiconductor Devices. America (NY)*, Wiley-Interscience.

Tit, N., Obaidat, I. M., and Alawadhi, H. (2009). “Origins of bandgap bowing in compound-semiconductor common-cation ternary alloys.” *J. Phys. Condens. matter*, 21(7), 75802.

Tripathi, S. K. (2010). “Temperature-dependent barrier height in CdSe Schottky diode.” *J. Mater. Sci.*, 45(20), 5468–5471.

Wang, L., Yoon, M. H., Lu, G., Yang, Y., Facchetti, A., and Marks, T. J. (2006). “High-performance transparent inorganic-organic hybrid thin-film n-type transistors.” *Nat. Mater.*, 5(11), 893–900.

Wu, D., Xu, T., Shi, Z., Tian, Y., Li, X., Yu, Y., and Jiang, Y. (2017). “Two-terminal nonvolatile resistive switching memory devices based on n-CdSe NR/p-Si heterojunctions.” *J. Alloys Compd.*, 695, 1653–1657.

Yacobi B.G. (2003). *Semiconductors Materials An Introduction to Basic Principles. Thin Solid Films*.

Yadav, A. A., Barote, M. A., and Masumdar, E. U. (2010). "Studies on cadmium selenide (CdSe) thin films deposited by spray pyrolysis." *Mater. Chem. Phys.*, 121(1–2), 53–57.

Yang, L., McCue, C., Zhang, Q., Uchaker, E., Mai, Y., and Cao, G. (2015). "Highly efficient quantum dot-sensitized TiO<sub>2</sub> solar cells based on multilayered semiconductors (ZnSe/CdS/CdSe)." *Nanoscale*, 7(7), 3173–3180.

Zeng, Q., Chen, Z., Liu, F., Jin, G., Du, X., Ji, T., Zhao, Y., Yue, Y., Wang, H., Meng, D., Xie, T., Zhang, H., and Yang, B. (2017). "Aqueous-Processed Polymer/Nanocrystals Hybrid Solar Cells: The Effects of Chlorine on the Synthesis of CdTe Nanocrystals, Crystal Growth, Defect Passivation, Photocarrier Dynamics, and Device Performance." *Sol. RRL*, 1(1), 1600020.

Zeng, Q., Chen, Z., Zhao, Y., Du, X., Liu, F., Jin, G., Dong, F., Zhang, H., and Yang, B. (2015). "Aqueous-Processed Inorganic Thin-Film Solar Cells Based on CdSexTe1-x Nanocrystals: The Impact of Composition on Photovoltaic Performance." *ACS Appl. Mater. Interfaces*, 7(41), 23223–23230.

Zhang, S., Wei, S. H., Zunger, A., and Katayama-Yoshida, H. (1998). "Defect physics of the chalcopyrite semiconductor." *Phys. Rev. B - Condens. Matter Mater. Phys.*, 57(16), 9642–9656.

Zhao, Y., Zeng, Q., Liu, X., Jiao, S., Pang, G., Du, X., Zhang, K., and Yang, B. (2016). "Highly efficient aqueous-processed polymer/nanocrystal hybrid solar cells with an aqueous-processed TiO<sub>2</sub> electron extraction layer." *J. Mater. Chem. A*, 4(30), 11738–11746.

## LIST OF PUBLICATIONS

### PUBLICATIONS IN INTERNATIONAL JOURNALS

---

1. “Band gap engineering of mixed  $\text{Cd}_{(1-x)}\text{Zn}_{(x)}\text{Se}$  thin films”, **Santhosh T.C.M.**, Kasturi V. Bangera., G.K. Shivakumar., *Journal of alloys and compounds*, Vol. 703, (2017) 40 - 44.
2. “Synthesis and bandgap tuning in  $\text{CdSe}_{(1-x)}\text{Te}_{(x)}$  thin films for solar cell application”. **Santhosh T.C.M.**, Kasturi V. Bangera., G.K. Shivakumar., *Solar Energy*, Vol. 153, (2017) 343 - 347.
3. “Effect of Bi doping on the properties of CdSe thin films for optoelectronic device applications”, **Santhosh T.C.M.**, Kasturi V. Bangera., G.K. Shivakumar., *Material Science in Semiconductor Processing*, Vol. 68, (2017) 114 -117
4. “Effect of Ag in CdSe thin films prepared using thermal evaporation”, **Santhosh T.C.M.**, Kasturi V. Bangera., G.K. Shivakumar., *Semiconductors*, Vol. 51, (2017) 1597- 1603.

### CONFERENCE PROCEEDINGS

---

1. “Preparation of vacuum deposited cadmium selenide thin films for optoelectronic applications”, **Santhosh T.C.M.**, Kasturi V. Bangera., G.K. Shivakumar., *Materials Today Proceedings*, Vol. 3, (2016) 2220-2224.
2. “Effect of annealing on the structural, electrical and optical properties of CdSe thin films”, **Santhosh T.C.M.**, Kasturi V. Bangera., G.K. Shivakumar. (2016) *Advance science letters (ASL)* (Accepted May- 25<sup>th</sup>, 2017).



**Contact Information** Santhosh T. C. M  
S/o Veeraiah T.C.M.  
#1360, 16<sup>th</sup> Cross, 'D' Block  
Karnataka Housing Board colony,  
Kundwada, Davanagere - 577566  
Tel. no.: 9663450264  
santhu.990m@gmail.com

### Education

- July, 2013 - **National Institute of Technology Karnataka, Surathkal, India.**  
Present Ph.D., Physics (Pursuing)  
**“Preparation and Properties of cadmium-zinc chalcogenide thin films for device applications”**
- July, 2010 – P.G. Centre Chitradurga, Davanagere University, Davanagere  
July, 2012 M.Sc., Physics (Condensed Matter Physics)

### JOURNAL PUBLICATIONS

---

1. Preparation of vacuum deposited cadmium selenide thin films for optoelectronic applications., Santhosh T.C.M., Kasturi V. Bangera., G.K. Shivakumar., Materials Today Proceedings, Vol. 3, (2016) 2220-2224.
2. Band gap engineering of mixed  $\text{Cd}_{(1-x)}\text{Zn}_{(x)}\text{Se}$  thin films., Santhosh T.C.M., Kasturi V. Bangera., G.K. Shivakumar., Journal of alloys and compounds 703, (2017) 40 – 44.
3. Effect of Ag in CdSe thin films prepared using thermal evaporation., Santhosh T.C.M., Kasturi V. Bangera., G.K. Shivakumar., Semiconductors 51, (2017) 1597 – 1603.
4. Effect of annealing on the structural, electrical and optical properties of CdSe thin films., Santhosh T.C.M., Kasturi V. Bangera., G.K. Shivakumar. Advance science letters (ASL) (Accepted May- 25<sup>th</sup>, 2017).
5. Synthesis and bandgap tuning in  $\text{CdSe}_{(1-x)}\text{Te}_{(x)}$  thin films for solar cell application., Santhosh T.C.M., Kasturi V. Bangera., G.K. Shivakumar., Solar Energy 153, (2017) 343-347.

6. Effect of Bi doping on the properties of CdSe thin films for optoelectronic device applications., Santhosh T.C.M., Kasturi V. Bangera., G.K. Shivakumar., Material Science in Semiconductor Processing 68, (2017) 114-117.

#### **PAPERS PRESENTED IN NATIONAL/ INTERNATIONAL CONFERENCE.**

1. Santhosh T.C.M., Bangera. K. V., Shivakumar G.K., (2015), “Growth and characterization of cadmium selenide thin films.” Presented in national conference on “Condensed Matter Physics and Applications-2015”, held at Manipal Institute of Technology, during 27<sup>th</sup>- 28<sup>th</sup>, March 2015.
2. Santhosh T.C.M., Bangera. K. V., Shivakumar G.K., (2015) “Preparation of vacuum deposited cadmium selenide thin films for optoelectronic applications” Presented in International conference on “Recent Advances in Nano Science and Technology-2015” held at Sathyabama University, Chennai during 8<sup>th</sup> – 10<sup>th</sup>, July 2015.
3. Santhosh T.C.M., Bangera. K. V., Shivakumar G.K., “Effect of annealing on the structural, electrical and optical properties of CdSe thin films”. Presented in International Conference on Nanoscience and Nanotechnology (ICNAN’16)” held at Vellore Institute of Technology (VIT), Vellore, during 19<sup>th</sup> – 21<sup>st</sup>, October 2016.

#### **WORKSHOPS ATTENDED**

1. Participated in the “Nano Structured Materials and Their Applications in Catalysis and Fuel Cells (NMCF-2016)”, 29<sup>th</sup> September to 1<sup>st</sup> October, 2016, at Department of Chemical Engineering, National Institute of Technology Karnataka (NITK), Surathkal.
2. Participated in the Global Initiative for Academic Networks course on “Novel Functional materials for Energy Conversion” October-2016 at National Institute of Technology Karnataka (NITK), Surathkal.